Phase Field Theory Modeling of CH_4 and CO_2 Fluxes from Exposed Natural Gas Hydrate Reservoirs

Master of Science Thesis in Process Technology

by

Khuram Baig

Department of Physics and Technology

University of Bergen, Norway

2009

Abstract

Natural gas hydrates are widely distributed in sediments along continental margins, and harbor enormous amounts of energy. Gas hydrates are crystalline solids which occur when water molecules form a cage like structure around a non-polar or slightly polar (eg. CO_2, H_2S) molecule. These enclathrated molecules are called guest molecules and obviously have to fit into the cavities in terms of volume. Massive hydrates that outcrop the sea floor have been reported in the Gulf of Mexico (MacDonald, et al., 1994). Hydrate accumulations have also been found in the upper sediment layers of Hydrate ridge, off the coast of Oregon and a fishing trawler off Vancouver Island recently recovered a bulk of hydrate of approximately 1000kg (Rehder, et al., 2004). Håkon Mosby Mud Volcano of Bear Island in the Barents Sea with hydrates openly exposed at the sea bottom (Egorov, Crane, Vogt, Rozhkov, & Shirshov, 1999). In oil and gas industry the most common guest molecules are methane, ethane, propane, butane, carbon dioxide and hydrogen sulfide. But hydrocarbons with up to seven carbons can create hydrate.

The worldwide energy contained in hydrates is huge. But at the same time many of the natural hydrate resources are not well trapped below clay and shale layers and dissociate through contact with under saturated water. Arctic hydrates may be covered by ordinary geological trapping mechanisms and ice layers of varying thickness. The integrity of the geological trappings in these areas are, to a large extent unknown and many potential scenarios can occur when the ice is shrinking in these areas.

One of the largest environmental problems facing mankind in the 21st century is the impacts on global weather patterns due to greenhouse gases like methane, carbon dioxide and chlorofluorocarbons. It also effects the distribution of ecosystems and sea level change due to the impact of increased temperature on the melting of arctic ice and the shrinking of other permafrost ice like for instance glaciers. As a greenhouse gas CH_4 is in the order of 25 times as aggressive as carbon dioxide. It is therefore an important global challenge to be able to make reasonable predictions of the dissociation flux of exposed hydrate reservoirs, and the associated CH_4 that escapes to the atmosphere after biological consumption and conversion through inorganic and organic reactions.

There are several possible methods for reduction and stabilization of the CO_2 content in the atmosphere, ocean disposal and storage stands out as one solution. There are several options for this (different depths). The seafloor lake alternative, which implies disposal of CO_2 at depths for which the density of CO_2 is higher than that of seawater, might be the most promising. None of the ocean storage options for CO_2 are permanent. But the presence of a CO_2 hydrate film at the interface between water and CO_2 in the seafloor lake will significantly reduce the dissolution of CO_2 into the ocean water.

The primary focus in this thesis is on the dissociation of methane and carbon dioxide hydrates due to thermodynamic instabilities through direct contact with under saturated water. For this purpose Phase Field Theory (PFT) was chosen as the scientific method. This is the first work on these types of systems with this level of theoretical methods and the scope have initially

been limited to PFT without hydrodynamics. This puts an inherent limit on the types of phenomena that can be studied since the implicit assumption is then that the dilution of the released molecules from the hydrate is faster than the dissociation rate itself, meaning that no bubble formation is accounted for. This task has done by using phase field code made by Tamasz Puztai.

The simulations were run with conditions relevant to the Nyegga site located on the edge of the Norwegian continental slope and the northern flank of the Storegga Slide (Hovland, et al., 2005).

The results presented in this work were not yet stabilized due to technical problems and limited computer resources. The interface between the liquid and solid perfectly follows the power law which is proportional to square root of time showing a diffusion control process. To compare the values of dissolution rates, the fluxes were extrapolated to experimental time scales. Observed fluxes were larger than what can be expected from hydrate dissociating and molecularly diffusing into the surrounding water. The reason for these differences might be the effect of porosity, salinity, hydrodynamics etc. The further work will involve an up scaling of the code with regards to optimization of numerical routines, hydrodynamics and salinity.

Acknowledgements

First, I would like to sincerely thank my supervisor Professor Bjørn Kvamme for his valuable insights, enthusiasm, support and encouragements. I greatly appreciate the time that he spent and his effort for guiding me through this research experience and providing me with invaluable feedback on this thesis. I always believed that sometimes it's too difficult to find some words to express feelings, but I should acknowledge that now, it's really impossible for me to find any word to appreciate him.

I would like to thank Professor Tatiana Kuznetsova for her assistance on modification of code and Phd. Student Pilvi Helina for providing initial knowledge about the code. I would like to thank Phd. Student Muhammad Qasim for his excellent computer skills contributions on building of MatLab codes. I also would like to thank other Phd. Students for their help and valuable time.

Thanks to my fellow students for a memorable period of study and great social set. Especially, I would like to thank Archana, Alusine, Bjørnar and Amir for a very good and valuable cooperation.

Thanks to my family for their encouragement, understanding, warm support and patience.

Contents

List of Figures

List of Tables

1 Introduction

Hydrates, also called clathrates, are crystalline solids which look like ice, and which occur when water molecules form a cage-like structure around a non-polar or slightly polar (eg. CO_2, H_2S) molecule. These enclathrated molecules are called guest molecules and obviously have to fit into the cavities in terms of volume. In the oil and gas industry the most common guest molecules are methane, ethane, propane, butane, carbon dioxide and hydrogensulfide. This work will focus on methane and carbon dioxide as guest molecules. The methane guest molecules in gas hydrates are mainly microbially generated; however, thermogenic methane is observed in gas hydrate of the Gulf of Mexico, the Caspian Sea, and a few other places where there are known petroleum systems (K. A Kvenvolden, 1995). The most remarkable property of methane hydrates are that it compresses the guest molecule into a very dense and compact arrangement, such as $1m^3$ of solid methane hydrate with 100 percent void occupancy by methane will release roughly 164 m^3 of methane (Davidson, El-Defrawy, Fuglem, & Judge, 1978) at standard conditions of temperature and pressure.

Natural gas hydrates are widely distributed in sediments along continental margins, and harbor enormous amounts of energy. Massive hydrates that outcrop the sea floor have been reported in the Gulf of Mexico (MacDonald, et al., 1994). Hydrate accumulations have also been found in the upper sediment layers of Hydrate ridge, off the coast of Oregon and a fishing trawler off Vancouver Island recently recovered a bulk of hydrate of approximately 1000kg (Rehder, et al., 2004). Håkon Mosby Mud Volcano of Bear Island in the Barents Sea with hydrates openly exposed at the sea bottom (Egorov, et al., 1999). These are only few examples of the worldwide evidences of unstable hydrate occurencies that leaks methane to the oceans and eventually may be a source of methane increase in the atmosphere.

The primary focus in this thesis is on the dissociation of methane and carbon dioxide hydrates due to thermodynamic instabilities. Hydrates in reservoirs are subject to potential contact with minerals, aqueous solution and gas, depending on the state of the system and the fluid fluxes through the hydrate section. From a thermodynamic point of view the first question that arises is whether the system can reach equilibrium or not according to Gibbs phase rule. Equilibrium requires the equality of temperature, pressure, and chemical potential in all phases. In the case of dissociation, gas hydrate generally becomes unstable by changing the P/T conditions in a way that the hydrate phase is not stable anymore, i.e., that the chemical potential of the gas component is lower in the free gas phase than in the hydrate phase (Rehder, et al., 2004) and/or water is more stable as a liquid or ice phase. In a reservoir the local temperature is given by the geothermal gradient and the pressure is given by the static column above. Equilibrium in this system can only be achieved if the number of degrees of freedom is 2 (Gibbs phase rule). This implies that a hydrate surrounded by mineral (and corresponding adsorbed phase on the surface), aqueous phase and only methane will be over determined and cannot reach a unique equilibrium situation. These systems will progress dynamically towards local and global minimum free energy at all times.

Leakage of methane from reservoirs that are exposed towards the ocean floor will have an impact on the local ecological environments. Biological organisms will consume some of the released methane. Other portions of the methane will react with sulphur and other inorganic compounds. Released carbon dioxide from the biologically catalyzed sulphur reactions will to a large degree dissolve in the aqueous phase and may result in precipitation of solid carbonates. Some portion of the released methane will also be distributed in the ocean as methane and might end up in the atmosphere. (Sassen & MacDonald, 1997) Sassen et al. have analyzed such hydrates reservoir from outside the Gulf of Mexico where released gas from exposed hydrate reservoirs form free gas bubbles. The kinetic rates of dissociation of hydrate exposed to seawater are essential in the understanding of the carbon balance related to released methane and subsequent amounts of released methane that reaches the atmosphere. Methane is in comparison 24 times greater in the creation of the green house effect than carbon dioxide (Wuebbles & Hayhoe, 2002).

In the formulation below it is important to distinguish the human made changes from the fluctuations in temperature which occur over longer time scales according to natural cycles.

The greenhouse gases like methane and chlorofluorocarbons have been the main cause of rapid global warming, which has been discussed in several publications during the past (Bains, Norris, Corfield, & Faul, 2000; Beerling, Lomas, & Gröcke, 2002; Dickens, 2003; Glasby, 2003; Hesselbo, et al., 2002; Kennett, Cannariato, Hendy, & Behl, 2000). Therefore, an important global challenge is to be able to make reasonable predictions of the dissociation flux of exposed hydrate reservoirs, and the associated methane that escapes to the atmosphere after biological consumption and conversion through inorganic and organic reactions.

Humanity's largest contribution to global warming is CO_2 emission from the combustion of fossil fuels. Ocean deposits of CO_2, either as CO_2 lakes at depths where CO_2 is heavier than seawater or at intermediate depths is still a promising alternative for long term storage of CO_2 from this combustion (Ohsumi, 1995; Shindo, Fujioka, & Komiyana, 1995). These storage sites are characterized by high pressure as well as low temperature, conditions that will favour rapid formation of CO_2 hydrate on the interface between CO_2 and seawater. This hydrate will significantly reduce the dissolution of CO_2 into the surrounding water (Tatyana Kuznetsova & Kvamme, 2002).

The thesis is divided into in two parts. The first part consists of four chapters with review of the knowledge on hydrate as relevant for this work is briefly summarized. Chapter 2 provides background information on what hydrates are, how they form, how they can be used and some possible approaches for reductions of the impact of CO_2 on the environment. Chapter three explains the phase field theory, which is used in the building of the code for this work. Chapter four gives the thermodynamics used in this work, which is also a part of phase field theory. The second part of this thesis consists of four chapters; simulations, results & discussion, conclusions and proposals for future work.

2 HYDRATES

This chapter starts with brief history of hydrate and than an overview of what the most common hydrates look like and their most important properties are given in section 2.1. Special attention is given to hydrate structure I, which is the most relevant to the rest of this work. The scope of this thesis is on the kinetics of hydrate phase transitions, therefore, in section 2.2 I have presented some existing models and hypotheses. Rest of the chapters emphasis on what the potential uses of hydrates are, effects of hydrates on environment and how these effects can be reduced.

As mentioned in chapter 1, natural gas hydrates are crystalline solids composed of water and gas. Historically, the first discovery of hydrates was done in 1810 and after this a quarter of a century later – hydrates remained only of academic interest as a laboratory curiosity. The major revolution came in 1934 when E.G. Hammerschmidt discovered the plugging in the gas pipelines caused by gas hydrates. From that time on lots of efforts were done to predict and prevent hydrate formation in equipments and pipelines during processing or transport. From mid of 1960s, the discovery of hydrate formation in deep oceans and permafrost regions has gained much fame and lots of publication done on hydrate phase transition. (E.D Sloan, 1998)

2.1 The structure of hydrate

Natural gas hydrates belong to the three crystal structures, cubic structure I (sI), cubic structure II (sII), or hexagonal structure H (sH) shown in Figure 2-1. The scope of this work is on hydrates with carbon dioxide or methane as guests. These two components both form the structure I hydrate and the focus in this thesis will therefore be on this specific structure.

Structure I is formed with guest molecules having diameters between 4.2 and 6 Å, such as methane, ethane, carbon dioxide, and hydrogen sulfide. Structure II and structure H contains larger cavities and are formed from larger molecules, such as propane and iso-pentane respectively. More information about these structures is given in the book by Sloan 1998 (E.D Sloan, 1998).

The unit cell of structure I contains 46 water molecules which enclose two different types of cavities. This is the smallest symmetric unit of this hydrate structure and a hydrate crystal of any size can be constructed by adding unit cells. The size of the unit cell is slightly dependent on temperature due to the temperature dependence of the hydrogen bonds (Shpakov, Tse, Tulk, Kvamme, & Belosludov, 1998). The size of this unit cell is measure from crystallography to be 12.01 Å at temperature 0^{o}C (Stackelberg & Muller, 1951).

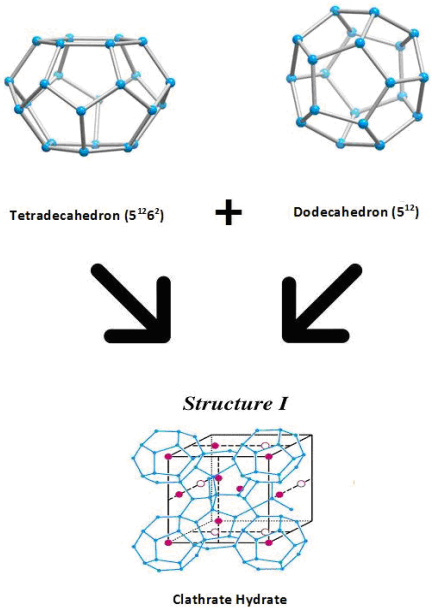

Figure 2-1: : The unit cell of hydrate structure I, and the cavities constituting the structure. The figure content is taken from USGS Geological Survey ((http://geology.usgs.gov/connections/mms/joint_projects/methane.htm) and (http://chem.ps.uci.edu/~kcjanda/Group/gas_hydrate_structure.html) websites dated. 2nd May 2009, time 16:07

The smaller cavities are each formed by a pentagonal dodecahedron with one water molecule at each of its 20 vertices. They are located at the centre and at the vertices of the unit cell, giving an average of 2 small cavities per unit cell. The remaining 6 molecules form bridges between the smaller cavities in such a way that a second type of cavity is formed, a tetradecahedron, having two opposite hexagonal faces and 12 pentagonal faces adding up to 24 water molecules per cavity. There are 6 of these larger cavities per unit cell giving a small to large cavity ratio of 1:3. The smaller cavities are close to spherical and the average distance from the oxygen molecules in the water to the centres of the cages are 3.95Å.

The larger cavities are slightly oblate and the distance from the oxygen to the centre of cavity varies between 4.04Å and 4.65Å. This small dimensional difference determines the size of the occupant. If all the cavities were occupied by guest molecules the mole percent of water would be about 85%. Methane is small enough to be able to fill both the large and the small cavities. CO_2 molecules, on the other hand, are bigger and do not fit into the small cavities. This means some of the cavities will be left empty, thus the actual mole per cent water will be larger. With such high water content the properties of hydrates are assumed to depend very little on the guest molecules, other than determining which structure of hydrate will be formed. Based on the similarities in the water crystal structure, one would also expect variations in properties between different hydrate structures to be less than the variation between hydrates and ice. The most striking property of hydrates is that they can be formed at temperatures higher than 0°C. The phase transition point also depends considerably on the pressure. The freezing temperature of ice on the other hand varies very little with pressure, and when ice becomes less stable with increasing pressure, hydrate becomes more stable up to certain limits in pressure. There are extreme pressure measurements (Dyadin, Aladko, & Larionov, 1997) which says something else.

When water freezes, the specific volume increases by 9%. For most substances the volume decreases from liquid to solid, so this is a very special property. Hydrates have an even larger expansion and increases 26-32% during the phase transition, if we only consider the water molecules. The thermal expansion of ice and hydrate structure II is about the same, while it is some 40% larger for structure I. Thermal conductivity is 5 times larger in ice than hydrates.

2.2 Hydrate formation

Hydrate formations are generally divided into two stages, the process of nucleation, and the steady growth stage. Hydrate nucleation is the process during which small clusters of water and gas (methane or carbon dioxide) grow and disperse in an attempt to achieve critical size for continued growth. When the cluster attains a critical size, monotonic growth occurs if it is not disturbed by competing clusters that are in a state of lower free energy (see section 4.1). The induction time or lag time is the time from the system is brought into a condition of super-saturation and until solid formation is observed. As such the induction is not a physically determined unique state of the systems since it depends on the resolution of the observation of hydrate, which can be everything from visual observations and downwards in scale.

It is important to keep in mind that this does not imply that there is no hydrate present during the lag time. The implication is simply that initial hydrate size below visible range is slowing down transport of the hydrate building blocks across a heterogeneous system – where the hydrate formers are in one phase and on the other side of the solid hydrate is the aqueous phase. Heterogeneous nucleation occurs on the interface between hydrate former phases, for instance a gas mixture and liquid water or ice. It can also be nucleation from water and gas on water which is adsorbed on solid surfaces like for instance a metal or rust surface in a pipeline. Nucleation can also happen somewhere inside the bulk of pure solution which is called homogeneous nucleation. Homogeneous nucleation is a solidification process occurring in the absence of impurities. It involves many more molecules than could collide simultaneously, thus a sequence of bimolecular collisions of an autocatalytic nature is more probable. Homogeneous from aqueous solution extracts both water and former from solution and might not be delayed much but is slow for other reasons (low concentrations of hydrate formers). In the open literature there are also experimental observations that have been discussed in terms of homogeneous nucleation while there exists photographic evidence that they most likely are heterogeneous because the dissolved hydrate formers have adsorbed onto a metal surface or other surfaces. The guest molecules are therefore extracted from an adsorbed phase while the water is taken from the solution and the nucleation is, by definition, heterogeneous. Homogeneous nucleation of hydrates is considered an anomaly because heterogeneous nucleation occurred much more frequently.

For the simplest case of a spherical particle the Gibbs free energy difference (ΔG) between a small solid particle and the solution can be expressed in terms of the surface free energy (ΔG_S) and the volume free energy (ΔG_V):

$$\Delta G = \Delta G_S + \Delta G_V = 4\pi r^2 \gamma + \frac{4}{3}\pi r^3 \Delta g_v \qquad (2.1)$$

Δg_v is the free energy change per unit volume and γ is the interface free energy. The interface free energy is the work needed to create the actual interface between the new phase and the "mother" phase(s), in contrast to the interfacial tension which is proportional to surface stress between two phases. Interface free energy and interfacial tension are related by $\sigma = \gamma + A_s d\gamma / dA_s$, where σ is the interfacial tension and A_s is the interface area. The surface gives a positive contribution to the free energy, while the free energy change from liquid to solid is negative. Adding the surface and volume contribution gives a maximum value for ΔG at a specific radius, which corresponds to the critical size. Below the critical radius there is a free energy penalty in getting larger, consequently the crystals will fluctuate by either growing or re-dissolving. The critical radius represents the minimum size for which a nucleus will only grow. A foreign particle or surface may reduce the critical radius if the solid surface changes the chemical potential and concentrations of the building blocks in a favorable fashion, and hydrates are more likely to occur. The above formulation is for Classical Theory which presumes a sharp interface and not accurate for solid/liquid. Solid/liquid interface has substantial interface (1 – 1.5 nm is common). In industrial systems with natural gas or CO_2 in pipelines and equipment solid metal surfaces are examples of surfaces which will enhance the hydrate formation rates. In addition to the thermodynamic conditions for nucleation, the history of the water has also been shown to influence the induction time. It is a common preception that when ice or hydrate is dissociated a substantial amount of the water structure remains in the form of clusters of water with local number of average hydrogen bonds higher than average for “uniform” water. When the temperature is decreased for a second time, the observed induction time is typically considerably shorter. Many experimental results imply some apparatus dependence as well as experimental procedure dependence, which makes it difficult to deduce any general conclusions that can be directly transferable to other experimental situations or real scenarios.

The solubility of guest molecules in water is normally very low, suggesting that formation of hydrate in bulk water phase is not very likely. This is particularly true for hydrocarbons. Gases like for instance CO_2 and H_2S has higher solubility and homogeneous formation of hydrate from solution is absolutely feasible. Hydrate formation from bulk hydrate former phase (for instance a natural gas phase) is not likely due to the limited water content in this phase. Concentrations close to the 15% (as mentioned in section 2.1) in hydrate can be found at the vapour-water interface and at the surface of the container through adsorption of guest molecules to the container walls, making these sites more likely for nucleation. Since hydrate nucleation normally occurs at the vapour-water interface this has also been the basis for

molecular models. There are only some few hypotheses attempting to describe the nucleation of hydrate at a molecular level.

Christiansen and Sloan (E.D Sloan, 1998; E. D Sloan & Fleyfel, 1991) proposed a hypothesis following the classical nucleation theory. Water molecules are here assumed to form clusters around dissolved guest molecules. These clusters then combine to form unit cells, and when the size of agglomerated clusters reaches a critical size, growth begins. Another hypothesis has been proposed by Kvamme (B. Kvamme, 1996). Gas molecules are here assumed to travel to a suitable site at the vapour-water interface where the water molecules first form partial, and then complete cages around the adsorbed species. Clusters join and grow on the vapour side of the surface until critical size is achieved. There is very limited experimental verification of these hypotheses. In the abscence of experimental verification they remain speculations and may be considered, with critical perspective, as potential possible mechanisms.

It is obvious from equation 2.1 that mass have to be supplied through diffusional processes and potentially induced transport through stirring and other means which can increase the contact area for heterogeneous hydrate formation on water/gas interface. Since the phase transition by itself is exothermic there is obviously also heat transport involved in the dynamics. But since the rate of heat transport is at least two orders of magnitude faster than mass transport for this particular phase transition (dominated by water) the heat transport is only a limiting factor when the kinetic rate of the phase transition itself (4.2) is slow. This might be the case when pressure reduction is used for generating hydrate dissociation in a reservoir.

In the second phase, which is the growth phase, mass (and possibly heat transfer) becomes increasingly important. Especially in growth from aqueous solutions, where the guest solubility is much less than the guest mole fraction in the hydrate, the mass transfer will be important, and may very well dominate the entire process. In this situation heat transfer is very rapid due to the heat transport properties of water and hydrate. Transport of heat is more than two orders of magnitude faster than mass transport rate and heat transport limitations may normally be omitted from the considerations of kinetics (Buanes, Kvamme, & Svandal, 2006). Two major models for hydrate growth exist, the work by Englezos et. al. (Engelezos, Kalogerakis, Dholabhai, & Bishnoi, 1987) and the modified Englezos model by Skovborg et al. (Skovberg & Rasmussen, 1994). In simplified model for crystal growth the change in the rate of crystal growth is frequently expressed in terms of

$$\frac{dm}{dx} = KA\left(c - c^{eq}\right) \qquad (2.2)$$

where A is the crystal surface area, c and c^{eq} the supersaturated and equilibrium concentration respectively. K is an overall transfer coefficient expressed in terms of diffusion and reaction coefficients k_d and k_r as

$$\frac{1}{K} = \frac{1}{k_d} + \frac{1}{k_r} \qquad (2.3)$$

The concentrations in equation 2.2 are sometimes replaced by fugacities as in the Englezos model. To make this replacement one has to assume ideal liquid solutions, conservation of mass and constant temperature and pressure. By observing some restrictions and limitations in the Englezos model, Rasmussen and Skovborg were able to simplify the model. They assumed the process could be modelled as a mass transfer restriction through liquid film at the gas-liquid interface and reduced the number of differential equations from 5 to a single equation. These two models have yet only been shown to fit the experiment data for which the parameters were derived from.

2.3 Potential uses and impact of gas hydrates

The important amounts of gas hydrates in the Earth's crust might be considered as a new source of sustainable energy (Y. F. Makogon, 1965). Kvenvolden (Kvenvolden, 1988) and Makogon (Y. F. Makogon, 1998) pointed out that the amount of gas in known hydrate reserves up until 1988 was at least twice as much as the energy contained in the total fossil fuel reserves. Indeed, one volume of methane hydrate can yield 164 times more methane than one volume of gaseous methane under the same pressure conditions and at standard temperature (Davidson, et al., 1978). Gas hydrate deposits, principally considered as the result of a permanent migration of natural gases throughout Earth fractures, are mainly distributed offshore due to the high pressure and low temperature conditions at the seabed and more parsimoniously encountered in permafrost (Keith A. Kvenvolden, 1995; E.D Sloan, 1998). Nevertheless, fossil fuel resources are currently sufficient to face worldwide energy needs, and thus, gas-hydrate exploitation is dedicated to being a distant prospect, especially for offshore hydrates (Grauls, 2001).

Gas recovery is generally based on in situ hydrate dissociation by either heating or depressurization (Holder, Zetts, & Pradhan, 1988). The thermal approach generates huge heat losses and, therefore, seems less exploitable than (Lee & Holder, 2001) depressurization that requires high porosity hydrate deposits (Burshears, O_Brien, & Malone, 1986). Moreover, the transport stage can be technically challenging, since extracted gas and water may re-crystallize into gas hydrates inside the transmission lines and then provoke pipe plugging. Even though they are considered as the main hydrocarbon source for the future, gas hydrate deposits might also represent a real threat to the environment. Indeed, when considering offshore hydrates as a global methane reservoir, exploitation of these sediments in unfavorable circumstances could drastically modify the marine ecosystem and even generate underwater gas blowouts (Glasby, 2003). Moreover, destabilizing hydrate sediments plays an undeniable role in climate change. According to Brewer (P.G. Brewer, 2000), a slight global warming would raise the hydrate temperature above the equilibrium point, involving dissociation and the release of a great quantity of methane. Given that a mole of methane is

about 24 times more effective at absorbing infrared radiation and affecting the climate than a mole of carbon dioxide (Wuebbles & Hayhoe, 2002), such discharge would cause a chain reaction mechanism. However, methane hydrate sediments may be reinforced by injecting chemical promoters and, thus, limiting the predictable safety risks. An original perspective proposed by other authors (Seo, Lee, & Yoon, 2001; Warzinski & Holder, 1988) would consist in swapping methane, encased in hydrate, with carbon dioxide and, thus, limiting disturbances in underwater layers and preventing sub-oceanic landslides.

About 64% of the enhanced greenhouse gas effect is due to carbon dioxide emissions (Bryant, 1997), of which more than 6 Gt/yr are attributed to anthropogenic activities (Desideri & Paolucci, 1999). Given that the greenhouse effect is undeniably responsible for climate warming (Smith & Thambimuthu, 1993), reducing the quantities of CO_2 released into the atmosphere is a major environmental challenge. Carbon dioxide can be partially taken up by various methods such as chemical absorption in amines (Chakma, 1997; Desideri & Paolucci, 1999; Gray, et al., 2004) and then degassed from the amine solution. The separated CO_2 phase must then be deposited in an appropriate fashion. Several approaches have been proposed during the last three decades, ranging from ocean disposal at different depths, including CO_2 lakes at depths where CO_2 is heavier than the seawater above, mineralization and sequestration in geological media and oceans (Bachu, 2002; Hendriks & Blok, 1993). A schematic overview of some options can be listed with reference to fig. 1 as follows:

- Direct injection of the captured CO_2 gas into near-shore shallow ocean about 200-400 m depth from ocean surface (Qi, Zhishen, & Xiaochun, 2008).
- Disposal of liquid CO_2 into the shallow sub-seabed less than 300 m depth from ocean surface (Qi, et al., 2008).
- Sequesteration of liquid CO_2 into deep sub-seabeds about 300-500 m depth from ocean surface (Qi, et al., 2008).
- Injection of liquid CO_2 in deep ocean over 3000 m to form lake (Nealson, 2006).
- Disposal of liquid CO_2 into a membrane containment at the super deep sea floor (>3000 m depth from ocean surface).
- Release of liquid CO_2 into 1000-2500 m depth from ocean surface from moving ship Handa et al. (Handa & Ohsumi, 2003).
- Injection of liquid CO_2 into super deep sub-seabed, greater than 3000 m depth from ocean surface (Qi, et al., 2008).

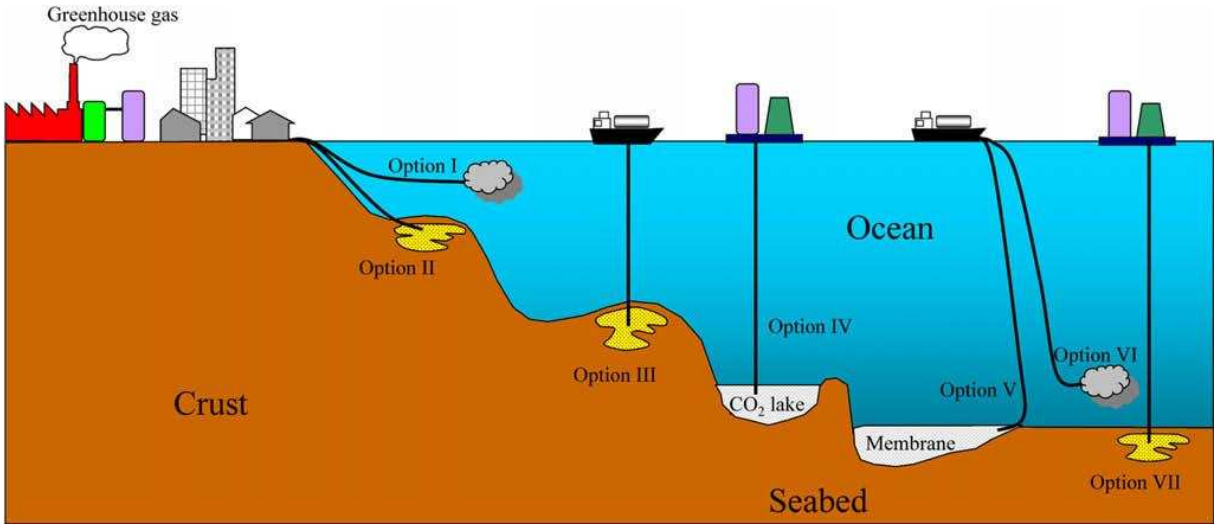

Figure 2-2: : Schematic illustration of some ocean storage strategies (Qi, et al., 2008)

Most of injected CO_2 into the ocean will dissolve as bicarbonate, and unfortunately, a large fraction of the sequestered CO_2 will be released to the atmosphere after a few hundred years because of ocean currents and local supersaturation (Jain & Cao, 2005). Injection of CO_2 in deep ocean over 3000 m is the one studied closer in this thesis.

2.3.1 Sequestration of CO_2 in deep ocean

Long-term storage of carbon dioxide might be more effective if CO_2 were stored on the sea floor in liquid or hydrate form below 3000 meters, where CO_2 is denser than sea water (Ohsumi, 1995; Shindo, et al., 1995). Liquid carbon dioxide could be introduced at depth to form a lake of CO_2 on the sea floor (Ohsumi, 1993). In the special case in their study a large CO_2 lake would form on the bottom and slowly disappear due to CO_2 dissociation into the surrounding sea water. On the basis of their estimates they argued that the efficiency of storage would be several hundred years. Fujioka et al. (Y. Fujioka, 1995; Y Fujioka, et al., 1995) discussed another deep ocean storage case of liquid CO_2 in which the CO_2 was injected into a small deep depression on the deep ocean floor. The idea here is that the smaller surface area will lead to less dissolution of CO_2. At the same time, if the depression is not be completely filled, the dissolved CO_2 will make the sea water denser, and this will presumably result in stagnant layer of sea water with high concentrations of CO_2 above the lake in the depression. The higher concentrations of CO_2 will again reduce the driving forces towards CO_2 dissociation, and make the entire dissolution process slow down. Extreme cases of deep ocean storage, at depths approaching 6000m in the Japanese trench, have also been discussed. In this case CO_2 hydrate will be less dense than liquid CO_2, and there will not be the same possibility of the hydrate breaking up and sinking. Here it is most probable that a stable hydrate film will form at the interface and prevent the dissolution of CO_2 into the sea water. Brewer et al. (P.G. Brewer, Friederich, Peltzer, & Orr Jr., 1999) have calculated that at a depth of more than 4500m, a floating skin of hydrate probably would have formed over the

denser liquid CO_2. Their direct experiments from 349 to 3627m did show massive hydrate growth, but no floating film at the interface.

The injection of large quantities of liquid CO_2 to the deep ocean is technically difficult and thus expensive (P.G. Brewer, Peltzer, Friederich, Aya, & Yamane, 2000). This work also illustrates how injected CO_2 behaves on intermediate depths. Due to the relatively small rising CO_2 droplets, the pure CO_2 will dissociate quickly into the surrounding water (P.G. Brewer, Peltzer, Friederich, & Rehder, 2002). It is also argued that CO_2 injection and dispersal in mid-ocean will reduce environmental impacts, since the mole fraction of CO_2 could be minimized by the rapid dilution of dissolved CO_2 in large volumes of sea water (Ozaki, 1998). Knowledge on the dissolution rates of the rising droplets will help us determine where it is ideal to dispose the CO_2 for long term storage in the ocean.

Commercial CO_2 capture technology is still expensive, but the technology is there. The ability to dispose of large amounts of CO_2 is the uncertain part. The atmosphere and the ocean will eventually equilibrate on a time scale of 1000 years regardless of where the CO_2 is disposed (Herzog, et al., 1997). What will be achieved by deep ocean injection is a reduction in peak atmospheric concentrations expected to occur in the next few centuries. The magnitude of reduction depends on quantity of CO_2 injected in the ocean, and the depth and location of the injection. Permanent disposal of CO_2 as a hydrate on the sea floor is not realistic, but with long residence time in the hydrate, and then later as dissociated CO_2 in the ocean waters, this might lessen the damaging effects CO_2 has in the atmosphere.

2.3.2 Impact on the marine environment

There is always concern at the prospect of using the oceans to store waste materials. Dumping hazardous substances in the ocean, such as nuclear waste, has been banned. But using the oceans to sequester more CO_2 would be different as the oceans already hold vast quantities of CO_2. In fact, what is being proposed with ocean sequestration of CO_2 is merely an acceleration of an existing natural process. This acceleration may assist in protecting the atmosphere and the terrestrial environment in which we live. Nevertheless, it is important to understand the effect that sequestration of CO_2 would have on the oceans.

It is well known that dissolving CO_2 in sea water will decrease the pH of the water, due to the formation of bicarbonate and carbonate ions. It is also known that marine animals are, in general, intolerant to changes in the pH of the water in which they live (Knutzen, 1981). Higher concentration of CO_2 in ocean causes the organism to go into a condition which is known as Hypercapnia. Under these conditions, CO_2 enters the organisms by diffusion across body and especially respiratory surfaces and equilibrates with all body portions. This internal accumulation of CO_2 will be responsible for most of the effects observed in animals (Ishimatsu, Kikkawa, Hayashi, Lee, & Kita, 2004; **Pörtner**, **Langenbuch** , & Michaelidis, 2005; **Pörtner**, **Langenbuch** , & **Reipschlager**, 2004; **Pörtner** & **Reipschlager**, 1996; Seibel & Walsh, 2001). Respiratory distress, narcosis, and mortality are the most obvious

short-term effects at high CO_2 concentrations, but lower concentrations may have important effects on longer time scales. The CO_2 level to which an organism has acclimated may affect its acute critical CO_2 thresholds, however, the capacity to acclimate has not been investigated to date.

The dissolve inorganic carbon (DIC) concentration in surface ocean waters is already higher than in pre-industrial times as a result of the elevated CO_2 concentration in the atmosphere. Calculations show (Haugan & Drange, 1996) that there has been a decrease in pH of the ocean surface water of almost 0.1 pH-units due to the increase of atmospheric CO_2 from pre-industrial times. This study predicts a reduction in pH of about one unit, from an ambient level of pH ~7.8, extending for several kilometers from the point of injection; this would have an impact on marine life. However, the study also showed a way in which the near-field environmental impact could be substantially reduced. This would be achieved by dispersing the CO_2 over large volumes of seawater so as to reduce the loading of CO_2 at any point in the ocean. A suitable engineering design could involve, for example, increasing the number of independent discharge points at which CO_2 is injected into the ocean. Other techniques have been examined which involve injecting liquid CO_2 through a vertical pipe housed on a moving ship. Both this technique and the dropping of solid blocks of CO_2 through the water column are efficient methods of dispersing the CO_2 and minimizing pH changes; both procedures should, therefore, have minimum impact on the marine environment.

That means the impacts can be reduced to very low levels, small changes in pH could have sub-lethal effects on marine animals and, over a period of time, affect the marine ecology. For example, reproduction and growth rates might be reduced. An important concern would be for those pelagic species that migrate vertically, either daily or seasonally, as a layer of low pH water could present a physiological barrier to such processes. It has also been established (Poetner & Reipschlager, 1996) that pelagic species with high metabolic rates, such as squid, are much less tolerant to changes in pH than less active species, such as worms living in marine sediments.

3 Scientific methods

As discussed in the first two chapters hydrate stability in reservoirs is undefined in the sense that Gibbs phase rule cannot be fullfilled when both temperature and pressure are defined at a given location (depth). This means that the system will progress towards lowest free energy possible under the constraints of mass- and heat-transport. Heat transport in these systems, which are dominated by water, is fast and 2 orders of magnitude faster than mass transport (A Svandal, 2006). Practically this means that it is possible to consider the phase transitions as isothermal. It might be possible to set up systems of non-equilibrium Monte Carlo but since time information is crucial that is not an option. Non-equilibrium molecular dynamics might also be theoretically possible although scaling of water molecules according to the method applied by Kuznetsova & Kvamme (T. Kuznetsova & Kvamme, 1999) would result in a breakdown of the hydrate. But other scaling approaches might be feasible. Scaling relative to water in other thermodynamic conditions might be possible. The problem is still the small scale in volume and even more crucial the limited scale in time. Hydrate dissociation towards pure water are slow compared to limits of molecular dynamics (nano seconds).

Density functional theory (DFT) is also limited in geometry since the kinetics of the phase transition is proportional to the change in molecular structure across the interface from the old to the new phase. As such the molecular scale is still a limiting factor here since also the parameters which go in are related to processes on atomistic to molecular scale. Molecular structure is directly related to free energy and this is the original basis for formulation of Phase Field Theory (PFT). Replacing structure with corresponding free energies opens up for a scale which is only limited by the scale of the thermodynamic description. On the other hand it is also so that the phase transition will be proportional to the capillary waves and the thermal fluctuations of the interface. So practically there is a link to at least some nano scale processes (Evans & Sluckin, 1980; Tarazona & Evans, 1984).

Another feature which may complicate the picture is the potential of bubble formations through dissociation. If the dissociation rate is slower than the diffusion controlled dilution in the surrounding water then there is no bubble formation during the dissociation itself and hydrodynamic impact on the phase transition process can be ignored. As mentioned in the introduction there are several places where large bubbles are observed but there are also many cases where at least not visible bubbles have been observed (that does not mean that nano to micro bubbles can be ignored).

In view of the discussion above PFT is chosen as the primary tool and at this stage the focus is limited to PFT without hydrodynamics.

3.1 Phase Field Theory

This chapter is the presentation of phase field theory for two component system. At first the most basic equations and concepts are given in section 3.2. This model follows the

formulation of Wheeler et al. (Wheeler, Boettinger, & McFadden, 1992), which historically has been mostly applied to descriptions of the isothermal phase transition between ideal binary-alloy liquid and solid phases. Only a short review of the model is given here, but full details of the numerical method can be found elsewhere (Gránásy, Börzsönyi, & Pusztai, 2002; B. Kvamme, et al., 2003; Wang, et al., 1993; Warren & Boettinger, 1995). Section 3.2 deals with how the model can be extended to take into account anisotropy, polycrystalline growth and temperature dependence. The most of the contents of this chapter is taken from Svandal et al. (A Svandal, 2006).

3.2 The governing equations

Phase field models are models which from a free energy functional depending on the phase field and other variables like temperature, concentrations & etc. model the time evolution of systems involving different phases. In this work the model is applied to essentially only two phases in the sense that the fluid thermodynamics is treated appropriately but in the absence of hydrodynamics there is no need to distinguish between gas phase and liquid phase other than making sure that the transport properties are handled appropriately. The diffusivity of water is lower than gas diffusivity so provided that the gas density is high enough to provide access to guest molecules the water movement and reorganization is expected to be the kinetic rate limiting within the implicit mass transport contributions. The phase field is an order parameter describing the phase of the system as a function of spatial and time coordinates. The field ϕ is allowed to vary continuously on the range from solid to liquid.

An isothermal solution of two different components A and B were considered which may exist in two different phases, solid and liquid, contained in a fixed region Ω. For the hydrate system the component A is water and component B is some guest molecule. Within the scope of this work B is methane or carbon dioxide. The solid state is represented by the hydrate and an aqueous solution is the liquid phase. The solidification of hydrate is described in terms of the scalar phase field $\phi(x, t)$ and the local solute concentration of component B denoted by $c(x, t)$. The field ϕ is a structural order parameter assuming the values $\phi = 0$ in the solid and $\phi = 1$ in the liquid. Intermediate values correspond to the interface between the two phases. The starting point of the model is a free energy functional,

$$F = \int d^3x \left(\frac{\varepsilon_\phi^2 T}{2} |\nabla \phi|^2 + f(\phi, c) \right) \tag{3.1}$$

Which is an integration over the system volume of the free energy density $f(\phi, c)$ and a gradient term correction to ensure a higher free energy at the interface between phases. Note that the integration variable x in the integrand is not to be confused with mole fraction as this is an indication of a length variable and the integral is over the system volume. The free energy density is given by

$$f(\phi, c) = WTg(\phi) + (1 - p(\phi))g_S + p(\phi)g_L \tag{3.2}$$

The phase field switches on and off the solid and liquid contributions g_S and g_L through the function $p(\phi)=\phi^3(10-15\phi+6\phi^2)$, and note that $p(0)=0$ and $p(1)=1$. This function was derived from density functional theory studies of binary alloys and has been adopted also for our system of hydrate phase transitions. The binary alloys are normally treated as ideal solutions. The thermodynamics for the hydrate system is treated more rigorously and the free energy densities are presented in chapter 4. The quadratic function $g(\phi)=\phi^2(1-\phi)^2/4$ ensures a double well form of the $f(\phi,c)$ with a free energy scale $W=(1-c)W_A+cW_B$, with $g(0)=g(1)=0$. In the phase field literature the concentration c is the mole fraction of component B, $c=n_B/(n_A+n_B)$, i.e. the fraction of component B to the total. With the assumption that the molar volume is constant the mole fraction concentration and the volume concentration are related by $c_m=c_v v_m$, where v_m is the average molar volume. In chapter 4 the term x is use for the mole fraction, but following the phase field formulation c will be used here. Without hydrodynamics the impact of density difference is not accounted for and molar density is approximated constant. And as such the mole fractions of a certain element in the grid will be equal to the volume fractions. In order to derive a kinetic model it is assume that the system evolves in time so that its total free energy decreases monotonically. Given that the phase field is not a conserved quantity, the simplest form for the evolution that ensures a minimization of the free energy is

$$\dot{\phi}=-M_\phi\frac{\delta F}{\delta\phi} \tag{3.3}$$

With $M_\phi>0$. It may also allow M_ϕ depending on composition writing $M_\phi=(1-c)M^A+cM^B$

where,

$$M^A=[1-p(\phi)]M^A_{solid}+p(\phi)M^A_{fluid}$$

$$M^B=[1-p(\phi)]M^B_{solid}+p(\phi)M^B_{fluid}$$

For the conserved quantity this may associate a flux to the concentration by writing

$$\dot{c}=-\nabla\cdot J_c \tag{3.4}$$

Following classical linear irreversible thermodynamics it is assume that near equilibrium the flow is linearly proportional to the force that drives it.

$$J_c=-M_c\nabla\frac{\delta F}{\delta c} \tag{3.5}$$

Inserting (3.5) into (3.4) gives

$$\dot{c}=\nabla\cdot M_c\nabla\frac{\delta F}{\delta c} \tag{3.6}$$

where,

$M_c = c(1-c)(v_m / RT)D$

$D =$ Diffusion coefficient

Above equation of M_c is taken to reproduce the Fick's law of diffusion in the bulk phase. In order to allow the diffusion coefficient for different diffusivities in the solid and liquid can be expressed in terms of the respective diffusivity coefficient governed by the phase field,

$$D = D_S + p(\phi)(D_L - D_S)$$

Now using the form of the free energy as in Eq. (3.1) the governing equations can be written as

$$\dot{\phi} = M_\phi\left(\varepsilon_\phi^2 T\nabla^2\phi - WTg'(\phi) - p'(\phi)(g_L - g_S)\right) \quad \textbf{(3.7)}$$

And

$$\dot{c} = \nabla\left(\frac{v_m}{RT} D_c(1-c)\nabla\left((W_A - W_B)Tg(\phi) + (1-p(\phi))\frac{\partial g_S}{\partial c} + p(\phi)\frac{\partial g_L}{\partial c}\right)\right) \quad \textbf{(3.8)}$$

The model parameters ε_ϕ, W_A, W_B, M^A and M^B can be related to measurable quantities, just as M_c is related to diffusivity. The mobility for the phase field will also be related to diffusivity but is expected to be more complex and also reflect dynamic characteristics of the water rearrangement. Molecular dynamics simulations can be one method for obtaining more insight into this and might even be able to provide a tool for estimating values for the mobility. At this stage, however, the same value as for the concentration mobility is used. Considering the equilibrium condition the parameters can be related to the interface energy $\sigma_{A,B}$, the temperature of melting $T_{A,B}$ and the interface thickness $\delta_{A,B}$.

3.3 Extended model

To include the flow of heat in the simulation, an energy or thermal field is introduced. Example of this is given in the work by Conti (Conti, 1997, 2000). The energy field is a conserved quantity and the time derivative can be derived by associating a flux to the flow of energy and a driving force as in equations (3.4) and (3.6).

$$\dot{e} = -\nabla \cdot J_c \quad \textbf{(3.9)}$$

$$\dot{e} = \nabla \cdot \left(M_e \nabla \frac{\delta F}{\delta e}\right) \quad \textbf{(3.10)}$$

For hydrate dissociation with low solvent concentration as used in our simulation, the guest component diffusion is assumed to completely dominate the process. This is shown in earlier

work by Svandal et al. (A Svandal, Kvamme, Gràsàsy, & Pusztai, 2005b), which demonstrated that diffusion of CO_2 in the aqueous phase is the governing parameter for growth of hydrate from CO_2 in aqueous solution as well as dissociation rates of hydrate towards pure water. As discussed earlier the release of heat has little or no effect on the growth and dissociation rates (A Svandal, et al., 2005b). Constant temperature is therefore assumed for our system, and a thermal field has not been included in our models.

We specifically demonstrated that heat transport was actually more than two orders of magnitude faster than mass transport. Heat transport will therefore rapidly dissipate the heat away from the phase transition site.

3.4 Simulation of hydrate system

Classically the phase field theory has been applied to model alloy solidification. There are some very important differences between binary metals and our hydrate systems. The most apparent is the very low solubility of the solutes, CO_2 and CH_4, in water. The simplest scenario for growth is from an initial nucleus in a supersaturated homogeneous solution. Presently no phase field models published on heterogeneous growth, even though this is a necessary element in hydrate kinetics since most natural hydrate growth happens this way. For hydrate dissociation, a larger hydrate nucleus is placed in a strongly undersaturated solution of almost pure or pure water. Extensive work on applying the phase field model on both hydrate growth and dissociation have been conducted by Bjørn Kvamme, Atle Svandal, László Gránásy, Tamás Pusztai and several others (Buanes, et al., 2006; B. Kvamme, et al., 2003; A Svandal, Kuznetsova, & Kvamme, 2006a; A Svandal & Kvamme, 2005a; Tegze, Gránásy, & Kvamme, 2007) . Svandal et al. (A Svandal, et al., 2005b) used phase field simulations to study homogeneous growth of hydrate from aqueous solution and also dissociation of hydrate towards undersaturated aqueous solution. The results obtained from these studies indicated that the kinetic rates of growth and dissociation of CO_2 hydrate are dominated by diffusion of carbon dioxide in aqueous phase. The simulations also indicated that the most important parameter when it comes to growth and dissociation rates is the initial mole fraction of CO_2 in the aqueous phase. The same authors also demonstrated that CH_4 dissociation rate is much slower than for carbon dioxide (A Svandal & Kvamme, 2005a). This can be explained by the much lower solubility of CH_4 in water.

4 Thermodynamics

This chapter treats the development of the thermodynamic functions needed for the phase field theory presented in chapter 3. Much of the theory in section (4.1) & (4.2) was found in a book on classical theoretical physics (Greiner, Neise, & Stocker, 1995). Section (4.3) & (4.4) much of the data taken from Svandal et al. (2006).

4.1 Free energy

The conservation of energy is critical in all aspects of physics, and is also the principle that gives rise to the 1st law of thermodynamics. The 2nd law of thermodynamics tells us that any isolated system will strive towards maximum entropy. Combining the two laws gives for the changes in internal energy for phase *i*:

$$dU^i \leq T^i dS^i - pdV^i + \sum_{l=1}^{n} \mu_l^i dN_l^i \qquad (4.1)$$

Here, the summation is done over all present phases $i = 1,2,\ldots,n$. S is the entropy, μ the chemical potential and N the number of particles of a specific compound. The equality is for reversible changes, which is only a theoretical possibility. So, for all real and irreversible changes will have the "less than" situation. Transformation of the natural variables is accomplished through Legendre transforms by subtracting $d\left(T^i S^i\right)$ on both sides. The resulting function is termed Helmholtz free energy:

$$dF^i \leq -S^i dT^i - p^i dV^i + \sum_{l=1}^{n} \mu_l^i dN_l^i \qquad (4.2)$$

Free energy can, in a simplified sense, be considered as the "available" energy level under the constraints of losses associated to entropy generation. $-p^i dV^i$ is termed technical work, or shaft work, since the work involved in pushing fluids internally in the systems is subtracted. The last term on the right hand side is called chemical work and is the work related to extracting or inserting particles. Removing a molecule from the system involves releasing the molecule from the interaction energy of the surroundings and also involves an entropy contribution related to reorganisation of the system. Free energy is an extensive state quantity, so to get the total for an entire system, which may consist of more than one phases, one just adds the contributions from the different phases.

$$F^{tot} = \sum_{l=1}^{n} F^i \qquad (4.3)$$

For changes at constant pressure and temperature equations (4.1) and (4.2) gives:

$$dF^{\,i} \le \sum_{l=1}^{n} \mu_l^i dN_l^i \tag{4.4}$$

In an isothermal, isobaric system (like the one simulated in this thesis) left on its own, irreversible processes happen until a minimum total free energy is achieved, given by:

$$\begin{aligned} dF^{\,tot} &= 0 \\ dF^{\,tot} &= dF^{\,tot}_{\min} \end{aligned} \tag{4.5}$$

This means that differences in the free energy between two phases can be seen as a driving force, and the system will strive towards minimum free energy. The final limit of free energy minimum can easily be verified to be the situation where chemical potential of each component is the same in all co-existing phases if the number of degrees of freedom is so that full equilibrium can be reached.

4.2 The Gibbs phase rule and hydrate phase transition

A phase is any physically separable material in the system. It is possible to have two or more phases in the same state of matter (e.g. solid, liquid and gaseous,…). Phases may either be pure compounds or mixtures such as solid or aqueous solutions--but they must "behave" as a coherent substance with fixed chemical and physical properties.

Gibbs' phase rule provides the theoretical foundation, based in thermodynamics, for characterizing the chemical state of a system, and predicting the equilibrium relations of the phases present as a function of physical conditions such as pressure and temperature. To this end, an isolated system which contains C different particle species (methane and carbon dioxide etc.) and P different phases were started. Each phase can be understood as a partial system of the total system and on can formulate the first law for each phase, where it denotes quantities of the i^{th} phase by superscript $i = 1,2,...,P$. For reversible changes of state the equation becomes:

$$dU^{(i)} = T^{(i)} dS^{(i)} - p^{(i)} dV^{(i)} + \sum_{l=1}^{C} \mu_l^i dN_l^i \tag{4.6}$$

In Equation (4.6), $U^{(i)}$ of phase i is a function of the extensive state variables $S^{(i)}, V^{(i)}, N_1^{(i)}, ..., N_C^{(i)}$; i.e. it depends on $C+2$ variables (if further terms appear in eq. (4.6), the number of variables is larger). Altogether this gives $P(C+2)$ extensive state variables. If the total system is in thermodynamic equilibrium, the following conditions for the intensive state quantities results:

$$T^{(1)} = T^{(2)} = \cdots = T^{(P)} \qquad \text{Thermal equilibrium}$$

$$P^{(1)} = P^{(2)} = \cdots = P^{(P)} \qquad \text{Mechanical equilibrium} \qquad \textbf{(4.7)}$$

$$\mu_l^{(1)} = \mu_l^{(2)} = \cdots = \mu_l^{(P)} \qquad l = 1,...,C \qquad \text{Chemical equilibrium}$$

Each line contains $P-1$ equations, so that equation (4.7) is a system of $(P-1)(C+2)$ equations. Since $T^{(i)}, p^{(i)},$ and $\mu_l^{(i)}$ are functions of $S^{(i)}, V^{(i)},$ and $N_l^{(i)}$ can eliminate one variable with each equation.

$$(C+2)P-(C+2)(P-1)=(C+2) \qquad \textbf{(4.8)}$$

This only require extensive variable to determine the equilibrium state of the total system. As shown in equation (4.8), this number is independent of the number of phases. If its now consider that exactly P extensive variables (e.g., $V^{(i)}$, $i=1,2,...,P$) determine the size of the phases (i.e., the volumes occupied by each), one needs intensive variables.

$$F = C + 2 - P \qquad \textbf{(4.9)}$$

The above equation is known as Gibbs` phase rule. It is readily understood with the help of concrete examples. Let us consider the potential for hydrate formation from methane and water. Since the components are methane and water $(C=2)$ and the phases are three (L_w-H-V) then one intensive variable $(F=1)$, such as either T or P must be specified in order to obtain a unique solution for the formation of hydrates. A unique solution means that it could theoretically reach equilibrium if left to itself for long times (E.D Sloan, 1998).

Now for our system, with two components $C=2$ (water and methane or water and carbon dioxide) and two phases ($L_{solution}$-H) then two intensive variables $(F=2)$, such as temperature and pressure must be defined to achieve unique solution. Considering the situation in natural systems like carbon dioxide lake at the sea bottom, assuming that the ions and/ or corresponding salt act as inert in the sea water with respect to phase transition. But ionic contents do have impact on the thermodynamic properties of the aqueous phase. The system is thermodynamically over determined since there are three phases and two components participating in the actual phase transitions. Degree of freedom (F) is equal to 1 but 2 independent variables are defined. For this situation the system is not able to establish complete three phase equilibrium and the combination of the first and second laws of thermodynamics will dictate this system to approach a state of minimum free energy. Since the system is inside the hydrate stability zone, this implies that hydrate is more stable form of water than liquid water or ice, and that the total free energy changes over to hydrate represent reduction in Gibbs' free energy (E.D Sloan, 1998).

A system including hydrate will always strive towards thermodynamic equilibrium or lowest possible Gibbs free energy if equilibrium cannot be reached due to Gibb's phase rule. Than it is clear that there are three factors, high temperature, low pressure and lower chemical

potential of one of the hydrates components in the surroundings that can provoke hydrate dissociation:

In this work temperature and pressure are assumed as fixed thermodynamic state properties. Chemical potential differences and corresponding free energy differences related to concentration differences and phase are the driving forces for hydrate dissociation. Hydrate dissociation involves breaking the bonds in the hydrate structure, and diffusing the guest molecules into the bulk liquid. Dissociating hydrate is an endothermic process, meaning the system absorbs energy in the form of heat. This results in heat transfer towards the dissociating hydrate, and mass transfer away from the dissociating hydrate.

4.3 Hydrate thermodynamics

The theory for hydrate thermodynamics built on van der Waals' and Platteuw's approach relies on the approximation that the water lattice remains undisturbed by the presence of guest molecules. While this might be an adequate approximation for guest molecules which are small compared to the cavity they occupy. Molecules which are not small compared to the cavity size, for instance CO_2 in the large cavities of structure I hydrate, do affect the water vibration movement and thus affects the free energy of the water lattice. For CO_2, this effect may be of the order of 1 kJ/mole at 0±C and thus significant. In this work, a revised adsorption theory due to Kvamme et al. (B. Kvamme & Tanaka, 1995) is used.

The expression for chemical potential of water in hydrate is

$$\mu_w^H = \mu_w^{O,H} - \sum_i RTv_i \ln\left(1 + \sum_j h_{ij}\right) \qquad (4.10)$$

This equation is derived from the macro canonical ensemble under the constraints of constant amount of water, corresponding to an empty lattice of the actual structure. Details of the derivation are given elsewhere (B. Kvamme & Tanaka, 1995) and will not be repeated here. $\mu_w^{O,H}$ is the chemical potential for water in an empty hydrate structure and h_{ij} is the cavity partition function of component *j* in cavity type *i*. The first sum is over cavity types, and the second sum is over components j going into cavity type *i*. In this work , only one type of guest occupying the hydrates in a given simulation, the second sum will thus be reduced to a single term. Here v_i is the number of type i cavities per water molecule. For hydrate structure I, there are 3 large cavities and 1 small per 23 water molecules, $v_l = 3/23$ and $v_s = 1/23$. In the classical use of equation (4.10), the cavity partition functions are integrated under the assumption that the water molecules are fixed and normally also neglecting interactions with surrounding guest molecules. This may be adequate for small guest molecules with weak interactions. On the other hand, molecules like CO_2 are large enough to have a significant impact on the librational modes of the water molecules in the lattice. An alternative approach

(B. Kvamme & Tanaka, 1995) is to consider the guest movements from the minimum energy position in the cavity as a spring, and evaluate the free energy changes through samplings of frequencies for different displacements in the cavity. A molecule like methane will, as expected, not have significant impact on the water movements (B. Kvamme & Tanaka, 1995). CO_2 on the other hand, will change water chemical potential by roughly 1 kJ/mole at 0°C when compared to the assumption of undisturbed fixed water molecules. The cavity partition function may thus be written as:

$$h_{ij} = e^{\beta\left(\mu_j^H - \Delta g_{ji}^{inc}\right)} \tag{4.11}$$

Where Δg_{ji}^{inc} now is the effect of the inclusion of the guest molecule j in the cavity of type i, which as indicated above is the minimum interaction energy plus the free energy of the oscillatory movements from the minimum position. At hydrate equilibrium the chemical potential is equal to that of the chemical potential of the guest molecule in its original phase (chemical potential of dissolved CO_2 or CH_4 for the case of hydrate formation from aqueous solution).

Equation (4.11) can be inverted to give the chemical potential for the guest as a function of the cavity partition function:

$$\ln h_{ij} = \beta\left(\mu_j^H - \Delta g_{ji}^{inc}\right)$$

Where $\beta = \frac{1}{RT}$

$$\ln h_{ij} = \frac{1}{RT}\left(\mu_j^H - \Delta g_{ji}^{inc}\right)$$

$$\mu_j^H = \Delta g_{ji}^{inc} + RT \ln h_{ij} \tag{4.12}$$

Equation (4.12) is basically derived from an equilibrium consideration but may be used as an approximation for bridging chemical potential to composition dependency. The relation between the filling fraction, the mole fractions and the cavity partition function is

$$\theta_{ji} = \frac{x_{ji}}{v_i\left(1 - x_T\right)} = \frac{h_{ji}}{1 + \sum_j h_{ji}} \tag{4.13}$$

Here x_T is the total mole fraction of all the guests. Because of CO_2 shape and size, it can only fit into the larger cavities, and unless some other guest molecule is present, the small cavities will then all be empty. For a system with only one component occupying the large cavities, the chemical potential of the guest molecule would be reduced to

$$\mu_w^H = \Delta g_{ji}^{inc} + RT \ln\left(\frac{\theta_{ji}}{1-\theta_{ji}}\right) \tag{4.14}$$

For methane, which can occupy both large and small cavities, a more cumbersome approach is needed. Initially assuming that chemical potential of methane in the two cavities is the same. This gives a proportional relation between the two partition functions independent on composition.

$$\mu_{ms}^H = \Delta g_{ms}^{inc} + RT \ln h_{ms}$$

$$\mu_{ml}^H = \Delta g_{ml}^{inc} + RT \ln h_{ml}$$

$$RT\left(\ln h_{ml} - \ln h_{ms}\right) = \Delta g_{ms}^{inc} - \Delta g_{ml}^{inc}$$

$$\left(\ln h_{ml} - \ln h_{ms}\right) = \frac{\Delta g_{ms}^{inc} - \Delta g_{ml}^{inc}}{RT}$$

$$\frac{h_{ml}}{h_{ms}} = e^{\left(\frac{\Delta g_{ms}^{inc} - \Delta g_{ml}^{inc}}{RT}\right)} = A \tag{4.15}$$

The mole fraction of methane x_m is the sum of the mole fraction in each cavity, i.e. large x_{ml} and small x_{ms}. The mole fractions are expressed in terms of the cavity partition function from equation (4.13)

$$x_{ms} + x_{ml} = x_m \tag{4.16}$$

$$\frac{h_{ms}}{1+h_{ms}} v_s + \frac{h_{ml}}{1+h_{ml}+h_{cl}} v_l = \frac{x_m}{1+x_T} = B \tag{4.17}$$

Here h_{ms}, h_{ml} and h_{cl} are the cavity partition functions of methane in small cavities, methane in large cavities and carbon dioxide in large cavities respectively. The denominator in the second term can be expressed in terms of the mole fraction and one of the partition functions from equation (4.13) and (4.16).

$$1+h_{ml}+h_{cl} \tag{4.18}$$

The partition function for CO_2 using equations (4.13) needs to be calculated as:

$$\frac{x_c}{v_l(1-x_T)} = \frac{h_{cl}}{1+h_{ml}+h_{cl}}$$

Rearranging the above equation in term of h_{cl} gives

$$h_{cl} = \frac{x_c(1+h_{ml})}{v_l(1-x_T)-x_c}$$

Inserting the value of h_{cl} in equation (4.18) gives:

$$1+h_{ml}+h_{cl} = 1+h_{ml}+\frac{x_c(1+h_{ml})}{v_l(1-x_T)-x_c}$$

$$1+h_{ml}+h_{cl} = (1+h_{ml})\left(1+\frac{x_{cl}}{v_l(1-x_T)-x_{cl}}\right) \qquad \textbf{(4.19)}$$

The factor right side in the above equation is a known constant because CO_2 only go into large cavities. This gives the constant C:

$$C = 1+\frac{x_{cl}}{v_l(1-x_T)-x_{cl}} \qquad \textbf{(4.20)}$$

Using equations (4.15), (4.19) & (4.20) results:

$$1+h_{ml}+h_{cl} = (1+Ah_{ms})C \qquad \textbf{(4.21)}$$

Equation (4.17) can be written in terms of single partition function:

$$\frac{h_{ms}}{1+h_{ms}}v_s + \frac{Ah_{ms}}{(1+Ah_{ms})C}v_l = B \qquad \textbf{(4.22)}$$

Now the equation (4.22) can be reduce to get second order equation:

$$h_{ms}(1+Ah_{ms})Cv_s + Ah_{ms}(1+h_{ms})v_l = B(1+h_{ms})(1+Ah_{ms})C$$

$$(v_sCA+v_lA-BCA)h_{ms}^2 + (v_sC+v_lA-BCA-BC)h_{ms} - BC = 0 \qquad \textbf{(4.23)}$$

Equation (4.23) can be written in the form of second constant:

$$a_1(h_{ms})^2 + a_2(h_{ms}) + a_3 = 0 \tag{4.24}$$

$$a_1 = A(v_l + v_s C - BC)$$
$$a_2 = v_s C + A v_l - BC(1 + A)$$
$$a_3 = -BC$$

For Pure Methane

In the presence of only one guest equation (4.17) can be rewritten in term of one component:

$$\frac{h_{ms}}{1+h_{ms}} v_s + \frac{h_{ml}}{1+h_{ml}} v_l = \frac{x_m}{1+x_m} = B \tag{4.25}$$

Now from equation (4.15) & (4.18)

$$1 + h_{ml} = (1 + A h_{ms}) \tag{4.26}$$

Equation (4.25) can be reduced to second order term using equation (4.26):

$$\frac{h_{ms}}{1+h_{ms}} v_s + \frac{A h_{ms}}{1+A h_{ms}} v_l = B$$

$$(v_s A + v_l A - BA) h_{ms}^2 + (v_s + v_l A - BA - B) h_{ms} - B = 0 \tag{4.27}$$

Now in terms of second constant:

$$a_1(h_{ms})^2 + a_2(h_{ms}) + a_3 = 0 \tag{4.28}$$

$$a_1 = A(v_s + v_l - B)$$
$$a_2 = v_s + A v_l - B(1 + A)$$
$$a_3 = -B$$

Solving this with respect to the cavity partition function h_{ms}, all partition functions are known and the chemical potentials in equation (4.10) and (4.14) can be calculated. The free energy densities for the hydrate as a function of mole fractions are shown in figure (Figure 4-1).

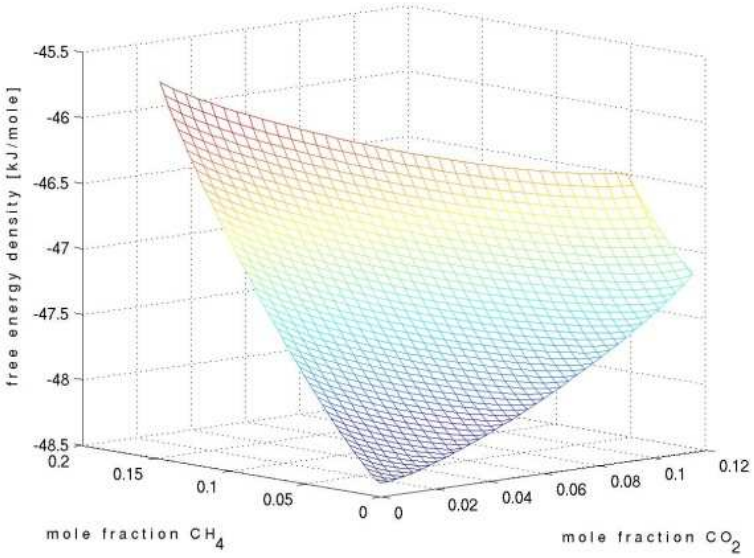

Figure 4-1: Free energy density (KJ/mole) as a function of the mole fractions of CH4 and CO_2 at 1oC and 40 bar (A Svandal, 2006)

The surface in Figure (Figure 4-1) is restricted by the complete filling of the cavities $x_c + x_m \leq 4/27$. However CO_2 only goes into the large cavities so for mole fractions of CH_4 less than the filling of small cavities $x_m \leq 1/27$, the hydrate can never be fully occupied, as can be seen from equation (4.13). Still, the theoretical limit of the thermodynamics for full occupancy can be evaluated. This can be seen as the cut-off region to the right in the figure. Here, the large cavities are fully occupied by the carbon dioxide and the small cavities are partly occupied by methane. In this work, in which only pure CO_2 or pure CH_4 hydrate is used and only the corresponding two-dimensional projections of the graph in fig. (Figure 4-1) is used. Also note that the plot is simplified and only approximate if mixtures were to be used since the intermediate regions in this figure is simply plotted as an ideal mixture of the CO_2 hydrate and the methane hydrate. As such it will not correctly represent situations where CO_2 hydrate obtains extra stability through methane filling of the small cavities.

4.4 Aqueous solution

The chemical potential of CO_2 and CH_4 has the general form in the aqueous phase derived from excess thermodynamics

$$\mu_i = \mu_i^{\infty} + RT \ln\left(x_i \gamma_i^{\infty}\right) + v_i\left(P - P_0\right) \qquad \textbf{(4.29)}$$

μ_i^{∞} is the chemical potential of component i in water at infinite dilution, γ_i^{∞} is the activity coefficient of component i in the aqueous solution in the asymmetric convention (γ_i^{∞} approaches unity in the limit of x becoming infinitely small). The chemical potentials at infinite dilution as a function of temperature are found by assuming equilibrium between fluid and aqueous phases ($\mu_i^L = \mu_i^{aq}$). This is done at low pressures where the solubility is very low, using experimental values for the solubility and extrapolating the chemical potential down to a corresponding value for zero concentration. The activity coefficient can be regressed by using the model for equilibrium to fit experimental solubility data. The chemical potential of water can be written as:

$$\mu_w = \mu_w^p + RT\ln\left((1-x)\gamma_w\right) + v_w\left(P - P_0\right) \tag{4.30}$$

Where μ_w^p is pure water chemical potential. The activity coefficient in water can be calculated from the Gibbs-Duhem equation, but it will be close to unity.

$$x d\ln\left(\gamma_c\right) + \left(1-x\right) d\ln\left(\gamma_c\right) = 0 \tag{4.31}$$

γ_c is the activity coefficient of CO_2 for the water/CO_2 system and CH_4 in the water/CH_4 system. x is the mole-fraction of dissolved hydrate former (CO_2 or CH_4).

4.5 Fick's second law of diffusion

When unsteady-state diffusion takes place in a solid or stagnant fluid, the governing differential equation, called Fick's second law of diffusion.

$$\frac{\partial c_A}{\partial t} = D\frac{\partial^2 c_A}{\partial x^2} \tag{4.32}$$

Where,

$c_A =$ Concentration, $kgmol/m^3$
$D_A =$ Diffusivity, m^2/hr
$x =$ Distance in direction of diffusion, m
$t =$ Time, hr

The equation (4.32) is used in the formation of phase field theory and thermodynamics involved in the hydrate kinetics (McCabe, Smith, & Harriott, 2005).

5 Simulations

This chapter is divided into two sections. Sections (5.1) provide information about the background of simulations and references taken to run the simulations. In section (5.2), setup of the simulations has discussed.

5.1 Simulations Basis

Unfortunately there is no experimental data available for naturally existed hydrates and this may be due to lack of pressurized core sampling (Long, Lovell, Rees, & Rochelle, 2009). So the references taken are not directly comparable with this work but can give an idea about the fluxes presence around these areas. The thermodynamic conditions for the first four simulations taken from the following Figure 5-1

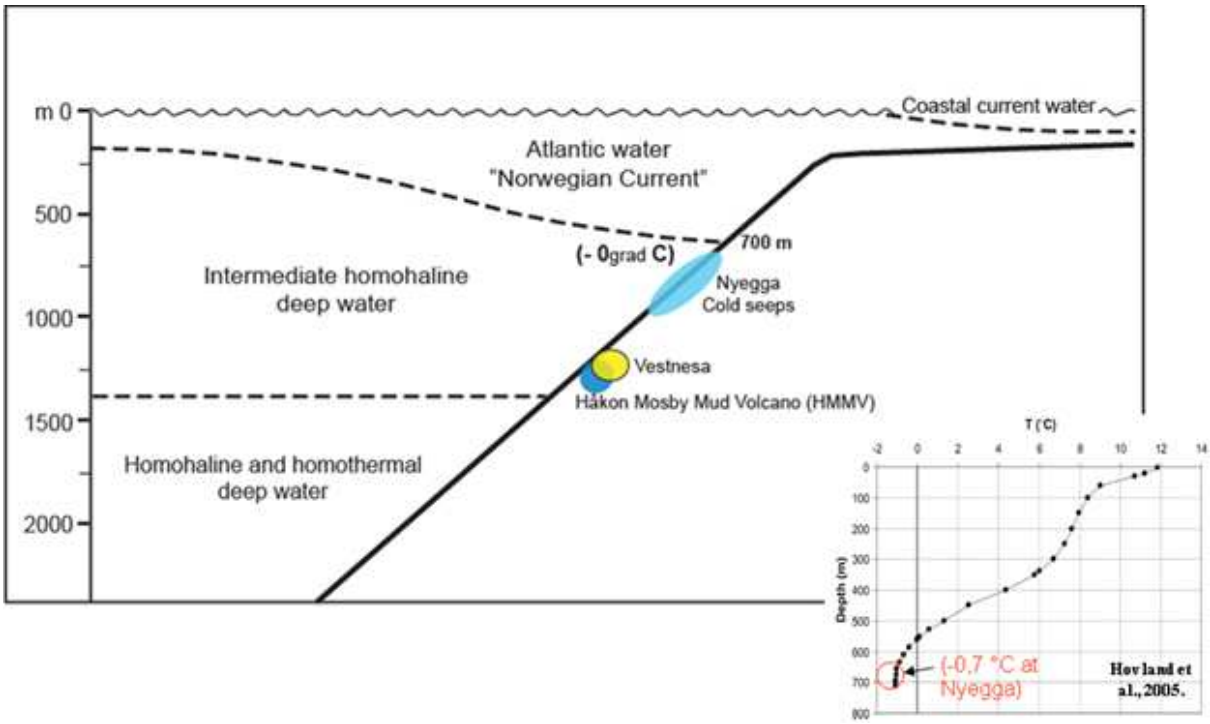

Figure 5-1: Thermal gradient at Nyegga site. (Hovland, et al., 2005)

Chen and Haflidason (Chen, Haflidason, & knies, 2008) are working on a project in which they have taken six gravity cores up to 3.5 m long from the Nyegga region at depths of 639 to 740 m. The place is located on the edge of the Norwegian continental slope and the northern flank of the Storegga Slide, on the border between two large oil/gas prone sedimentary basins— the Møre Basin to the south and the Vøring Basin to the north (Bünz, Mienert, & Berndt, 2003). Totally 41 pore waters were obtained and sulfate gradients measured in the southeast of Nyegga indicate that methane fluxes are 15 to 49 mmol/m^2/yr, which are high in

comparison with other known methane hydrate sites (W S Borowski, Hoehler, Alperin, Rodriguez, & Paull, 2000; D'Hondt, et al., 2004). The Yifeng work is part of GANS (Gas Hydrates on the Norway Barents Sea Svalbard Margin) project. The main objective of GANS project is to determine the gas accumulations in the form of hydrates in sediments on the Norway –Barents Sea – Svalbard (NBS) margin; including an assessment of their dynamics and impacts on the seabed, and their response on the sediments and biota, to provide knowledge vital for a safe exploitation in oil and gas production (http://folk.uib.no/nglbh/GANS/index.html dated 06 Sep. 09 at time 14:14).

(Lijuan, Matsubayashi, & Lei, 2006) estimated methane fluxes from sulfate gradient at each site using the method of Boroski et al. (Walter S. Borowski, Paull, & Ussler, 1996). Methane fluxes converted from the sulfate gradient are very low at ODP sites 1178 and 1176, only 6 or 8 mol / m^2kyr respectively. The methane flux values at site HP04 (Toki, Gamo, & Yamanaka, 2001) and ODPsite 1174 similar(77 mol/m^2kyr), being the highest among all these sites. ODP site 808 has an estimated methane flux of 62 mol m^{-2} kyr^{-1}. The methane flux values of 18 mol $m^{-2}kyr^{-1}$ for Carolina rise and Black Ridge estimated by Borowski et al. (1996) using the same method. In contrast, the methane flux values at site HP04, ODP Sites 1174 and 808 are distinctly higher and close to those predicted by modeling at ODP Site 1043 (70 mol $m^{-2}kyr^{-1}$) offshore Costa Rica (Ruppel & Kinoshita, 2000).

Rehder et al (Rehder, et al., 2004) have calculated the fluxes of CO_2 and CH_4 at depth of 1028 m in Monterey Bay located in the subsurface of Monterey Canyon approximately 15 Km off the coast of central California. In the experiment methane and carbon dioxide hydrates were formed by using method explained by stern et al (Laura A. Stern, Kirby, & Durham, 1996; L.A Stern, Kirby, Durham, Circone, & Waite, 2000). The sample were transferred to the pressurized vessel and transported to the depth of 1028 m using ROV (remotely operated vehicle) Ventana. The pressure and temperature condition at this depth were 10.48 Mpa and 3.5 ^oC respectively. The system is monitored for 27 hours using time-lapse and HDTV cameras. Video analysis showed that CO_2 hydrate samples were completely dissolved after 3 h: 55 min and the dissolution rates observed were 3.62 and 4.67 mmol CO_2 / m^2s. Where CH_4 hydrates dissolved in 26.3 to 27 hrs and the dissolution rates were observed 0.34 – 0.4 mmol CH_4 / m^2s.

These rates are generated from freshly formed hydrates and in Nyegga they have found pore water cores, in both cases the fluxes are not comparable because this thesis is based on naturally occurring hydrates which existed from 10000 years. But these fluxes can show the difference between the pressurized and none pressurized core sampling by comparing with theoretical work done in this thesis.

5.2 Simulations Setup

Some simulations ran on Linux clusters in IFT building and the rest of the simulation ran on hexagon operated by Bergen center of computational sciences (BCCS). The phase field code was programmed by Tamasz Puztai and than first used by László Gránásy for the hydrate system in collaboration with Bjørn Kvamme (B. Kvamme, et al., 2003; Nakashiki, 1998). Then this code is modified with the assistance of professor Tatayana to restart it from any instant time. Also manage to run the simulation independently on parallel processors. The small changes also made in the code to run on hexagon. The phase field model consists of a narrow 2D planar geometry see Figure 5-2. This square structure used to dissociate circle of hydrate placed in the center surrounded by pure liquid water. Two different sizes of the system (5000×5000) and (1500×1500) grids were used and each grid is calculated using Lagrange Method which is equal to 1.00E-10 m. The time is calculated using Lagrange method which is equal to stepmax × innerstepmax × 1.00E-15 s. Phase field model written on C language in which several inputs are changed to run the simulations like temperature, size of the hydrate, total size of the system and concentration in liquids and hydrate at time zero. The model also consists of a thermodynamic part made on MATLAB by Atle Svandal (A Svandal, 2006), which generates tables of the required thermodynamics parameters at given temperature and pressure. The simulation generates results for all grid points in the form of concentrations for all component and structural order ϕ at given time step intervals.

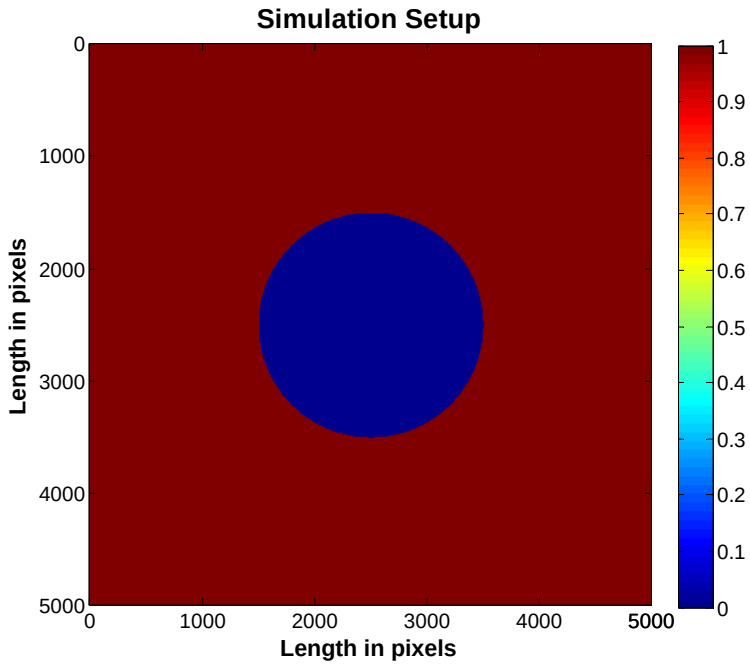

Figure 5-2: : Simulation at time zero, showing the initial picture of hydrate and liquid water with 5000x5000 grid points and a hydrate radius of 1500 grid points.

6 Results and Discussion

To see the effects of dissociation of methane, the simulations were run on different depths and temperatures. The change in temperature for case-I is so small that kinetics is only influence by mass transfer. The several other simulations were run with isothermal conditions at varying pressures and at constant pressure with varying temperatures to show that the kinetics of heat transfer is significantly faster than kinetics related to mass transfer. These simulations were run with different guest molecules to show the effect of dissociation. In order to replicate the realistic conditions the size of the hydrate considered was comparatively much smaller than the surrounding bulk liquid Less amounts of methane present in liquid will provide large thermodynamic forces throughout the length of simulations.

6.1 Calculations

The dissolution rates were calculated from the shrinkage rate using the following equation (Rehder, et al., 2004):

$$DR = SR \times \frac{\rho_{Hyd}}{M_G} \times \left(\frac{M_G}{M_G + (HN \times 0.018)} \right) \quad (6.1)$$

Where,

DR = Dissolution rate (mmol/m^{2}s)

SR = Radius shrinkage rate (mm/s)

ρ_{Hyd} = Density of hydrate (kg/m^3)

M_G = Molar weight of the guest (kg/mol)

HN = Hydrate number

To calculate the radius shrinkage rate (SR), the code is made on MATLAB which used phase ordering parameter ϕ already calculated by the phase field code. This MATLAB code is based on the following equation:

$$SR = \frac{(I_2 - I_1) \times 1.00E-10}{(t_2 - t_1) \times 1.00E-15} \quad (6.2)$$

where I_1 and I_2 are the integrals at times t_1 and t_2 respectively. Hydrate density ρ_{Hyd} is calculated using the following formulation by Sloan E. D (E. Dendy Sloan & Koh, 2008)

$$\rho = \frac{N_W MW_{H_2O} + \sum_{J=1}^{C} \sum_{i=1}^{N} \theta_{ij} v_i MW_J}{N_{Ava} V_{cell}} \quad \textbf{(6.3)}$$

Where,

θ_{ij} = fractional occupation of cavity i by component J

N_W = number of water molecules per unit cell (Table 6.3)

N_{Ava} = Avagadro's number, 6.023×10^{23} molecules/mol

MW_J = molecular weight of component J

MW_{H_2O} = molecular weight of water

v_i = number of type i cavities per water molecule in unit cell (Table 6.3)

V_{cell} = volume of unit cell (dimensions in Table 6.3)

N = number of cavity types in unit cell

C = number of components in hydrate phase

The fractional occupation θ_{ij} depends on pressure and temperature calculated by equation (6.4)

$$\theta_{iJ} = \frac{C_i P}{1 + C_i P} \quad \textbf{(6.4)}$$

where C_i is Langmuir constant and P is the dissociation pressure (E. Dendy Sloan & Koh, 2008). Langmuir constants for individual components depend on temperature and are calculated by the following equation (I. U. F. Makogon, 1981)

$$\lg C_i = 0.43429(A - BT) \quad \textbf{(6.5)}$$

where A and B are constants, the values of which are shown in Table 6.1 and T is temperature of the system being used in Kelvin (I. U. F. Makogon, 1981).

Table 6.1: Value of constants A and B for structure I (I. U. F. Makogon, 1981).

Component	Constants A and B (Structure I)			
	Small Cavities		Large Cavities	
	A_S	B_S	A_L	B_L
CH_4	6.9153	0.03155	6.0966	0.02792
CO_2	14.9976	0.05884	15.2076	0.05886

To calculate the dissociation pressures the stability curves for methane and carbon dioxide were generated as shown in Figure 6-1 using computer program CSM_{Gem} made by Sloan E. D (E. Dendy Sloan & Koh, 2008).

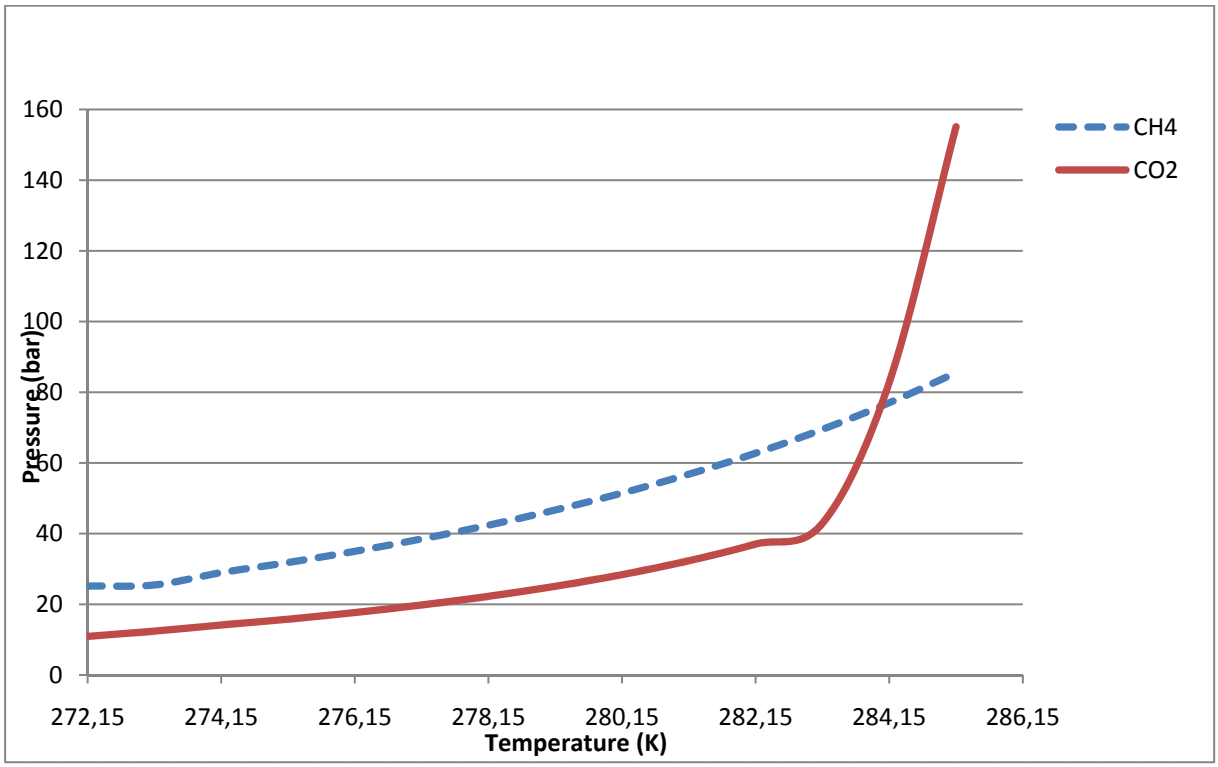

Figure 6-1: Stability curve for methane and carbon dioxide generated from computer programe (E. Dendy Sloan & Koh, 2008)

The dissociation pressures calculated at required temperatures as discussed in section (5.1) are shown in Table 6.2.

Table 6.2: Dissociation pressure at required temperatures.

Temperature (K)	CH_4 Dissociation pressure (bars)	CO_2 Dissociation Pressure (bars)
273.25	25.767	-
273.21	26.50	-
273.17	26.41	-
274.65	30.35	14.95
276.65	36.69	18.71
278.65	44.46	23.64
280.65	54.10	30.26
281.53	58.59	-
282.65	66.10	39.80

These temperatures and pressures used to calculate the fractional occupancy for large and small cavities. The other required values were N_W , v_i and V_{cell} , were taken from Table 6.3.

Table 6.3: Geometry of hydrate crystal structure I. (1) No. of oxygen atoms at the periphery of each cavity.(2) Lattice parameters are a fucnction of temperature, pressure and guest composition. Values given are typical average values. The table is modified using data from Sloan E. D (E. Dendy Sloan & Koh, 2008).

Geometry of Cage		
Hydrate crystal structure	Structure I	
Cavity	Small	Large
Description	5^{12}	$5^{12}6^2$
No. of cavities/unit cell (v_i)	2	6
No. of water molecules/cavity (N_W)	20	24
Lattice parameters	12Å ($\alpha = \beta = \gamma = 90^{\circ}$)	

The hydrate number is calculated by using the fractional filling of small and large cavities (equation (6.6)).

$$HN = \frac{46}{2\theta_S + 6\theta_L} \tag{6.6}$$

Simulation c was extrapolated till the depth of 730m (equation (6.7)) in order to study the effect of temperature and pressure near the stability curve (Figure 6-1).

$$P = P_o + \rho g(z - z_o)$$
$$T = T_o + 0.036\frac{℃}{m}(z - z_o) \tag{6.7}$$

Results from this section are presented in Appendix A.

6.2 Case I: Methane simulations at different depths

Four simulations a, b ,c and d for methane were run on different depths 500, 639, 730 & 740 meters respectively. The temperature and pressure conditions taken for the simulations a, b & d were from Nyegga cold seeps as shown in Figure 5-1, are well inside the stability region.

Table 6.4: Simulation run on different depths.

Simulations Name	Mpftsim1 (a)	Mpftsim2 (b)	Mpftsim4 (c)	Mpftsim3 (d)
Temperature (K)	273.25	273.21	281.53	273.17
Pressure (bar)	50	63.90	72.56	740

The size of the system was taken 5000×5000 grid points which correspond to area 2.5E-13 m^2. The total hydrate unit cells in the initial solid were 31.41676E+05 with radius of 1000 grids cells shown in Figure 5-2 which corresponds to circular area 3.1415E-14 m^2. All the simulations were run to 16.13E+06 total time steps this corresponds to the time of 16.13 ns. The ratio between solid and liquid was adjusted as to achieve the stability. In this case the solid to liquid ratio was taken as 1 : 2.5.

Table 6.5: The properties used to setup the simulations.

Grid points for all five simulations	5000×5000
Corresponding area in m^2	2.50E-13
No. of time steps	16.384E+06
Total time in seconds	16.384E-09
Mole fraction of CH_4 in hydrate	0.14
Mole fraction of water in liquid phase	1.0

The CH_4 concentration initially was adjusted to 0.14 in the hydrate (Table 6.5). The mole fraction in the liquid was adjusted to 1.00e-08. The concentration of methane in liquid was set to get the differences in concentration or more precisely the corresponding chemical potential differences which liberate the diffusion from hydrate towards liquid side.

The concentrations have been calculated inside and outside the hydrate at different time intervals for all the simulations shown in Figure 6-2 & Figure 6-3.

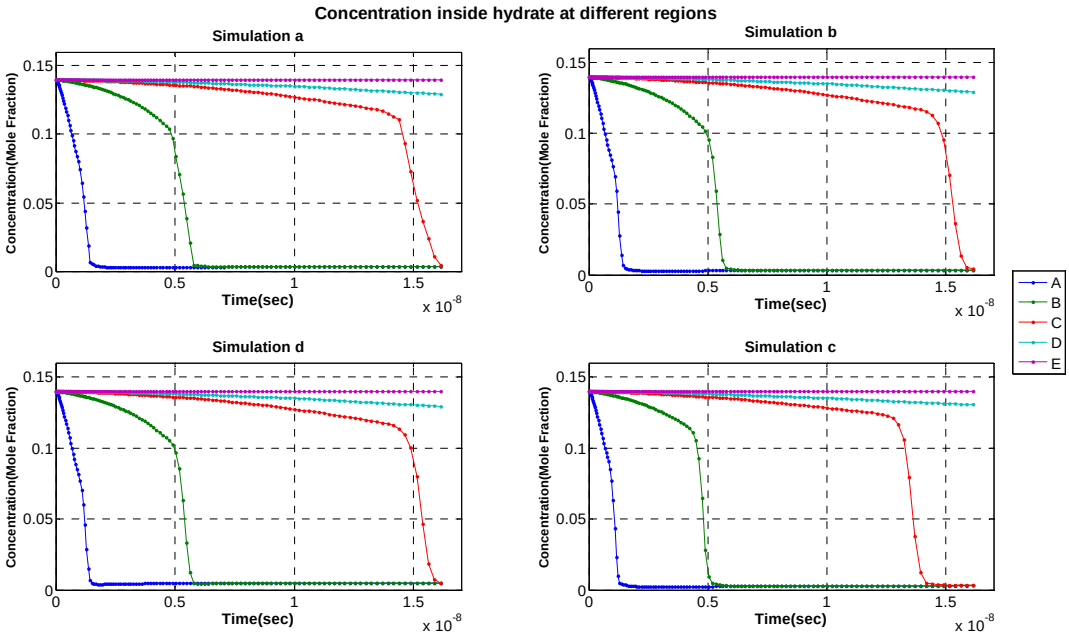

Figure 6-2: Methane concentration inside the hydrate at different points. A, B, C, D & E are points which 10.0E-9Å, 30.0Å, 60. 0Å, 80.0Å & 1000.0Å away from the original interface respectively.

Initially (t=0) Figure 6-2 & Figure 6-3, the mole fraction equals the initial values which show that CH_4 has not yet diffused. To get the clear vision of diffusion inside the hydrate, the concentrations have been taken on five points A, B, C, D & E corresponding to values 10Å, 30Å, 60Å, 80Å and 1000Å respectively, showing distance from the original interface. If the

concentration of methane drops below the hydrate stability limit for the given temperature and pressure, a chemical potential driving force towards dissociation will arise as shown in Figure 6-2 lines A, B, C and D. The sudden drop in concentrations in all four cases is due the dissociation pressure reached and hydrate completely dissociated. The maximum mole fraction decrease observed was 0.004469, 0.004565, 0.003219 and 0.004814 in all four cases respectively, this difference in fractions due to the effect of concentration gradient as moving away from the original interface.

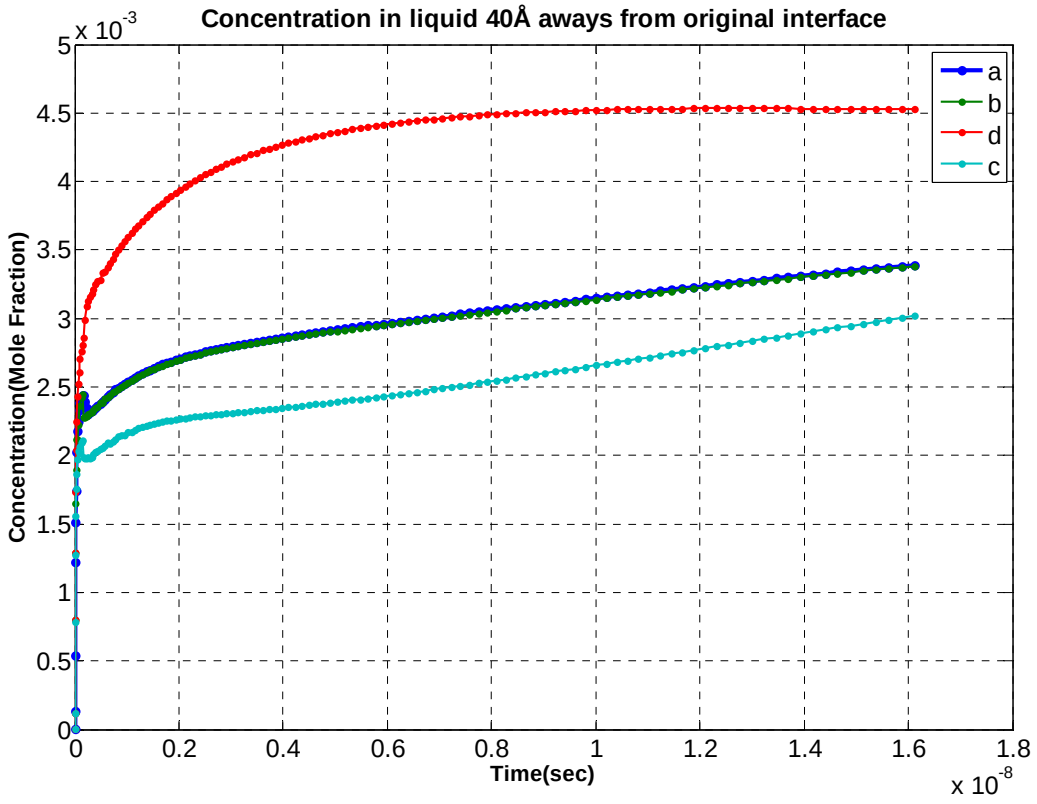

Figure 6-3: Methane concentration taken inside the liquid 40.0Å away from the original interface. a, b, c & d are simulations name which are at depths of 500, 639, 730 & 740 meters respectively.

Rapid increase in the concentration observed at far left side of the Figure 6-3 is an initial relaxation of a system into a physical realistical interface. Concentration gradually increased following the profile towards stability after this point. Simulation d at depth 740 meters has higher methane concentration due to higher thermodynamic driving force in comparison to other simulations (a &b). The higher amount of methane released in simulation c (Figure 6-2) from original hydrate phase to bulk liquid phase may tends to formation of hydrate due to this reason less gain in concentration of methane in simulation c have seen (Figure 6-3). Figure 2-1 on the right side of this curve the rate of concentration is decreased due to the driving force decreased is inversely proportional to the increasing concentration of methane in surrounding liquid.

To observe the movement of methane from solid phase to liquid, the velocity on the interface is determined by tracking the ϕ values. The velocity on the interface is calculated using

equation (6.2). From this velocity the dissolution rate was calculated using equation (6.1) and the data from these calculations saved in CD and attached with this thesis, from which the Figure 6-4 is generated.

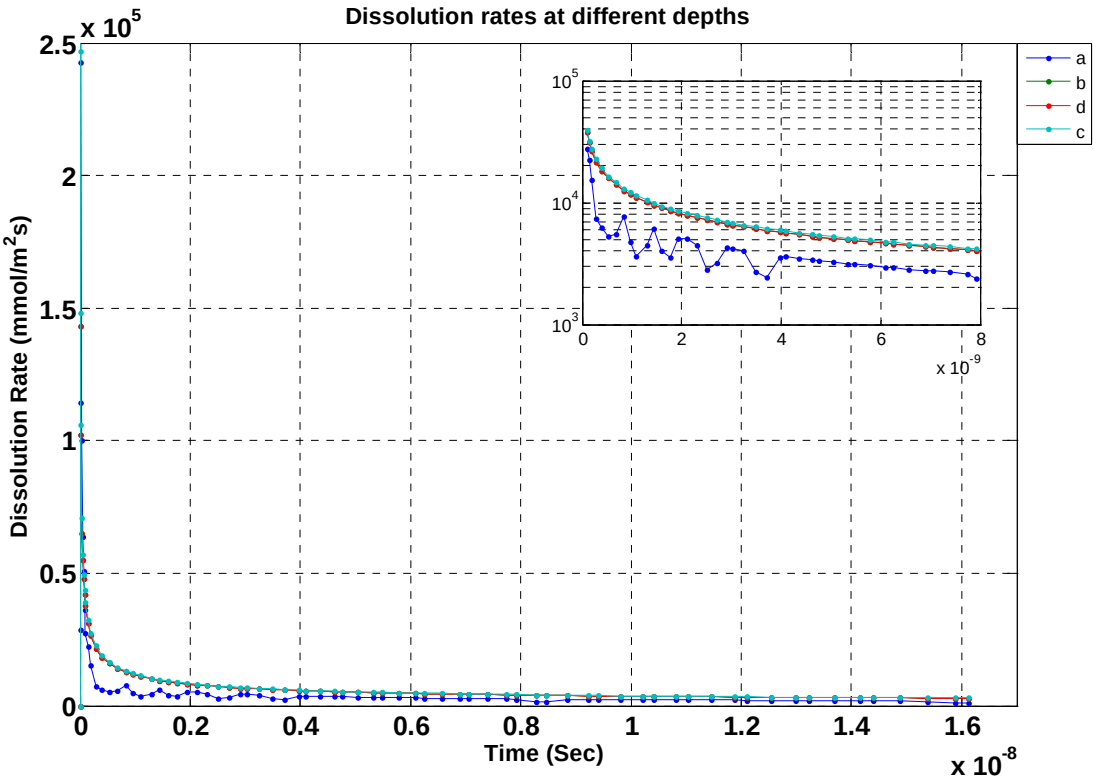

Figure 6-4: Methane Dissolution rate has been calculated at different depths and time upto 16.13 ns.

The initial value of flux was high due to the initial relaxation as mentioned above. To show the actual dependency of dissociation on driving forces the close look on the curve has shown in the Figure 6-4. The rate is decreasing gradually after this relaxed point on the curve. One reason for this is the decrease in thermodynamic driving force which is proportional to the increasing chemical potential in the surrounding aqueous solution. The noise seen on calculated curves that is due to the grid effects. It can be seen that increasing depths leads to increase in flux. Simulations a, b, c and d at the end of this plot have 1040, 2827, 2929 & 2827 mmol/m^{2}s respectively. These results cannot be comparable with the reference mentioned in section (5.1), one reason for such high fluxes that the system still not reached at equilibrium. This can be seen clearly from Figure 6-2 in which the point D in all four simulations just 80Å away from the original interface still at its initial stage showing the slight decrease in concentration and no change is observed at point E which is 1000Å away from the original interface. To compare the results with the references an extrapolation has done using power law.

The interface in this simulation is perfectly follows the power law which is proportional to square root of time showing a diffusion control process. To compare the values of dissolution rates (section (5.1)), the flux is extrapolated to experimental time scales.

6.2.1 Extrapolation

The extrapolation has done to 3.1536E+20 nano seconds from 16.384 nano seconds in all four simulations which is equal to 10^4 years (Figure 6-5).

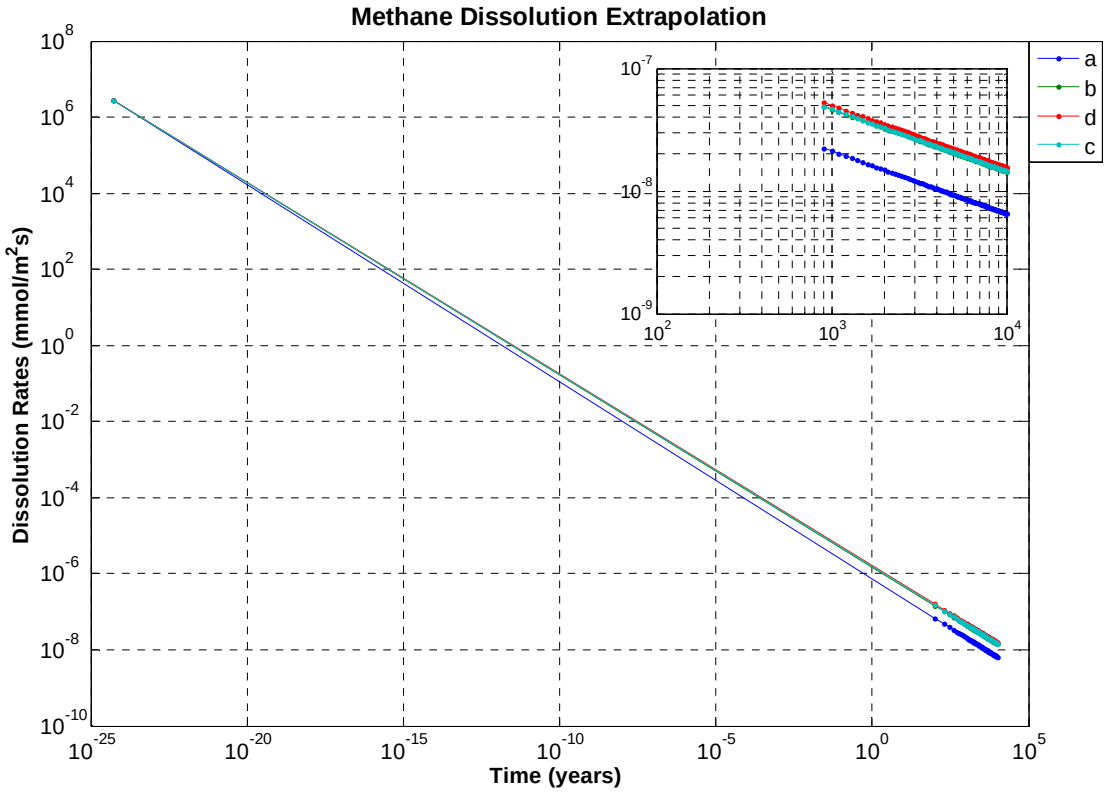

Figure 6-5: Extrapolation of dissociation rate uptil 10000 years.

Due to the length of the time scale the values were plotted in the figure with 100 years of time intervals. After 10000 years the dissociation rates were 6.539E-09, 1.441E-08, 1.45E-08 & 1.557E-008 mmol/m^{2}s converted to 0.2062, 0.4544, 0.4573 and 0.4910 mmol/m^{2}yr units for simulations a, b, c and d respectively.

Chen and Haflidason (Chen, et al., 2008) have calculated the fluxes in Nyegga region using cores from inside of pockmarks. Sulfate gradients measured in the southeast of Nyegga at depth 639 to 740 meters indicate that methane fluxes are 15 to 49 mmol/m^{2}yr. The simulation b and d runs on the same conditions and shows deviation from the experimental results. The reason for these slight differences might be the lack of pressurized core sampling as mentioned before. But these confirm that conditions in the south east of Nyegga are suitable for methane accumulation and gas hydrate formation. These results might still higher in comparison to the original condition present in situ. Because the porosity effects were not included in this work and the presence of salt ions in the water which will lower the chemical

potential of the water in the aqueous water phase and will also affect the chemical potential of the guest molecules in the aqueous phase. The ions will reduce water chemical potential and such imply a reduction in thermodynamics driving force. This will in turn reduce the rates of growth and dissociation of hydrate. But the total effect is more complex since it depends on the chemical potentials of guests in the electrolyte solution of given ionic content. Another effect is might be the lack of hydrodynamics which is not included in this system. From the limited background data on the Nyegga samples and the Nyegga system as such it remains very uncertain at this point what the observed values actually reflect. It could be methane fluxes from dissociating "massive" hydrate below the samples but it can also be fluxes where hydrate is forming and dissociating dynamically in addition to allowing free gas to pass and migrate upwards due to large size of channels (fractures, faults) which is not able to be blocked down to very low permeability.

6.3 Case II: Dissolution of methane at 104.8 bars pressure.

The simulations of methane run at 104.8 bars pressure on different temperature (Table 6.6) to see the effect of dissolution rate.

Table 6.6: The names and temperatures for all the simulations at 104.8 bars pressure.

Simulations Name	mmpft1 (m1)	mmpft2 (m2)	mmpft3 (m3)	mmpft4 (m4)	mmpft5 (m5)
Temperature (K)	274.65	276.65	278.65	280.65	282.65

The model has been used with a 2D narrow geometry dimension 1500×1500 grid resolution with 150 grid radius which corresponds to 2.25E-14 m^2 system area and 7.068E-16 m^2 hydrate area respectively. The methane concentration adjusted to 0.14 mole fraction assuming completely filling of small and large cavities.

The concentration in liquid has taken 1.00E-10 mole fraction to create the gradient of concentration between both phases. As mentioned before the concentration of water in liquid was assumed 1 mole fraction (Table 6.7). The hydrate to liquid ratio adjusted to 1 : 5 to achieve complete dissociation of hydrate. The simulations were run to 28.90E+06 total time steps this corresponds to the time of 28.90 ns.

Table 6.7: Properties used to setup the simulations.

Grid points for all five simulations	1500×1500
Corresponding area in m^2	2.250E-14
No. of time steps	28.90E+06
Total time in seconds	28.9E-09
Mole fraction of CH_4 in hydrate	0.14
Mole fraction of water in liquid phase	1.0

To see how the simulation behaving with time and length of the system three plot were plotted for phase ordering parameter ϕ and concentrations.

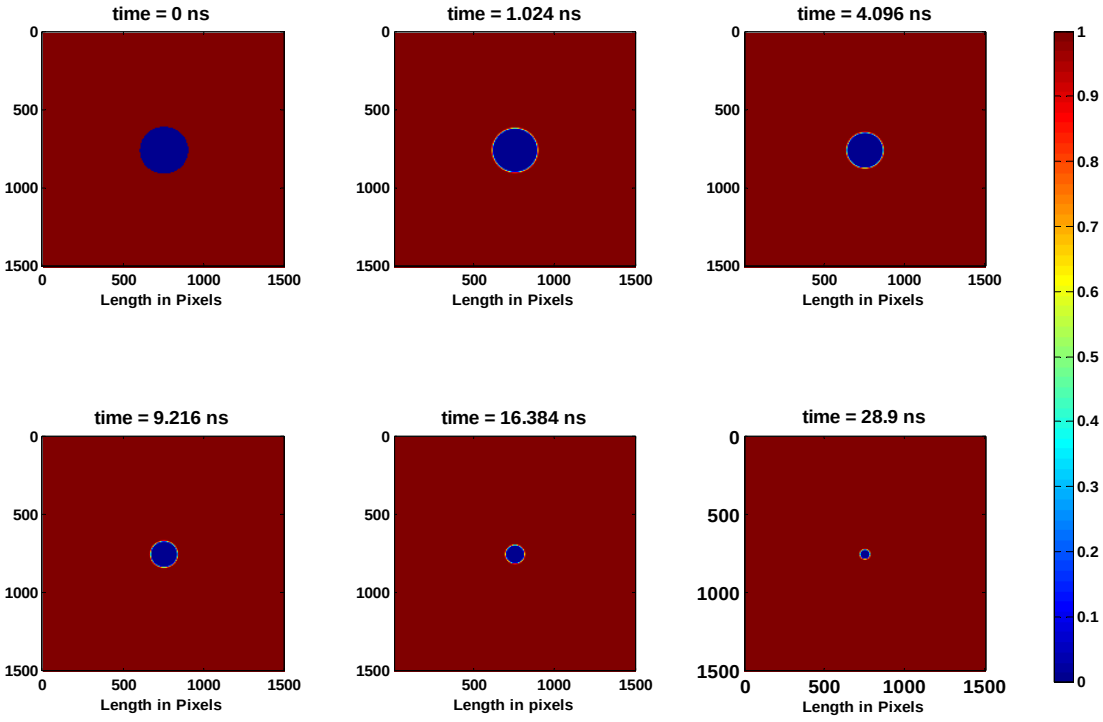

Figure 6-6: The phase ordering parameter ϕ of the dissociating hydrate at 104.8 bars pressure and 276.65 K temperature. Φ=0 denotes the solid and ϕ=1 corresponds to liquid shown in a color matching bar on right side of picture and interface is between these two phases shown with thin color circles around blue hydrate (mmpft2).

Figure 6-6 shows the dissocition of methane hydrate at 104.8 bars pressure and 276.65 K temperature with respect to time. And also explaining that how an interface between solid hydrate and liquid phases developed.

The Figure 6-7 plotted by making a cross section from 750 grids on x-axis till length of the y-axis for all the images. Figure 6-7 provide the clear vision of methane dissociation which is proportional to the reduction of well with respect to time. In Figure 6-8 the concentration of methane has shown that methane after dissociation reduced to 0.0044 mole fraction.

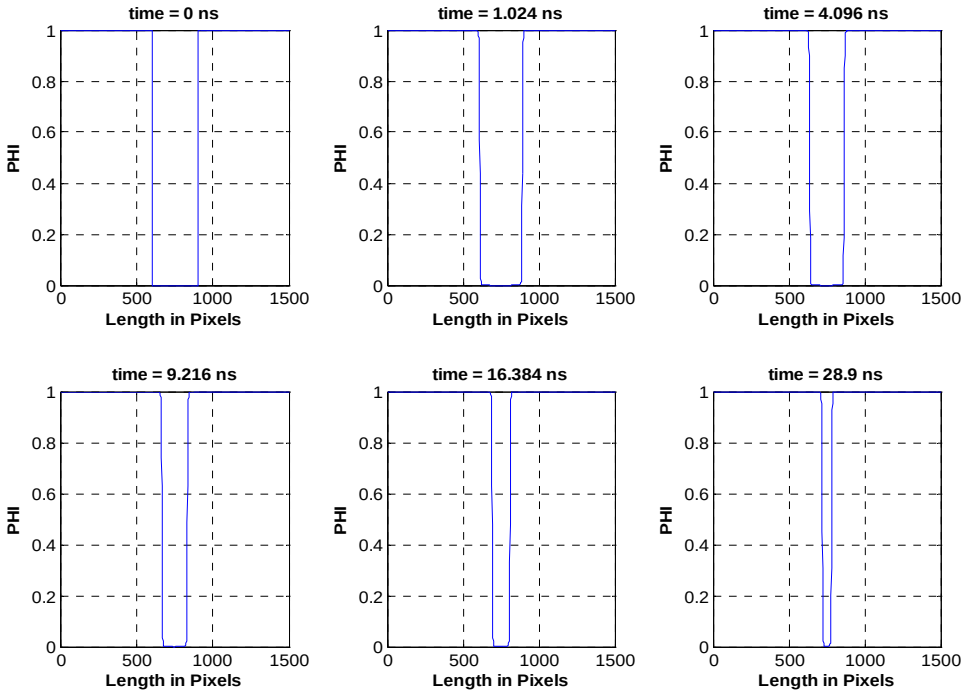

Figure 6-7: The phase ordering parameter ϕ of the dissociating hydrate at 104.8 bars pressure and 276.65 K temperature. The well in above graph shows the length of hydrate and solid line between phase Φ 1 and Φ 0 values is interface(mmpft2).

Figure 6-9 shows the fluxes of methane at different temperatures. These fluxes calculated using the same method as mentioned in (Case I). From original graph, it is difficult to see the change in flux with temperature rise, so zoom of the graph shown right side of the figure which clearify the hypothesis that flux is directly proportional to temperature.

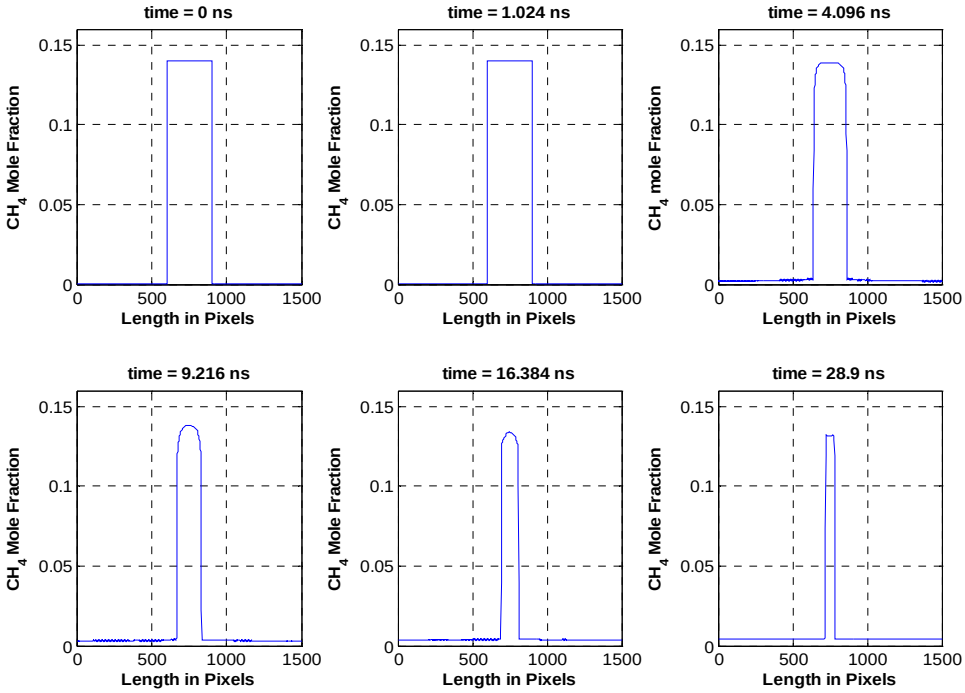

Figure 6-8: The mole fraction of methane at 750 grids cross section on x-axis pressure 104.8 bars and 276.65 K temperature. The mole fraction in solid shown is 0.14. The reduction in well with respect to time shows process of dissociation. (mmpft1).

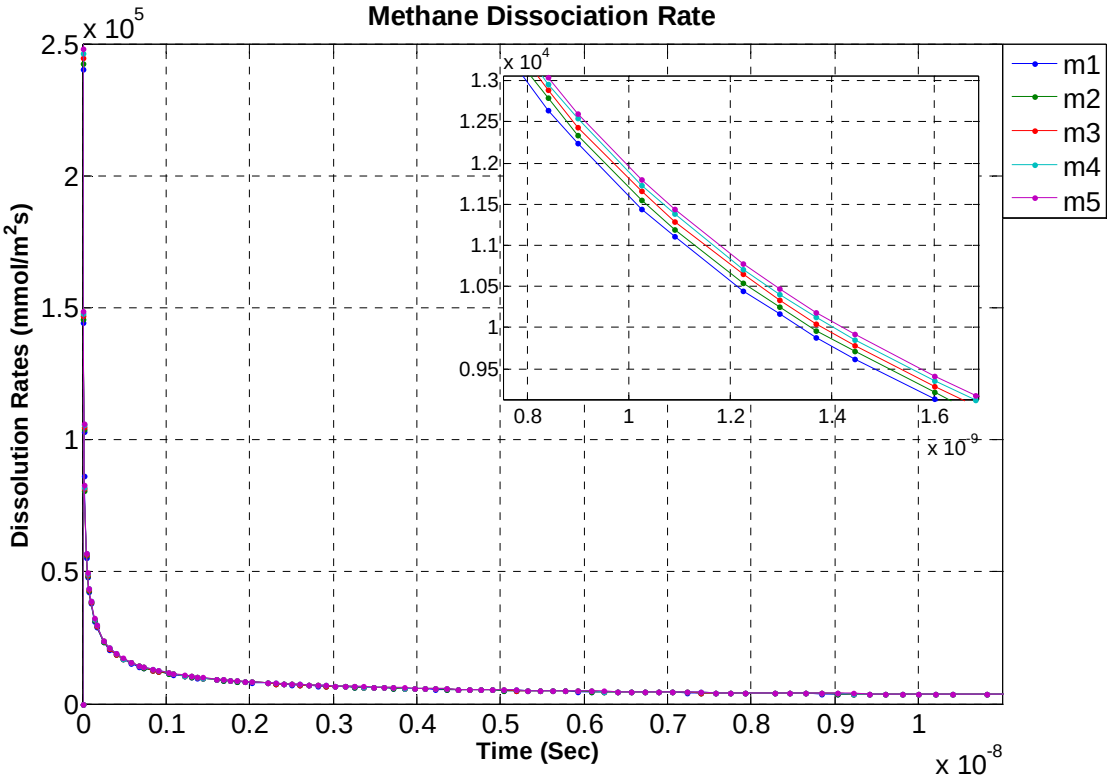

Figure 6-9: methane fluxes at constant pressure 104.8 bar and different temperature. the zoomed graph shows the increase in concentration with increase in temperature which is difficult to see from main plot.

To see the same effect clearly, the data from the above figure is ploted in 3-dimensional plot (Figure 6-10). The fluxes obtained from results after complete dissociation of hydrate are 2.1265e+003, 2.1468e+003, 2.1646e+003, 2.1801e+003 and 4.3875e+003 mmol/m^2s.

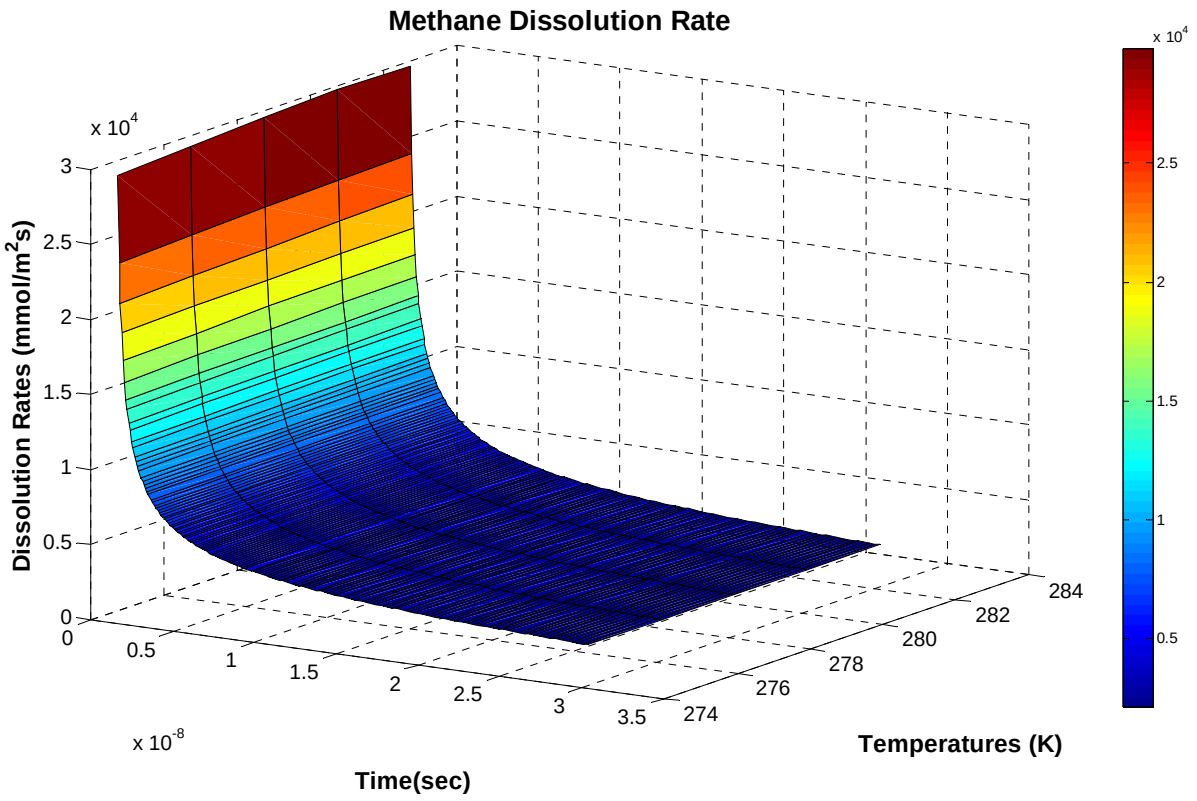

Figure 6-10: Dissociation of methane at different temperature.

6.3.1 Extrapolation

Figure 6-11 & Figure 6-12 shows that the simulation perfectly follows the power law $\alpha\ t^{1/2}$ showing the diffusion control process. The simulations were extrapolated to 3.1536E+20 ns which is equal to 10000 years. After 10000 years the dissociation rates were 1.867E-009, 1.857E-09, 1.835E-09, 1.235E-08, 1.24E-08 mmol/m^2s. These differences in fluxes in comparison with the fluxes shown in case 1 are due to the size of the system. The simulation at pressure 104.8 bar and temperature 276.65 k was extrapolated to 9.7200e+013 ns which is equal to 27 hours. The value after extrapolation is 3.021E-05mmol/m^2s. Rehder et al. (2004) calculated methane fluxes by taking the samples of methane at the depth of 1028 m using the

ROV (remotely operated vehicle) Ventana. The pressure and temperature condition at this depth were 104.8 bar and 276.65 K respectively. The higher pressure in the vessel is maintained to allow the sea water to flow through these samples. The methane fluxes dissolved in 26.3 to 27 hrs and dissolution rates were observed 0.34 – 0.4 mmol/m^2s.

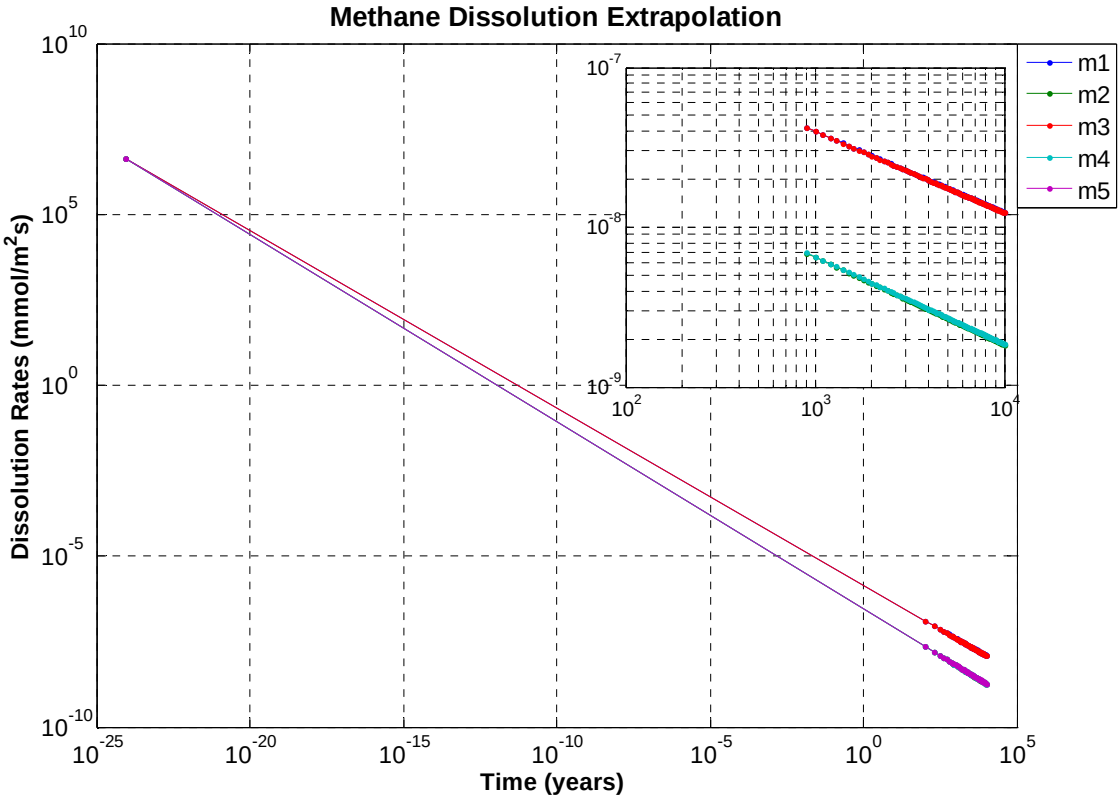

Figure 6-11: Extrapolation of dissociation rate at 104.8 bars pressure and different pressure upto 10000 years.

This experiment can not in any aspect be compared to the simulations presented here for two important reasons. The first is that the hydrate sample was artificially made and not aged like natural hydrate. By aging it is referred to the discussion of degrees of freedom and the system being overdetermined (section 4.2) in terms of Gibbs phase rule. Such a system will need long time to rearrange into compact hydrate since initial hydrate films on gas/water interface may encapsulate unconverted water as well as unconverted gas.

The second reason is that the mole fraction of methane in hydrate may be close to 0.14, which is orders of magnitude higher than seawater solubility at these conditions of temperature and pressure. This may result in some released methane being dissolved into seawater on a molecular level while large portions of the released methane can be distributed in seawater as bubbles ranging from nano scale up to visible scale. Hydrodynamics has not been included in this first work on estimating dissociation fluxes and is one of the issues proposed for further work along these lines.

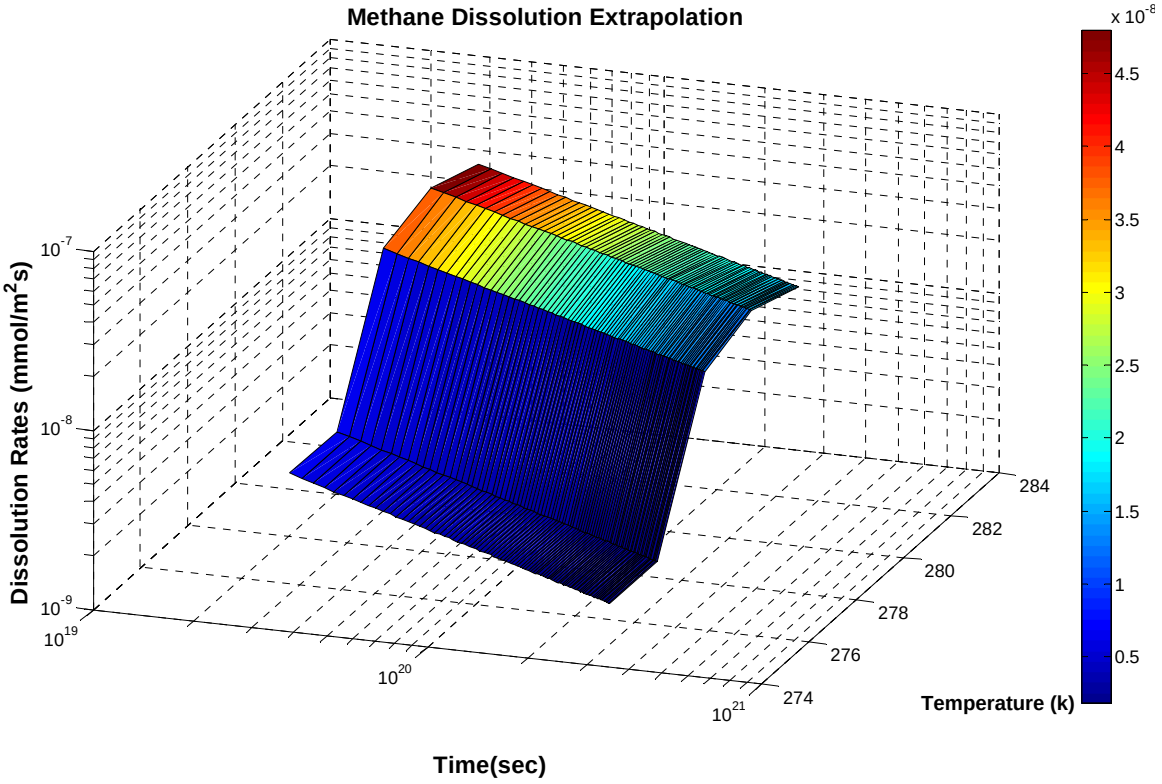

Figure 6-12: Extrapolation of dissociation rate at 104.8 bars pressure on different temperatures upto 10000 years.

There are several ways to incorporate hydrodynamics, ranging from algorithms which makes an external coupling to solution of Navier-Stokes to a more fundamental implicit scheme derived from the extensive formulation of the free energy functional. The reason behind this huge difference in fluxes might be the pressure gradient between the naturally existed gas hydrate and hydrate contained inside the vessel. The higher pressure caused higher flow of water through these samples and thus the rates should higher in comparison to the hydrates that exposed to the sea floor. Another reason for this is the size of the system which might be effective but again as mentioned before the hydrodynamics and sea water salinity is not included in this work due to this reason the rates calculated were assumed that higher in comparison to the originally existed hydrate. The other simulations have shown the same behavior (Figure 6-13).

6.4 Case III: Dissolution of CO_2 at 104.8 bars pressure at different temperatures.

The geometry of the system adjusted to 1500×1500 grids resolution which corresponds to total area 2.25E-14 m^2 of the system and the radius of the hydrate spreads over 150 grids. It means the area of the hydrate is 7.068 m^2. The simulations run for the complete dissociation of hydrate. To show the comparison between each simulation the same time was used namely

total dissociation time of mcpft5 (Table 6.8). The mole fraction of CO_2 in the hydrate is 0.11 and in liquid is 1.00E-10 mole fraction.

Table 6.8: The names and temperatures for all the simulations at 104.8 bars pressure.

Simulations Name	mcpft1 (C1)	mcpft2 (C2)	mcpft3 (C3)	mcpft4 (C4)	mcpft5 (C5)
Temperature (K)	274.65	276.65	278.65	280.65	282.65

As mentioned in Case II concentration of water in the liquid phase taken 1.00 mole fraction (Table 6.9).

Table 6.9: Properties used to setup the simulations.

Grid points for all five simulations	1500×1500
Corresponding area in m^2	2.250E-14
No. of time steps	10.82E+06
Total time in seconds	10.82E-09
Mole fraction of CO_2 in hydrate	0.11
Mole fraction of water in liquid phase	1.0

The hydrate to liquid ratio adjusted to 1 : 5 to achieve complete dissociation of CO_2 hydrate. At the end of all the simulations when all the hydrate dissociated, the mole fraction of CO_2 in aqueous solution is 0.0036. The initial value of flux was high due to the initial relaxation as mentioned in previous cases. To show the actual dependency of dissociation on driving forces the close look on the plot has shown that the increase in temperature leads to increase in dissociation of CO_2 (Figure 6-13).

Figure 6-14 generated to show the clear effect of decrease in dissolution rate. The dissolution rates calculated at the end of all the simulations when no hydrate left in the system were 2657, 2872, 3112, 3223 and 3379 mmol/m^2s. The dissociation of hydrate is proportional to the $t^{1/2}$ indicating diffusion control process (Figure 6-15 & Figure 6-16).

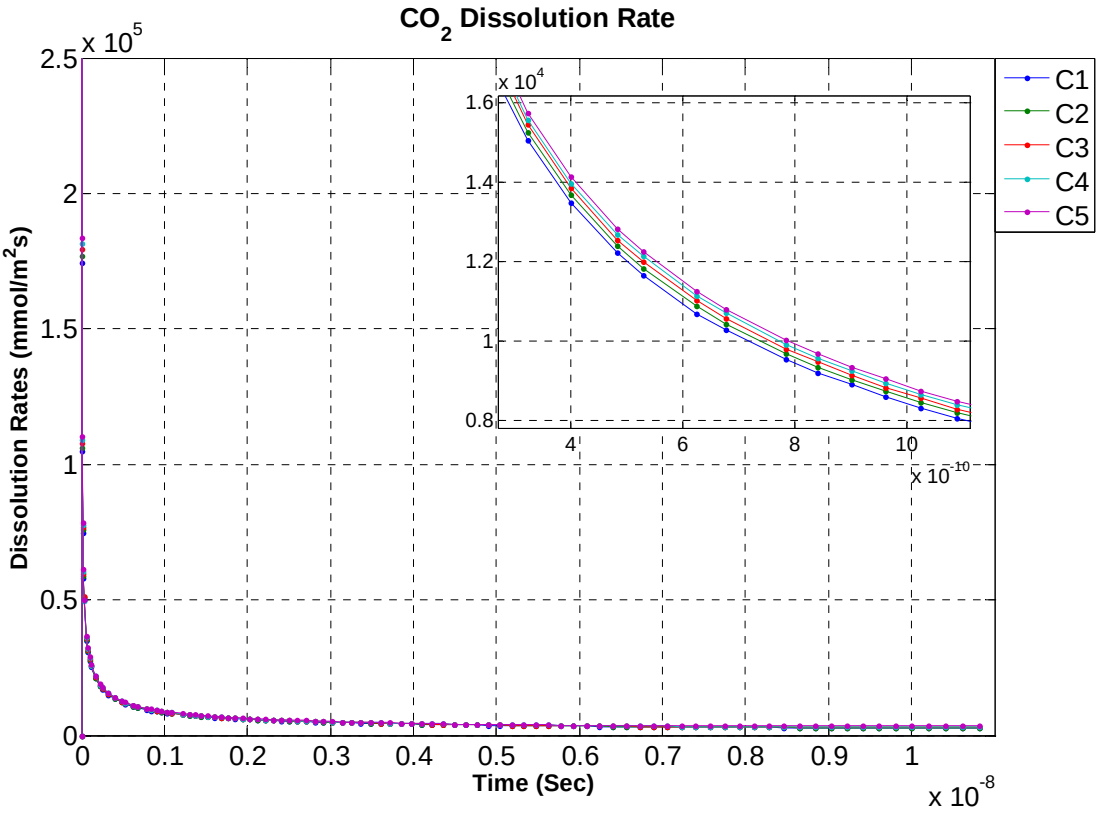

Figure 6-13: CO_2 fluxes at constant pressure 104.8 bar and different temperature. the zoomed graph shows the increase in concentration with increase in temperature which is difficult to see from original graph.

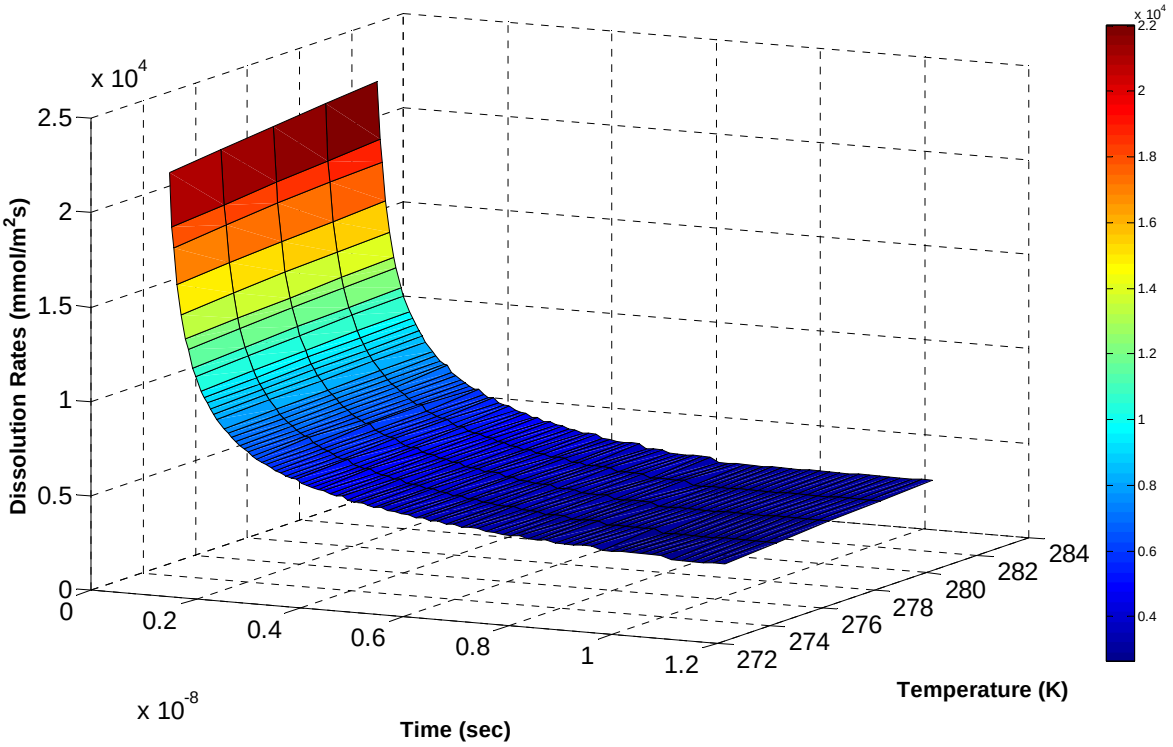

Figure 6-14: CO_2 fluxes at constant pressure 104.8 bar and different temperature.

6.4.1 Extrapolation

The extrapolation of the simulation done using power law as mention in previous sections it is perfectly follows it. Extrapolated results show that all the simulation following the same trend and change in their rates are so small that cannot be visible from Figure 6-15 . Figure 6-16 is plotted to provide clear behavior of all the simulations.

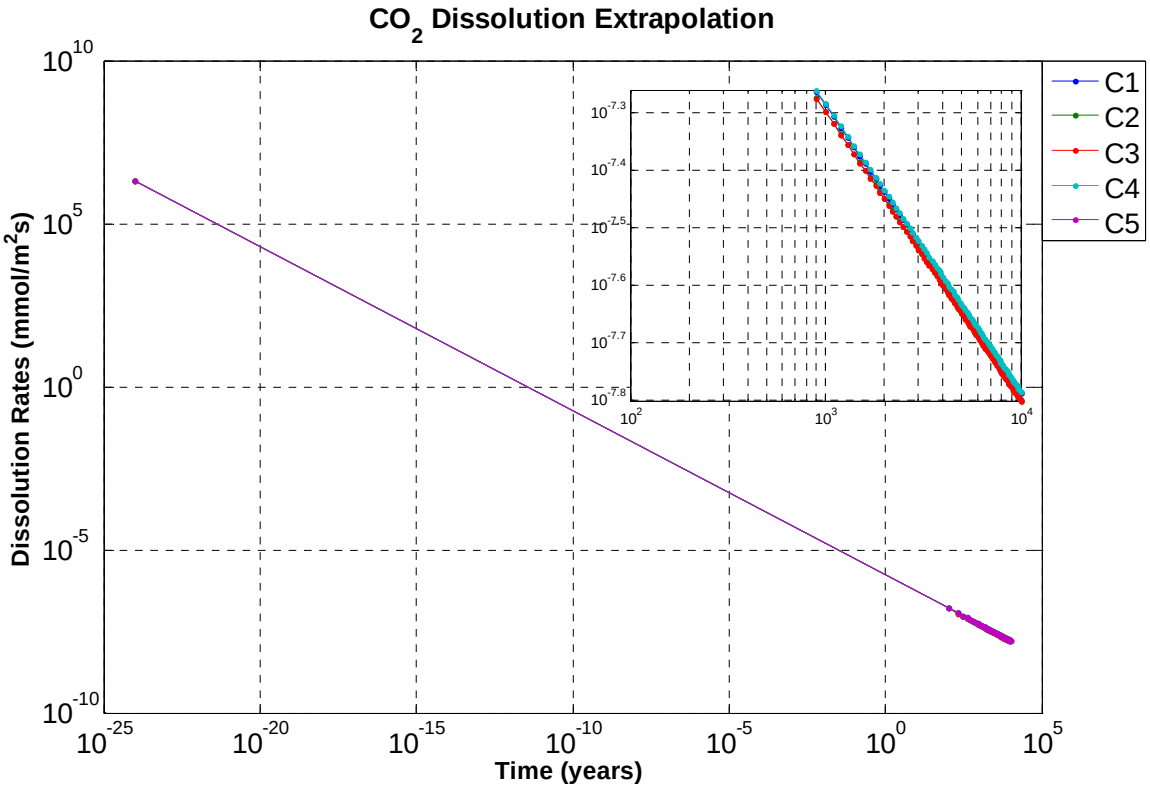

Figure 6-15: Extrapolation of dissociation rate at 104.8 bars pressure on different temperatures upto 10000 years.

The extrapolation done to compare the values with experimental scale, the dissolution rates after 10000 years 3.059E-10, 3.124E-10, 3.387E-10, 6.743E-10 and 6.936E-10 mmol/m^{2}s. The simulation with temperature 276.65 K and pressure 104.8 bar were extrapolated to 1.41E+13 ns which is equal to the 3 hours and 55 min. The rate obtained from this extrapolation is 1.735e-005. Rehder et al. (2004) has done experiment mentioned in previous case calculated the CO_2 fluxes on the same conditions. The CO_2 samples completely dissolved after 235 minutes and dissolution rates observed were 3.62 and 4.67 mmol/m^{2}s. These results are higher in comparison with this work. The reason might be the same as mentioned in previous section.

CO_2 fluxes are higher in comparison with the methane, To better compare the dissociation rates of CO_2 and CH_4 hydrate, simulations with similar initial conditions like temperature, pressure were used (Figure 6-17).

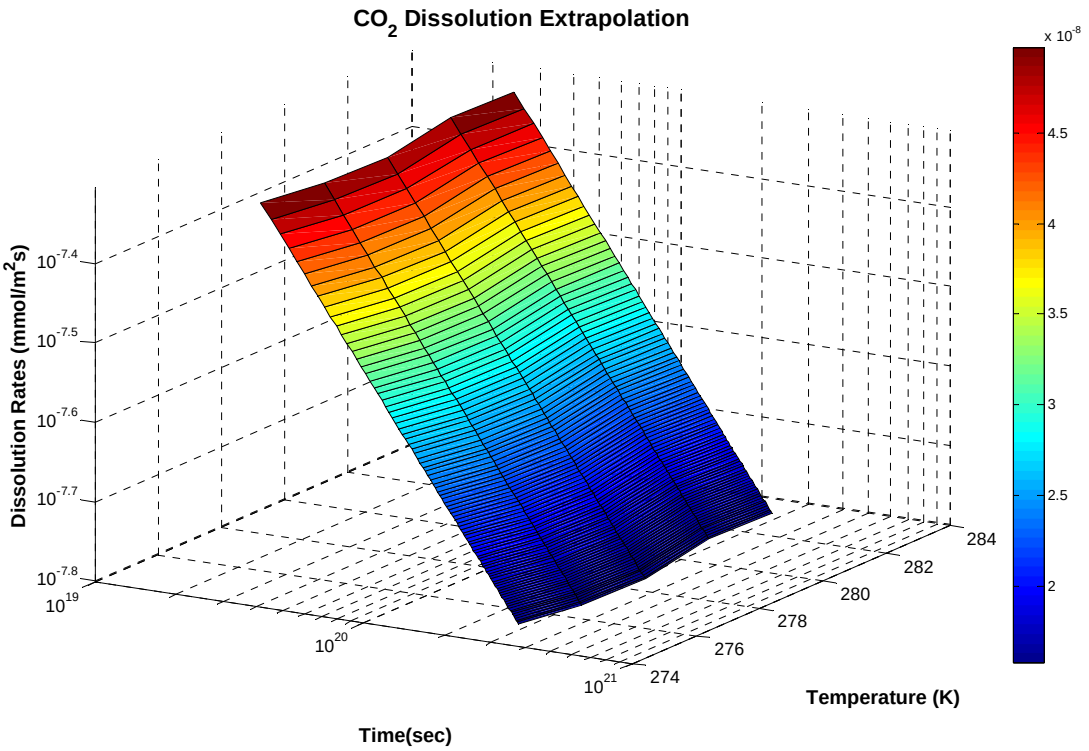

Figure 6-16: Extrapolation of dissociation rate at 104.8 bars pressure and different temperature upto 10000 years.

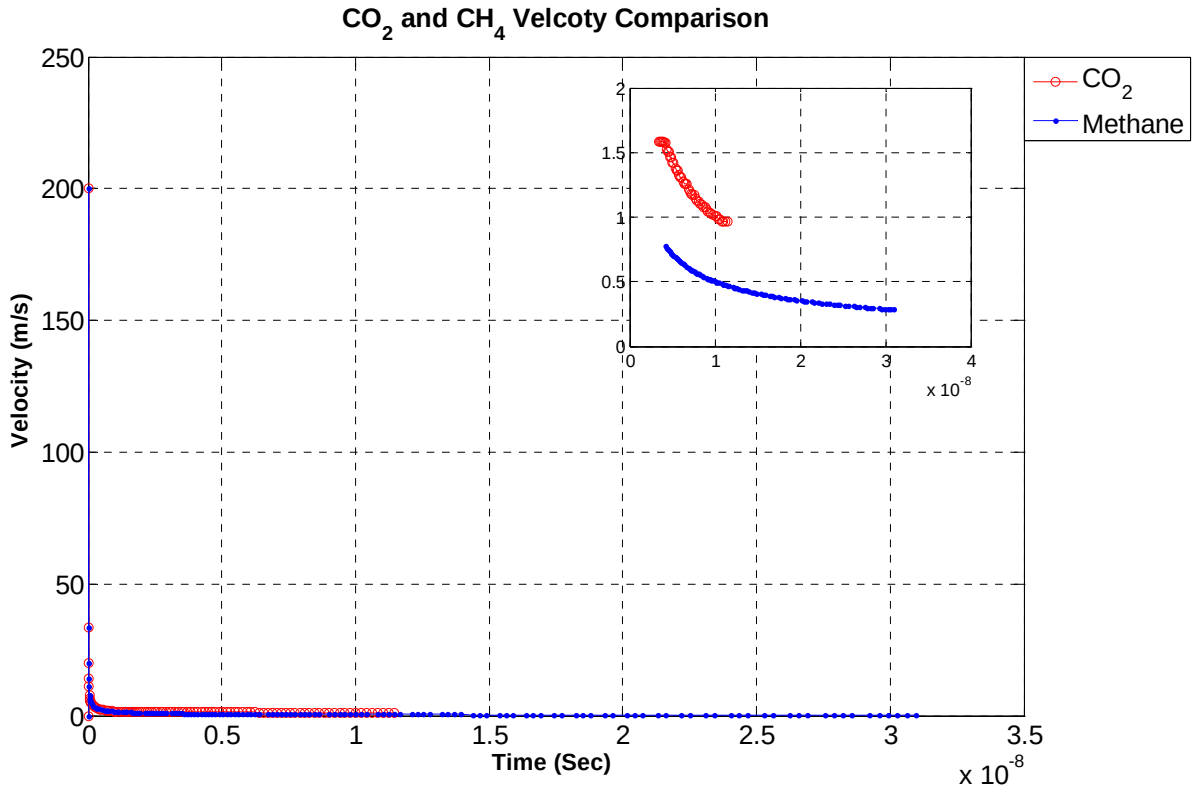

Figure 6-17: Comparison between CO_2 and CH_4 from simulation C3 and m3 simulations.

The simulations C3 and m3 were plotted to show the difference in dissociation rates. Initially the curves show strange behavior in which the rates decline rapidly and CO_2 rate is less than the CH_4. The reason behind this anomaly might be the hydrate solution needs time to stabilize itself from the unnatural initial with a steep concentration and phase field front. The system needs some time to relax into a natural state with a proper interface between the two phases. After this point the dissociation rate or interface velocity steadily decreasing and it has seen that CO_2 rates remain higher throughout the simulation. This is might be the reason that the CO_2 is more soluble than methane.

6.5 Case IV: Dissolution of Methane at 276.65 K temperature.

The setup of the system is shown in Table 6.11. The simulations of methane run at 276.65 K temperature on different pressures (Table 6.10) to see the effect of dissolution rate. The concentration in liquid has taken 1.00E-10 mole fraction to increase the transport rate in between two phases. As mentioned before the concentration of water in liquid was assumed to 1 mole fraction (Table 6.11). The hydrate to liquid ratio adjusted to 1 : 5 to achieve complete dissociation of hydrate. The simulations were run to 31.684E+06 total time steps this corresponds to the time of 31.684 ns. At the end of all the simulations when all the hydrate dissociated, the mole fraction of methane in aqueous solution is 0.0048.

Table 6.10: The names and temperatures for all the simulations at 104.8 bars pressure.

Simulation Name	Pressure (bars)
mmpftcT1 (m6)	24.8
mmpftcT2 (m7)	44.8
mmpftcT3 (m8)	64.8
mmpftcT4 (m9)	84.8
mmpftcT5 (m10)	104.8
mmpftcT6 (m11)	124.8
mmpftcT (m12)	144.8
mmpftcT (m13)	164.8
mmpftcT (m14)	184.8

The methane concentration adjusted to 0.14 mole fraction assuming completely filling of small and large cavities.

Table 6.11: Properties used to setup the simulations.

Grid points for all five simulations	1500×1500
Corresponding area in m^2	2.250E-14
No. of time steps	31.684E+06
Total time in seconds	31.684e-009
Mole fraction of CH_4 in hydrate	0.14
Mole fraction of water in liquid phase	1.0

The flux is calculated using the same method mentioned in previous cases. Figure 6-18 shows slight change in dissolution rate with increase in pressure at constant temperature. The rates are declining with increase in pressure. The values of dissociation rates from results are 4.099E+03, 4.054 E+03, 4.010E+03, 1.983E+03, 3.902E+03, 1.951E+03, 1.920E+03, 1.890E+03 and 3.685E+03 mmol/m^2s.

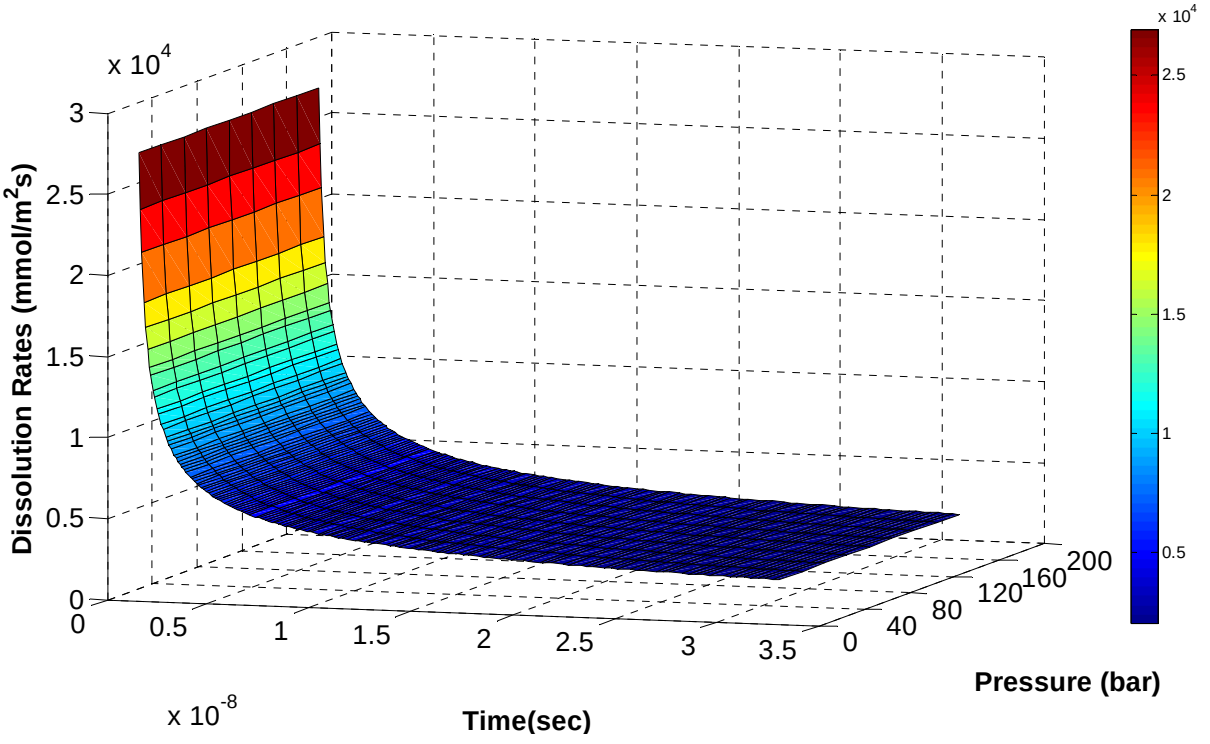

Figure 6-18: Dissociation of methane at different pressures.

6.5.1 Extrapolation

The dissolution curves do not follow exactly the power law $\alpha\ t^{1/2}$ under condition with lower driving forces the simulation shows deviation from this but the long time behavior converges towards the above power law (Figure 6-19). The values obtained from the extrapolations are 1.86e-009, 1.59e-008, 1.65e-008, 1.24e-008, 1.24e-008, 1.24e-008, 1.66e-008 and 1.82e-009 mmol/m^2s.

Lijuan et al. (2006) estimated fluxes from sulfate gradients at each ODP site of Nankai trauf. The fluxes converted from the sulfate gradients are very low at ODP sites 1178 and 1176, only 6 or 8 mol / m^2Kyr respectively in comparison to other sites like HP04 and ODP 1174 have shown 77 mol/m^2kyr being the highest among all these sites. ODP sites 808 has an estimated methane flux of 62 mol/m^2kyr. To compare the results with these references the result with higher pressure was converted to the referenced scale. The simulation m18 with pressure 184.8 bar and temperature 276.65 k converted to flux of 57.3955 mmol/m^2kyr, which is close to the values obtained from these ODP sites. Other simulations with lower pressure have shown higher dissociation rate, the reason behind this anomaly might be the factors mentioned in previous sectioned.

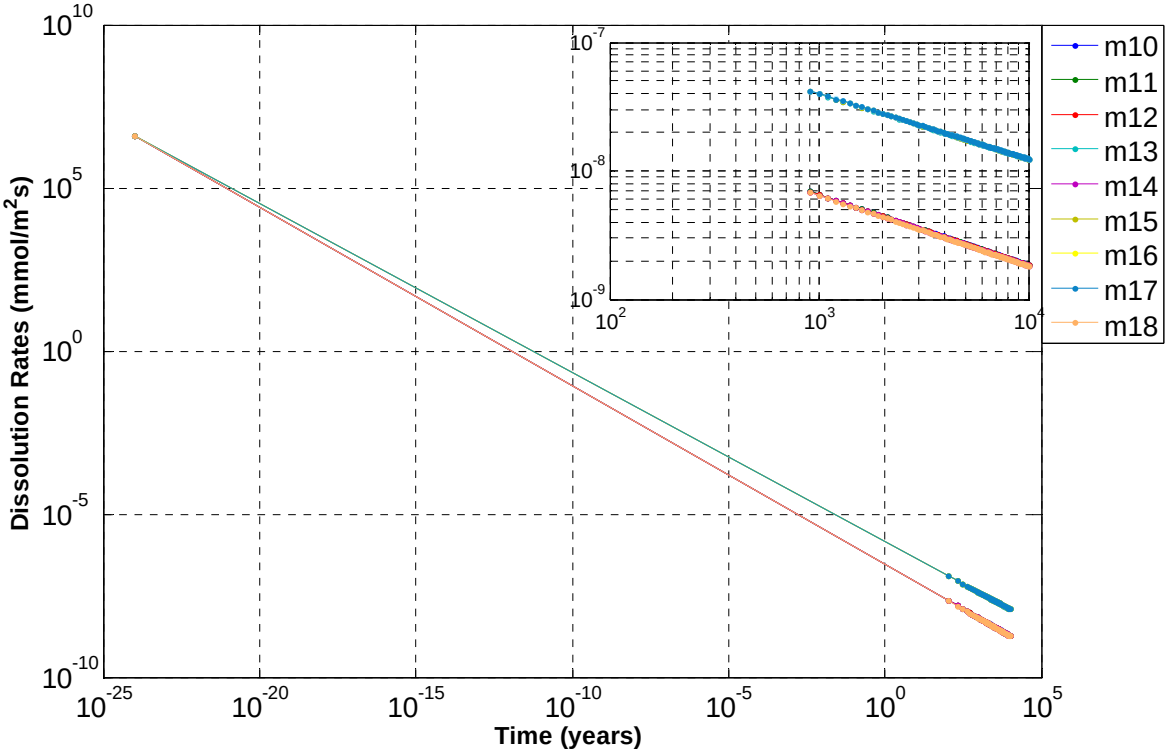

Figure 6-19: Extrapolation of dissociation rate at 276.65 temperature on different pressures upto 10000 years.

6.6 Case V: Dissolution rate of CO_2 at 276.65 K temperature

The simulations of CO_2 run at 276.65 K temperature on different pressures (Table 6.12) to see the effect of dissolution rate.

Table 6.12: The names and pressures for all the simulations at 276.65 K.

Simulation Name	Pressure (bars)
mcpftcT1 (m6)	24.8
mcpftcT2 (m7)	44.8
mcpftcT3 (m8)	64.8
mcpftcT4 (m9)	84.8
mcpftcT5 (m10)	104.8
mcpftcT6 (m11)	124.8
mcpftcT7 (m12)	144.8
mcpftcT8 (m13)	164.8
mcpftcT9 (m14)	184.8

The model has been used with a 2D narrow geometry dimension 1500×1500 grids resolution with 150 grids radius which corresponds to the area of 2.25E-14 m^2 and 7.068E-16 m^2 hydrate area respectively. The CO_2 concentration adjusted to 0.11 mole fraction assuming completely filling of small and large cavities.

Table 6.13: Properties used to setup the simulations.

Grid points for all five simulations	1500×1500
Corresponding area in m^2	2.250E-14
No. of time steps	11.025E+06
Total time in seconds	11.025e-009
Mole fraction of CO_2 in hydrate	0.11
Mole fraction of water in liquid phase	1.0

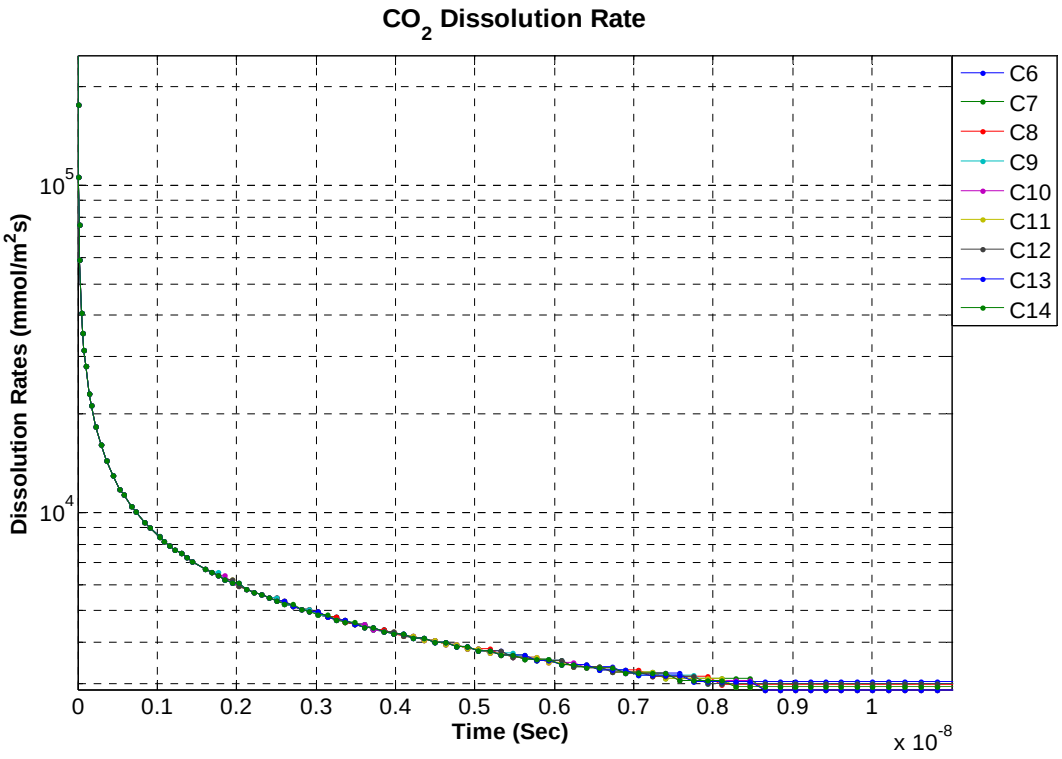

Figure 6-20: CO_2 fluxes at temperature 276.65 K and different pressures.

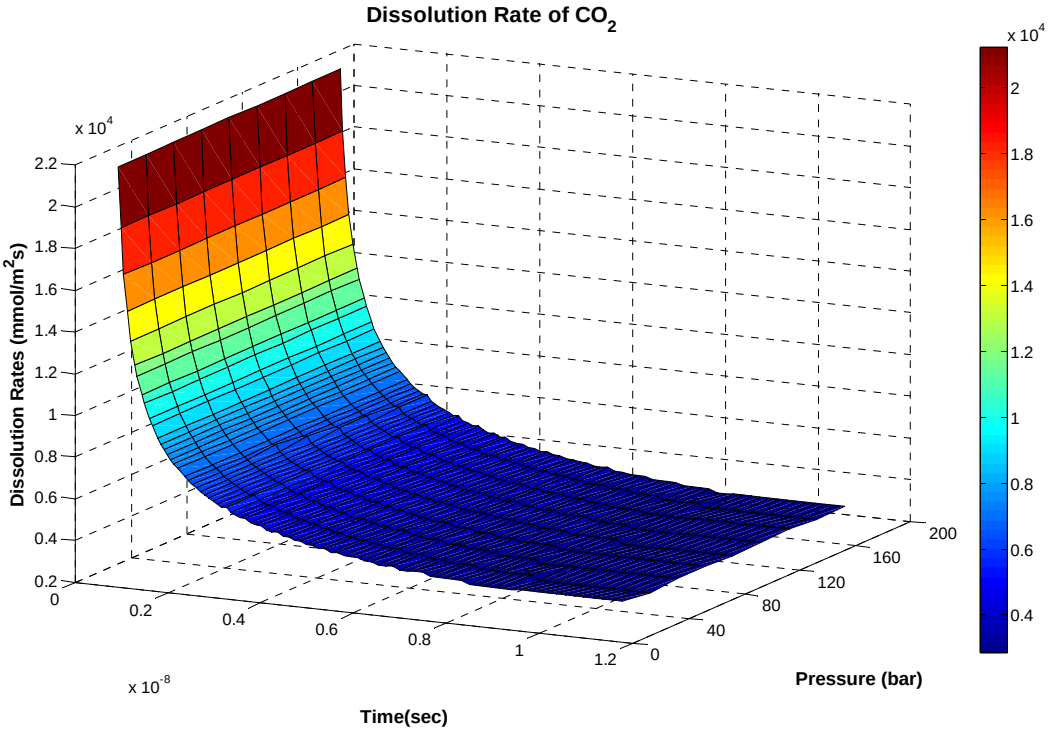

Figure 6-21: CO_2 fluxes at temperature 276.65 on different pressures.

The concentration in liquid has taken 1.00E-10 mole fraction to create the gradient of concentration between both phases. As mentioned before the concentration of water in liquid was assumed to 1 mole fraction (Table 6.13). The hydrate to liquid ratio adjusted 1 : 5 to achieve complete dissociation of hydrate.

The simulations were run to 11.025E+06 total time steps this corresponds to the time of 11.025 ns. After dissociation of complete hydrate the mole fraction in the liquid is 0.0037. The dissolution rates calculated at the end of all the simulations when no hydrate left in the system were 7413.20, 7344.88, 7344.88, 7344.88, 5084.02, 9703.74, 9703.74, 9703.74 and 7277.81 mmol/m^2s shown in figures (Figure 6-20 & Figure 6-21).

6.6.1 Extrapolation

Figure 6-22 shows that the simulation do not follow exactly the power law $\alpha\ t^{1/2}$ under condition with lower driving forces the simulation shows deviation from this but the long time behavior converges towards the above mentioned power law. The simulations were extrapolated to 3.1536E+20 ns.

The extrapolation done to compare the values with experimental scale, the dissolution rates after 10000 years 1.63e-08, 2.889e-08, 2.925e-08, 2. 889e-08, 8.140e-08, 2. 996e-08, 3.031e-08, 2. 960e-08 and 6.91e-08 mmol/m^2s.

Brewer et.al (P.G. Brewer, et al., 2002) measured the rise and dissociation rate of released CO_2 droplets by injecting CO_2 at a depth of 800 m and the sea temperature was 177.55 K. The initial dissolution rate under these conditions was 3.0 µmol/cm² s. This value in comparison is very high, as stated before the release of CO_2 from a rising droplet (Figure 6-21) is more likely to be dominated by breaking/release/reforming of hydrate film. Factor affecting bubble hydrodynamics is the fluid properties.

The fluid viscosity, and density, both of which vary with temperature, affects the drag force. If the dissociation rate is slower than the diffusion controlled dilution in the surrounding water then there is no bubble formation during the dissociation itself and hydrodynamic impact on the phase transition process can be ignored.

This work may not be directly applicable to the question of disposal of liquid CO_2 at the bottom of oceans, which requires depths greater than 3000 meters where liquid CO_2 becomes heavier than sea water (P.G. Brewer, et al., 1999). This is one of the planned task which was not completed due to the thermodynamic tables used by phase field model have pressure limitation up to 250 bars. The coworkers of this group still working to expand these tables and due to the time limitations it is impossible to complete this task.

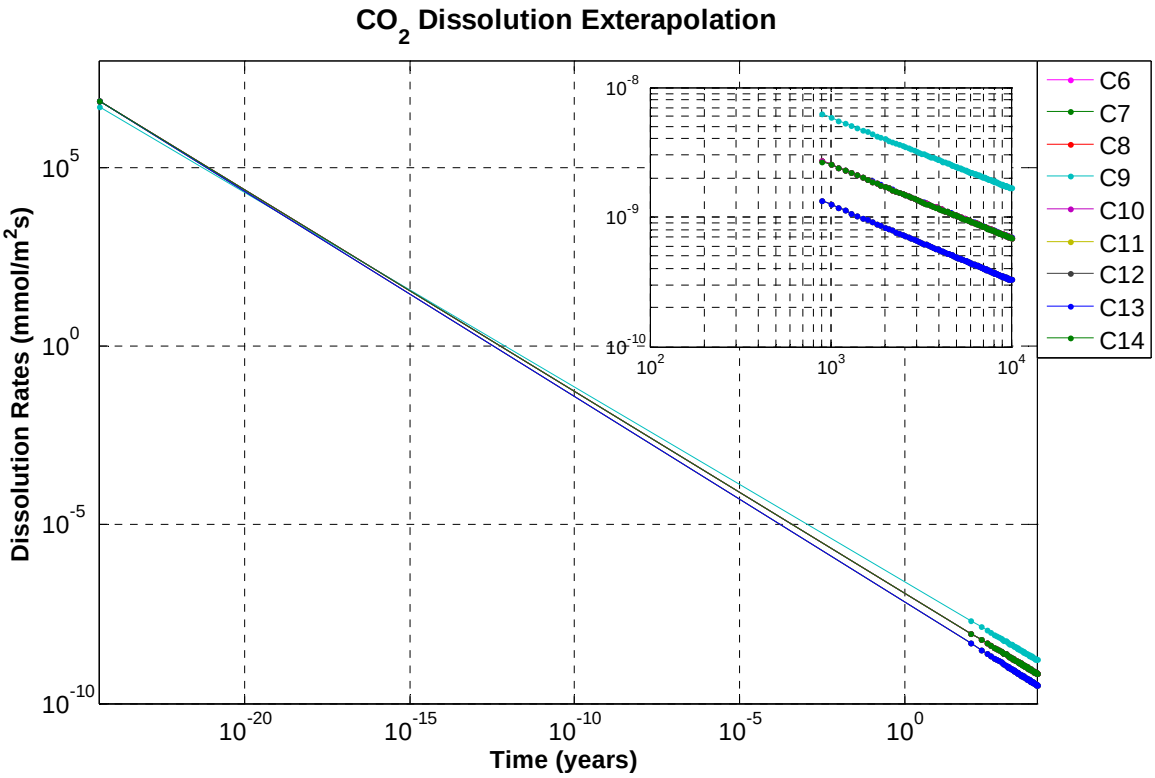

Figure 6-22: Extrapolation of dissociation rate at 276.65 temperature upto 10000 years using power law.

7 Conclusions

In this work, Phase Field Theory (PFT) has been applied to model the dissociation of methane and carbon dioxide hydrate towards pure water. The version of PFT applied in this work does not contain hydrodynamics and is as such limited to systems where distribution rate of dissolved methane in surrounding water through diffusion is faster than the dissociation rates. Or put in other words - appropriate for dissociation rates that does not involve bubble formation on any size level (nano to makro).

The concentrations of methane and CO_2 in liquid were set to get the differences in concentrations or more precisely the corresponding chemical potential differences which liberate the diffusion from hydrate towards liquid side.

The conditions of the model studies have been chosen to reflect some actual ***in situ*** sites, from which there exist measured fluxes of methane. There are very few data on this and it is very unclear what the published rates actually reflects. One of the systems, Nyegga, is not well described in the litterature and might not even be well understood at this point in terms of the origin of the methane fluxes. These fluxes could be from deeper dissociating hydrate but also from free methane gas from below, or combinations. Another system reported in the open litterature was created in laboratory and exposed to seawater at given depth, which makes this system questionable in the sense that the degree of convertion into hydrate in the first place is unknown. For both of these system the PFT estimated fluxes are orders of magnitude lower and the reason might be that the measured fluxes are dissolved methane as well as methane distributed as bubbles (nano scale and upwards in size).

In addition to the specific conditions related to these sites a limited sensitivity analyses of dissociating rates have been conducted. The model shows that at constant pressure the dissociation of CH_4 and CO_2 increases with increasing temperatures, while at constant temperatures the dissociation rates of these gas hydrates decreases with increasing pressures. This is reasonable according the chemical potential of water in the hydrate, for which the strength of the hydrogen bonding increases with decreasing temperatures (all temperatures are above ice freezing temperature). Increasing pressure lowers the chemical potential of water in hydrate due to the impact of the guest molecule chemical potential primarily. It was observed that CO_2 rates remain approximately 2 orders of magnitude higher than CH_4 throughout the simulation. One reason might be the thermodynamics of CO_2 in aqueous solution, which results in a substantially higher solubility than CH_4.

Due to technical problems and limited computer resources it has not been possible to run the simulations long enough for them to stabilize. The interface between the liquid and solid perfectly follows the power law which is proportional to square root of time showing a diffusion control process. To compare the values of dissolution rates, the fluxes are extrapolated to experimental time scales. Observed fluxes are larger than what can be

expected from hydrate dissociating and molecularly diffusing into the surrounding water. The reason for these differences might be the effect of salinity, hydrodynamics etc.

8 Future Work

Phase field theory is computationally very expensive as it a lot of time to run the simulations on computers. It is therefore important that the numerical routines are optimized for the best performance. Adaptive grid technique is another option to improve the code. Presently the simulations are done on a equidistant grid, which is not very efficient since the most important dynamics are taking place at the interface. Fewer grid points can be obtained by making the spatial resolution larger in the near bulk regions. The present thermodynamic package for the phase field model has pressure and temperature limitations with the upper pressure limit of 250 bars and lower temperature limit of 273.15 Kelvin. These limits need to be expanded. Due to this limitation a planned simulation set for lake type storage of CO_2 (a pressure of at least 300 bars needed) was not performed.

However, hydrodynamics is an important factor which needs to be defined into the code. Hydrodynamics is the study of fluids in motion. Factors affecting hydrodynamics are the fluid properties such as velocity, pressure, density, and temperature, as functions of space and time. Proper implementation of hydrodynamics should be able to account for dissociation with rapid agglomeration of released methane into bubbles as well as effects of merging bubbles through bubble collisions. Considering that is seems possible to simulate systems up to microscale this is expected to be a significant improvement in studies of the types of system discussed in this thesis. The effect of hydrodynamics is also expected to play a significant role in modeling a rising droplet surrounding by CO_2 hydrate, or the moving ocean water above a CH_4 reservoir or CO_2 lake. Therefore, there is a need of inclusion hydrodynamics in phase field code. There is a work going on to implement strategies for extensions of the PFT model to account for gravity, density and natural gas bubble formation in surrounding water. An example of a phase filed model which includes fluid flow is published by Tegze et. at. (2005).

Similarly, chemical potential of the water and guest molecules in the aqueous phase will be affected by the presence of salt ions in the water. In the presence of ions, thermodynamics driving force will be reduced due to the reduction in water chemical potentials. This will have impact on the growth and dissociation rates of hydrate. The chemical potentials of guests in the electrolyte solution of given ionic content will further make the total effect more complex. This problem can be handled if the properties and chemical potential of water is estimated as the function of salinity separately and used in the phase field simulation. Also, the guest solubility in electrolyte solution is calculated and the corresponding chemical potentials for these guests are estimated as the function of water ion content. On the other hand, since ions do not participate in the hydrate formation it should also be possible to include these ions in a straightforward fashion through extension of the phase field theory to the number of components needed. This would in principle make it able to study the impact of ion increase in the surrounding water during hydrate formation and a corresponding dilution during dissociation towards aqueous phase. Practically the CPU time would increase more than proportional to the number of components since the integration over concentration involves

differential equation of the fourth order in contrast to phase field which only extends to second order differential equations.

On the contrary, Implementation into ocean current and turbulence models to further enlighten us on where the dissolved CH_4 and CO_2 ends up, and how much eventually reaches the atmosphere. This implementation requires simplification of results into simple regression models of rigorous phase field simulations. A first step in this could be to investigate which proportions of the kinetics that can be explained by mass transport rate according to comparisons with solutions of Fick's law.

Moreover, Hydrates in reservoirs are formed within the pores. Thermodynamic properties of the fluids and hydrate molecules at the mineral surface are therefore an issue of significance that depends upon the size of the pores and the specific mineral surfaces. This system size can be within the reach for the phase field model to simulate.

Finally, development of a phase field theory that including the possible breaking of the hydrate film. Currents and turbulence can possibly break the hydrate film on top of a CO_2 lake, enabling large quanta of liquid CO_2 to escape. A rising CO_2 droplet will constantly shrink, and this could easily cause the thin hydrate film surrounding it to break up. Molecular simulations have proven to reproduce experimental hydrate equilibrium and we might therefore also use molecular simulations to estimate the mechanical strength of hydrate.

References

Bachu, S. (2002). Sequestration of CO_2 in geological media in response to climate change: road map for site selection using the transform of the geological space into the CO_2 phase space. *Energy Convers Manage, 43*(1), 87-102.

Bains, S., Norris, R. D., Corfield, R. M., & Faul, K. L. (2000). Termination of global warmth at the Palaeocene/Eocene boundary through productivity feedback. *Nature, 407*(6801), 171-174.

Beerling, D. J., Lomas, M. R., & Gröcke, D. R. (2002). On the nature of methane gas-hydrate dissociation during the Toarcian and Aptian oceanic anoxic events. . *American Journal of Science, 302*, 28–499.

Borowski, W. S., Hoehler, T. M., Alperin, M. J., Rodriguez, N. M., & Paull, C. K. (2000). 9. Signifiance of anarobic methane oxidation in methane rich sediments overlying the black ridge gas hydrates *Proc. ODP, Sci. results, 164*.

Borowski, W. S., Paull, C. K., & Ussler, W., III (1996). Marine pore-water sulfate profiles indicate in situ methane flux from underlying gas hydrate. *Geology, 24*(7), 655-658.

Brewer, P. G. (2000). Gas hydrates and global climate change. *Ann NY Acad Sci, 912*, 195-199.

Brewer, P. G., Friederich, G., Peltzer, E. T., & Orr Jr., F. M. (1999). Direct Experiments on the Ocean Disposal of Fossil Fuel CO2 (Vol. 284, pp. 943-945).

Brewer, P. G., Peltzer, E. T., Friederich, G., Aya, I., & Yamane, K. (2000). Experiments on the ocean sequestration of fossil fuel CO2: pH measurements and hydrate formation. *Marine Chemistry, 72*(2-4), 83-93.

Brewer, P. G., Peltzer, E. T., Friederich, G., & Rehder, G. (2002). Experimental Determination of the Fate of Rising CO2 Droplets in Seawater (Vol. 36, pp. 5441-5446).

Bryant, E. (1997). Climate Process and Change. *Cambridge, UK: Cambridge University Press, p.118*.

Buanes, T., Kvamme, B., & Svandal, A. (2006). Computer simulation of CO2 hydrate growth. *Journal of Crystal Growth, 287*(2), 491-494.

Burshears, M., O_Brien, T. J., & Malone, R. D. (1986). A multiphase multi-dimensional, variable composition simulation of gas production from a conventional gas reservoir in contact with hydrates. *In: SPE unconventional gas technol symposium. Louisville, KY*.

Bünz, S., Mienert, J., & Berndt, C. (2003). Geological controls on the Storegga gas-hydrate system of the mid-Norwegian continental margin. *Science, 209*(3-4), 291-307.

Chakma, A. (1997). CO_2 capture processes - opportunities for improved energy efficiencies. *Energy Convers Manage, 38*, S51-56.

Chen, Y., Haflidason, H., & knies, J. (2008). *Methane fluxes from pockmark areas in Nyegga, Norwegian Sea*. Paper presented at the International Geological Conference. from http://folk.uib.no/nglbh/GANS/publications.html

Conti, M. (1997). Solidification of binary alloys: Thermal effect studied with with the phase field. *Physical Review E, 55*(1), 765-771.

Conti, M. (2000). Thermal and chemical diffusion in the rapid solidification of binary alloys. *Physical Review E, 61*(1), 642-650.

D'Hondt, S., Jorgensen, B. B., Miller, D. J., Batzke, A., Blake, R., Cragg, B. A., et al. (2004). Distributions of Microbial Activities in Deep Subseafloor Sediments. *Science, 306*(5705), 2216-2221.

Davidson, D. W., El-Defrawy, M. K., Fuglem, M. O., & Judge, A. S. (1978). *Natural gas hydrates in northern Canada. In:3rd international conference on Permafrost. p. 938-43*.

Desideri, U., & Paolucci, A. (1999). Performance modelling of a carbon dioxide removal system for power plants. *Energy Convers Manage, 40*(18), 1899-1915.

Dickens, G. R. (2003). CLIMATE: A Methane Trigger for Rapid Warming? (Vol. 299, pp. 1017-).

Dyadin, Y. A., Aladko, E. Y., & Larionov, E. G. (1997). Decomposition of methane hydrates up to 15 kbar. *Mendeleev Communications*(1), 34-35.

Egorov, A. V., Crane, K., Vogt, P. R., Rozhkov, A. N., & Shirshov, P. P. (1999). Gas hydrates that outcrop on the sea floor: stability models. *Geo-Marine Letters, 19*(1), 68-75.

Engelezos, P., Kalogerakis, N., Dholabhai, P. D., & Bishnoi, P. R. (1987). Kinetics of formation of methane and ethane gas hydrates. *Chemical Engineering Science, 42*(11), 2647-2658.

Evans, R., & Sluckin, T. J. (1980). A Density Functional Theory for Inhomogeneous Charged Fluids - Application to the Surfaces of Molten-Salts. *Molecular Physics, 40*(2), 413-435.

Fujioka, Y. (1995). *Energy conversion and management, 36*(6-9), 551.

Fujioka, Y., Ozaki, M., Takeuchi, K., Shindo, Y., Yanagisawa, Y., & Komiyama, H. (1995). Ocean CO2 sequestration at the depths larger than 3700 m. *Energy Conversion and Management, 36*(6-9), 551-554.

Glasby, G. P. (2003). Potential impact on climate of the exploitation of methane hydrate deposits offshore. *Marine and Petroleum Geology, 20*(2), 163-175.

Gránásy, L., Börzsönyi, T., & Pusztai, T. (2002). Nucleation and Bulk Crystallization in Binary Phase Field Theory. *Phys. Rev. Lett., 88*(206105).

Grauls, D. (2001). Gas hydrates: importance and applications in petroleum exploration. *Marine and Petroleum Geology, 18*(4), 519-523.

Gray, M. L., Soong, Y., Champagne, K. J., Baltrus, J., Stevens, R. W., Toochinda, P., et al. (2004). CO_2 capture by amine-enriched fly ash carbon sorbents. *Sep Purif Technol, 35*(1), 31-36.

Greiner, W., Neise, L., & Stocker, H. (1995). *Thermodynamics and statistical mechanics*: Springer-Verlag New York Inc.

Handa, N., & Ohsumi, T. (2003). Direct ocean disposal of carbon dioxide. *1st ed. Tokyo: TERRAPUR.*

Haugan, P. M., & Drange, H. (1996). Effects of CO_2 on the ocean environment. *Energy Convers. Mgmt., 37*(6-8), 1019-1022.

Hendriks, C. A., & Blok, K. (1993). Underground storage of carbon oxide. *Energy Convers Manage, 34*(9-11), 949-957.

Herzog, H. J., Herzog, H. J., Adams, E. E., Caulfield, J. A., Auerbach, D. I. A., & Auerbach, D. I. (1997). *Environmental impacts of ocean disposal of CO2.* Paper presented at the Energy Conversion Engineering Conference, 1997. IECEC-97., Proceedings of the 32nd Intersociety.

Hesselbo, S. P., Gröcke, D. R., Jenkyns, H. C., Bjerrum, H. C., Farrimond, P., Bell, H. S. M., et al. (2002). Massive dissociation of gas hydrate during a Jurassic anoxic event. *Nature, 406* **392–395**.

Holder, G. D., Zetts, S. P., & Pradhan, N. (1988). Phase behavior in systems containing clathrate hydrates. *Rev Chem Eng, 5*(1-4), 1-70.

Hovland, M., Svensen, H., Forsberg, C. F., Johansen, H., Fichler, C., Fosså, J. H., et al. (2005). Complex pockmarks with carbonate-ridges off mid-Norway: Products of sediment degassing. *Marine Geology, 218*(1-4), 191-206.

Ishimatsu, A., Kikkawa, T., Hayashi, M., Lee, K.-S., & Kita, J. (2004). Effects of CO_2 on marine fish: larvae and adults. *Journal of Oceanography, 60*(4), 731-742.

Jain, A. K., & Cao, L. (2005). Assessing the effectiveness of direct injection for ocean carbon sequestration under the influence of climate change

Geophys Res Lett 2005 *Geophys Res Lett, 32*(L09609).

Kennett, J. P., Cannariato, K. G., Hendy, I. L., & Behl, R. J. (2000). Carbon Isotopic Evidence for Methane Hydrate Instability During Quaternary Interstadials (Vol. 288, pp. 128-133).

Knutzen, J. (1981). Effects of decreased pH on marine organisms. *Marine Pollution Bulletin*(12), 25-29.

Kuznetsova, T., & Kvamme, B. (1999). Grand canonical molecular dynamics for TIP4P water systems. *Molecular Physics, 97*(3), 423-431.

Kuznetsova, T., & Kvamme, B. (2002). Atomistic computer simulations for thermodynamic properties of carbon dioxide at low temperatures. *Energy Conversion and Management, 43*(18), 2601-2623.

Kvamme, B. (1996). A new theory for the kinetics of hydrate formation. *In 2nd International Conference on Natural Gas Hydrates*.

Kvamme, B., Graue, A., Aspenes, E., Kuznetsova, T., Gránásy, L., Tóth, G., et al. (2003). Kinetics of solid hydrate formation by carbon dioxide: Phase field theory of hydrate nucleation and magnetic resonance imaging. *Physical chemistry chemical physics, 6*(9).

Kvamme, B., & Tanaka, H. (1995). Thermodynamic stability of hydrate s for ethane, ethylene and carbon dioxide. . *J. Chem. Phys., 99*, 7114-7119.

Kvenvolden, K. A. (1988). Methane hydrate. A major reservoir of carbond in the shallow geosphere. *Chem Geol, 7*(1-3), 41-51.

Kvenvolden, K. A. (1995). A review of the geochemistry of methane in natural gas hydrate. *Organic geochemistry 23*, 997-1008.

Kvenvolden, K. A. (1995). A review of the geochemistry of methane in natural gas hydrate. *Organic Geochemistry, 23*(11-12), 997-1008.

Lee, S.-Y., & Holder, G. D. (2001). Methane hydrate potential as a future energy source. *Fuel Processing Technology, 71*(1-3), 181-186.

Lijuan, H., Matsubayashi, O., & Lei, X. (2006). Methane hydrate accumulation model for the Central Nankai accretionary prism. *Marine Geology, 227*(3-4), 201-214.

Long, D., Lovell, M. A., Rees, J. G., & Rochelle, C. A. (2009). *Sediment - Hosted Gas Hydrates: New Insights on Natural and Synthetic Systems (eds)* (Vol. 319). London The Geological Society, Special Publication.

MacDonald, I. R., Guinasso, N. L., Sassen, R., Brooks, J. M., Lee, L., & Scott, K. T. (1994). Gas hydrate that breaches the sea floor on the continental slope of the Gulf of Mexico (Vol. 22, pp. 699-702).

Makogon, I. U. F. (1981). *Hydrates of natural gas*. Tulsa, Okla.: PennWell Books.

Makogon, Y. F. (1965). Gazovaya Promyshlennost. *5*(14).

Makogon, Y. F. (1998). *Natural gas hydrates: the state of study in the ussr and perspectives for its use. In: Third chemical congress of North America. Toronto, Canada*.

McCabe, W. L., Smith, J. C., & Harriott, P. (2005). *Unit operations of chemical engineering* (seventh edition ed.): McGraw-Hill higher education.

Nakashiki, N. (1998). Lake-type storage concepts for CO2 disposal option. *Waste Management, 17*(5-6), 361-367.

Nealson, K. (2006). Lakes of liquid CO_2 in deep sea. *Proc Natl Acad Sci USA 103*(38), 13903-13904.

Ohsumi, T. (1993). Prediction of solute carbon dioxide behaviour around a liquid carbon dioxide pool on deep ocean basin. *Energy Conversion and Management, 33*(5-8), 685-690.

Ohsumi, T. (1995). CO_2 storage option in the deep sea. *Marine Technology Society Journal, 29*(3), 58-66.

Ozaki, M. (1998). CO2 injection and dispersion in mid-ocean depth by moving ship. *Waste Management, 17*(5-6), 369-373.

Poetner, H.-O., & Reipschlager, A. (1996). Ocean disposal of anthropogenic CO_2 : physiological effects on tolerant and intolerant animals' In :Ocean Storage of Carbon Dioxide. Workshop 2 - Environmental Impact. *IEA Greenhouse Gas R&D Programme, ISBN 1 898373 13 2*.

Pörtner, H. O., **Langenbuch** , M., & Michaelidis, B. (2005). Effects of CO_2 on marine animals: Interactions with temperature and hypoxia regimes. *Journal of Geophysical Research - Oceans, 110*, doi:10.1029/2004JC002561.

Pörtner, H. O., **Langenbuch** , M., & **Reipschlager,** A. (2004). Biological impact of elevated ocean CO_2 concentrations: lessons from animal physiology and Earth history. *Journal of Oceanography, 60*(4), 705-718.

Pörtner, H. O., & **Reipschlager,** A. (1996). Ocean disposal of anthroppgenic CO_2: Physiology effects on tolerant and intolerant animals. Ocean storage of CO_2-Environmental Impact. *B. Ormerod, M. Angel (eds), Massachusetts Institute of Technology and International Energy Agency, Greenhouse gas R&D Programme, Boston/Cheltenham, pp*, 57-81.

Qi, L., Zhishen, W., & Xiaochun, L. (2008). Prediction of CO_2 leakage during sequestration into marine sedimentary strata. *Energy Conversion and Management 50 (2009)*, 503-509.

Rehder, G., Kirby, S. H., Durham, W. B., Stern, L. A., Peltzer, E. T., Pinkston, J., et al. (2004). Dissolution rates of pure methane hydrate and carbon-dioxide hydrate in undersaturated seawater at 1000-m depth. *Geochimica et Cosmochimica Acta, 68*(2), 285-292.

Ruppel, C., & Kinoshita, M. (2000). Fluid, methane, and energy flux in an active margin gas hydrate province, offshore Costa Rica. *Earth and Planetary Science Letters, 179*(1), 153-165.

Sassen, R., & MacDonald, I. R. (1997, April 13-17). *Thermogenic Gas Hydrates, Gulf of Mexico Continental Slope.* Paper presented at the Proc. 213th ACS National Meeting.

Seibel, B. A., & Walsh, P. J. (2001). Potential impacts of CO_2 injections on deep-sea-biota. *Science, 294*, 319-320.

Seo, Y.-T., Lee, H., & Yoon, J.-H. (2001). Hydrate phase equilibria of the carbon dioxide, methane and water system. *Journal of Chemical & Engineering Data, 46*(2), 381-384.

Shindo, Y., Fujioka, Y., & Komiyana, H. (1995). Dissolution and dispersion of CO_2 from a liquid pool in the deep ocean. *International Journal of Chemical Kinectics, 27*(11), 1089-1095.

Shpakov, V. P., Tse, J. S., Tulk, C. A., Kvamme, B., & Belosludov, V. R. (1998). Elastic moduli calculation and instability in structure I methane clathrate hydrate. *Chemical Physics Letters, 282*(2), 107-114.

Skovberg, P., & Rasmussen, P. (1994). A mass transport limited model for the growth of methane and ethane gas hydrates. *Chemical Engineering Science, 49*, 1131-1143.

Sloan, E. D. (1998). *Clathrate hydrates of natural gases*

Sloan, E. D., & Fleyfel, F. (1991). A molecular mechanism for gas hydrate nucleation from ice. *AIChE Journal, 37*(9), 1281-1292.

Sloan, E. D., & Koh, C. A. (2008). *Clathrate hydrates of natural gases* (3rd ed.). Boca Raton, FL: CRC Press.

Smith, I. M., & Thambimuthu, K. V. (1993). Greenhouse gas emissions, abatement and control: the role of coal. *Energy Fuels, 7*, 7-13.

Stackelberg, M. V., & Muller, H. R. (1951). On the structure of gas hydrate. *J. Chem. Phys., 19*, 1281-1292.

Stern, L. A., Kirby, S. H., & Durham, W. B. (1996). Peculiarities of Methane Clathrate Hydrate Formation and Solid-State Deformation, Including Possible Superheating of Water Ice. *Science, 273*(5283), 1843-1848.

Stern, L. A., Kirby, S. H., Durham, W. B., Circone, S., & Waite, W. F. (2000). Synthesis of pure methane hydrate suitable for measurement of physical properties and decomposition behavior. *In Natural Gas Hydrate in Oceanic and Permafrost Environments (ed. M.D. Max, Kluwer, Dordrecht), pp.*(323 - 349).

Svandal, A. (2006). *Modeling hydrate phase transitions using mean-field approches.* University of Bergen, Bergen.

Svandal, A., Kuznetsova, T., & Kvamme, B. (2006a). Thermodynamic properties and phase transitions in the H2O/CO2/CH4 system. *Fluid Phase Equilibria, 246*(1-2), 177-184.

Svandal, A., & Kvamme, B. (2005a). Modeling the dissociation of carbon dioxide and methane hydrate using the Phase Field Theory. *Journal of Mathematical Chemistry, 3*, 1-3.

Svandal, A., Kvamme, B., Gràsàsy, L., & Pusztai, T. (2005b). The influence of diffusion on hydrate growth. *Journal of Phase Equilibria and Diffusion, 26*(5), 534-538.

Tarazona, P., & Evans, R. (1984). A Simple Density Functional Theory for Inhomogeneous Liquids - Wetting by Gas at a Solid Liquid Interface. *Molecular Physics, 52*(4), 847-857.

Tegze, G., Gránásy, L., & Kvamme, B. (2007). Phase field modeling of CH4 hydrate conversion into CO2 hydrate in the presence of liquid CO2. *Physical chemistry chemical physics, 9*, 3104-3111.

Toki, T., Gamo, T., & Yamanaka, T. (2001). Methane migration from the Nankai Trough accretionary prism. *Bulletin of the Geological Survey of Japan, 52*(0016-7665), 1-8 (in japanese with english abstract).

Wang, S. L., Sekerka, R. F., Wheeler, A. A., Murray, B. T., Coriell, S. R., Braun, R. J., et al. (1993). Thermodynamically-consistent phase-field models for solidification. *Physica D: Nonlinear Phenomena, 69*(1-2), 189-200.

Warren, J. A., & Boettinger, W. J. (1995). Predictions of dendritic growth and microsegragation patterns in a binary alloy using the phase-field method. *Acta metall. mater, 43*, 689-703.

Warzinski, R. P., & Holder, G. D. (1988). Gas clathrate hydrates. *Energy Fuels, 12*(2), 189-190.

Wheeler, A. A., Boettinger, W. J., & McFadden, G. B. (1992). Phase-field model for isothermal phase transitions in binary alloys. *Physical Review A, 45*(10), 7424-7439.

Wuebbles, D. J., & Hayhoe, K. (2002). Atmospheric methane and global change. *Earth-Science Reviews, 57*(3-4), 177-210.

Nomenclature

ΔG	Total Gibbs free energy	**(J)**
ΔG_S	Surface free energy	**(J/m^2)**
ΔG_V	Volume free energy	**(J/m^3)**
r	Radius	**(m)**
A_S	Interface area	**(m^{-1})**
A	Crystal surface area	**(m^2)**
A_S, B_S	Constants for small cavities structure I in section (6.1)	
A_L, B_L	Constants for large cavities structure I in section (6.1)	
K	Overall transfer coefficient	**(mol/m^{2}s)**
k_d, k_r	Reaction coefficients	**(mol/m^{2}s)**
dm	Change in mass	**(mole)**
dt	Change in time	**(s)**
c	Local solute concentration	**(moles/m^3)**
c^{eq}	Equilibrium concentration	**(moles/m^3)**
c	Mole fraction in Phase Field Theory	
F	Free energy functional	
f	Free energy density	**(J/m^2)**
v_m	Average molar volume	**(m^3/mol)**
W	Free energy scale	**(J/m^{3}K)**
D	Diffusion coefficient	**(m^2/s)**
D_L	Diffusivity coefficient for liquid	**(m^2/s)**
D_S	Diffusivity coefficient for solid	**(m^2/s)**

M_ϕ, M_c	Mobility coefficient	**(m^2/s)**
p	Pressure	**(Pascal, pa)**
J_c	Flux	**(mol/m^2s)**
T	Temperature of melting	**(K)**
R	Gas constant	**(J/Kmol)**
M^A, M^B	Molecular weights	**(g/mol)**
W_A		**(J/m^3K)**
W_B		**(J/m^3K)**
$\dot{e}$	Energy field	**(J)**
dU	Internal energy	**(J)**
N	No. of particles	
N	No. of cavity type in unit cell in section (6.1)	
N_W	No. of water molecules in section (6.1)	
S	Entropy	**(J/K)**
V	Volume	**(m^3)**
F	Helmholtz free energy in section (4.1)	**(J)**
C	No. of components	
F	Degree of freedom in section (4.2)	
P	No. of phases in section (4.2)	
v_i	No. of type I cavities per water molecule	
h_{ij}	Cavity partition function of component j in cavity type i	
Δg_{ji}^{inc}	Free energy of inclusion	**(J)**
x_T	Total mole fraction	
DR	Dissolution rate	**($Mmol/m^2s$)**
SR	Radius shrinkage rate	**(mm/s)**

M_G	Molecular weight of guest	**(Kg/mmoles)**
HN	Hydrate number	
V_{Cell}	Volume of unit cell	

Greek letters

γ	Interfacial free energy	**(mJ/m^2)**
σ	Interfacial tension	**(mJ/m^2)**
ϕ	Structural order parameter	
$б_{A,B}$	Interface energy	**(J/m^2)**
$\delta_{A,B}$	Interface thickness	**(m)**
β		**(moles/KJ)**
ε_ϕ	Model parameter	**(J/mK)**
μ	Chemical potential	**(J/moles)**
μ_w^o	Chemical potential of water in an empty hydrate structure	**(J/moles)**
μ_w^H	Chemical potential of water in hydrate	**(J/moles)**
Δ	Change	
θ_{ij}	Fractional occupancy of cavity i by component j	

Appendix A

The calculations to calculate the temperature and pressure near stability were done (Appendix A 1) using the equation .

Appendix A 1: Extrapolation of depth from 500 meters till 730 meters.

Sr#	P_o (bar)	P_o (Pa)	T_o (°C)	Z (m)	Z_o (m)	P (bar)	T (K)
1	50	5 000 000	0,1	510	500	50,98	273,61
2	50	5 000 000	0,1	520	500	51,96	273,97
3	50	5 000 000	0,1	530	500	52,94	274,33
4	50	5 000 000	0,1	540	500	53,92	274,69
5	50	5 000 000	0,1	550	500	54,91	275,05
6	50	5 000 000	0,1	560	500	55,89	275,41
7	50	5 000 000	0,1	570	500	56,87	275,77
8	50	5 000 000	0,1	580	500	57,85	276,13
9	50	5 000 000	0,1	590	500	58,83	276,49
10	50	5 000 000	0,1	600	500	59,81	276,85
11	50	5 000 000	0,1	610	500	60,79	277,21
12	50	5 000 000	0,1	620	500	61,77	277,57
13	50	5 000 000	0,1	630	500	62,75	277,93
14	50	5 000 000	0,1	640	500	63,73	278,29
15	50	5 000 000	0,1	650	500	64,72	278,65
16	50	5 000 000	0,1	660	500	65,70	279,01
17	50	5 000 000	0,1	670	500	66,68	279,37
18	50	5 000 000	0,1	680	500	67,66	279,73
19	50	5 000 000	0,1	690	500	68,64	280,09
20	50	5 000 000	0,1	700	500	69,62	280,45
21	50	5 000 000	0,1	710	500	70,60	280,81
22	50	5 000 000	0,1	720	500	71,58	281,17
23	50	5 000 000	0,1	730	500	72,56	281,53
24	50	5 000 000	0,1	740	500	73,54	281,89
25	50	5 000 000	0,1	750	500	74,53	282,25
26	50	5 000 000	0,1	760	500	75,51	282,61

Density Calculations

Appendix A 2: Calculation for the Langmuir Constant.

Langmuir Constant											
Temperature (K)	Eq-Pressure CH_4 (bar)	Eq-Pressure CO_2 (bar)	A1 CH_4S	B1 CH_4S	A2 CH_4L	B2 CH_4L	A2 CO_2L	B2 CO_2L	CS CH_4	CL CH_4	CL CO_2
273,17	26,41		6,9153	0,0316	6,0966	0,0279	15,2076	0,0589	0,4773	0,5145	-
273,21	26,5		6,9153	0,0316	6,0966	0,0279	15,2076	0,0589	0,4770	0,5142	-
273,25	25,767	12,81	6,9153	0,0316	6,0966	0,0279	15,2076	0,0589	0,4767	0,5140	0,6836
281,56	58,59		6,9153	0,0316	6,0966	0,0279	15,2076	0,0589	0,4254	0,4647	-
274,65	30,35	14,95	6,9153	0,0316	6,0966	0,0279	15,2076	0,0589	0,4677	0,5053	0,6596
276,65	36,69	18,71	6,9153	0,0316	6,0966	0,0279	15,2076	0,0589	0,4550	0,4932	0,6267
278,65	44,46	23,64	6,9153	0,0316	6,0966	0,0279	15,2076	0,0589	0,4427	0,4814	0,5955
280,65	54,1	30,26	6,9153	0,0316	6,0966	0,0279	15,2076	0,0589	0,4308	0,4699	0,5658
282,65	66,1	39,8	6,9153	0,0316	6,0966	0,0279	15,2076	0,0589	0,4191	0,4586	0,5376

Appendix A 3: Density and hydrate number calculations.

Density Calculation for Structure I hydrates									
Temperature (K)	Eq-Pressure CH_4 (bar)	Eq-Pressure CO_2 (bar)	θ_S CH_4	θ_L CH_4	θ_L CO_2	ρCH_4 Kg/m^3	HN CH_4	HN CO_2	Pure CO_2 Kg/m^3
273,17	26,41		0,9265	0,9314		910,1147	6,1814		
273,21	26,5		0,9267	0,9316		910,1379	6,1802		
273,25	25,767	12,81	0,9247	0,9298	0,8975	909,9076	6,1926	8,5422	1 023,3907
281,56	58,59		0,9614	0,9646		914,2450	5,9660		
274,65	30,35	14,95	0,9342	0,9388	0,9079	911,0284	6,1324	8,4442	1 026,0330
276,65	36,69	18,71	0,9435	0,9476	0,9214	912,1305	6,0744	8,3205	1 029,4564
278,65	44,46	23,64	0,9517	0,9554	0,9337	913,0947	6,0245	8,2113	1 032,5656
280,65	54,1	30,26	0,9589	0,9622	0,9448	913,9423	5,9813	8,1145	1 035,3922
282,65	66,1	39,8	0,9652	0,9681	0,9553	914,6820	5,9441	8,0250	1 038,0649

Appendix B

Long abstract submitted to seventh International Conference of Computational Methods in Science and Engineering {ICCMSE-2009}

Phase Field Theory modeling of methane fluxes from exposed natural gas hydrate reservoirs

Khuram Baig, Muhammad Qasim, Pilvi-Helinä Kivelä, Bjørn Kvamme[1]

University of Bergen, Department of Physics and Technology, Allégaten 55, N-5007 Bergen, Norway

Abstract. Fluxes of methane from offshore natural gas hydrate into the oceans vary in intensity from massive bubble columns of natural gas all the way down to fluxes which are not visible within human eye resolution. The driving force for these fluxes is that methane hydrate is not stable towards nether minerals nor towards under saturated water. As such fluxes of methane from deep below hydrates zones may diffuse through fluid channels separating the hydrates from minerals surfaces and reach the seafloor. Additional hydrate fluxes from hydrates dissociating towards under saturated water will have different characteristics depending on the level of dynamics in the actual reservoirs. If the kinetic rate of hydrate dissociation is smaller than the mass transport rate of distributing released gas into the surrounding water through diffusion then hydrodynamics of bubble formation is not an issue and Phase Field Theory (PFT) simulations without hydrodynamics is expected to be adequate [1, 2]. In this work we present simulated results corresponding to thermodynamic conditions from a hydrate field offshore Norway and discuss these results with in situ observations. Observed fluxes are larger than what can be expected from hydrate dissociating and molecularly diffusing into the surrounding water. Strategies for extensions of the PFT model to account for gravity and natural gas bubble formation in surrounding water is discussed.

Keywords: Phase Field Theory; Methane Fluxes, Hydrate
PACS: 30

INTRODUCTION

Hydrates, also called clathrates, are crystalline solids which look like ice, and which occur when water molecules form a cage-like structure around the guest molecule, which has to fit exactly into the cavity. The most common guest molecules are methane, ethane, propane, butane, carbon dioxide and etc. The most remarkable property of methane hydrates are that it compresses the guest molecule into a very dense and compact arrangement, such as 1 cubic meter of solid methane hydrate with 100 percent void occupancy by methane will release roughly 164 cubic meter of methane [3] at standard conditions of temperature and pressure. Unstable and dissociated gas hydrates are contributing to the global warming of the earth, but the main problems are hydrocarbon transmission in deepwater oil and gas production. Much scientific work has focused on the nucleation, growth, and dissociation of gas hydrates, as well as on the prevention of hydrate formation by adding chemical inhibitors [4]

Hydrates in reservoirs are subject to potential contact with minerals, aqueous solution and gas, depending on the state of the system and the fluid fluxes through the hydrate section. From a thermodynamic point of view the first question that arises is whether the system can reach equilibrium or not according to Gibbs phase rule. Equilibrium requires the equality of temperature, pressure, and chemical potential in all phases. In the case of dissociation, gas hydrate generally becomes unstable by changing the P/T conditions in a way that the hydrate phase is not stable anymore, i.e., that the chemical potential of the gas component is lower in the free gas phase than in the hydrate phase [5]. In a reservoir the local temperature is given by the geothermal gradient and the

pressure is given by the static column above. Equilibrium in this system can only be achieved if the number of degrees of freedom is 2. This implies that a hydrate surrounded by mineral (and corresponding adsorbed phase on the surface), aqueous phase and only methane will be over determined and can not reach a unique equilibrium situation. These systems will progress dynamically towards local and global minimum free energy at all times.

[1] bjorn.kvamme@ift.uib.no

SIMULATIONS

The theoretical aspects of the simulations namely phase field theory (PFT) and thermodynamics are presented elsewhere. Look for example [6-7] for PFT and [8-9] for thermodynamics of a hydrate system.

Unfortunately there is no experimental data available for naturally existed hydrates and this may be due to lack of pressurized core sampling [10]. So the references taken are not directly comparable with this work but can give an idea about the fluxes presence around these areas. Yifeng and Haflidi [12] are working on a project in which they have taken six gravity cores up to 3.5 m long from the Nyegga region at depths of 639 to 740 m. Totally 41 pore waters were obtained and sulfate gradients measured in the southeast of Nyegga indicate that methane fluxes are 15 to 49 mmol/m2/yr.

The code is described in [5,7, 11]. It was used a 2D planar geometry to dissociate circle of hydrate placed in the center surrounded by pure liquid water. Two different sizes of the system (5000×5000) and (1500×1500) grids were used and each grid is calculated using Lagrange Method which is equal to 1.00E-10 m. The time is calculated using Lagrange method which is equal to stepmax × innerstepmax × 1.00E-15 s.

RESULT AND DISCUSSION

To see the effects of dissociation of methane, simulations were run on different depths 500, 639, 730 & 740 meters respectively. The temperature and pressure conditions taken for the simulations were from Nyegga cold seeps, are well inside the stability region.

The results are shown here only for 639 m depth with temperature 273.21 Kelvin. The size of the system was taken 5000×5000 grid points which correspond to area 2.5E-13 m^2. The total hydrate unit cells in the initial solid were 31.41676E+05 with radius of 1000 grids which corresponds to circular area 3.1415E-14 m^2. The simulation was run to 16.13E+06 total time steps this corresponds to the time of 16.13 ns. The ratio between solid (hydrate) and liquid was adjusted as to achieve the stability. In this case the hydrate to system ratio was taken as 1 : 2.5. The concentrations have been calculated inside the hydrate at different points 10Å, 30Å, 60Å, 80Å & 100Å away from the original interface shown in Figure-1.

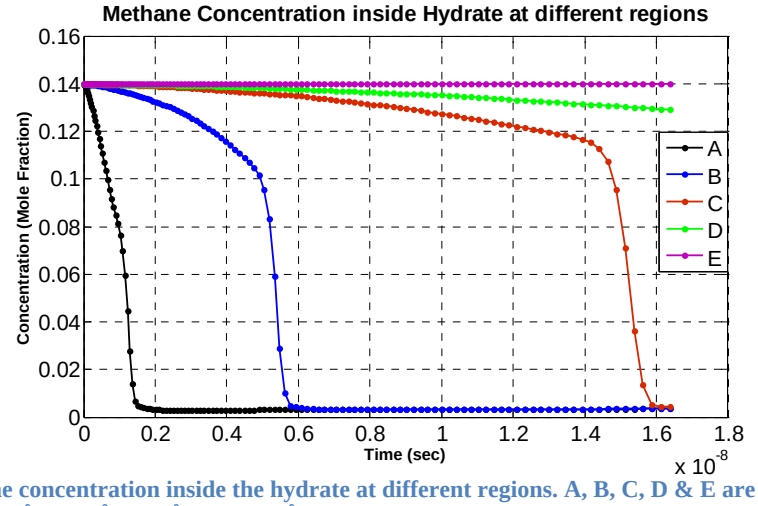

FIGURE 23: Methane concentration inside the hydrate at different regions. A, B, C, D & E are points which 10.0Å, 30.0Å, 60. 0Å, 80.0Å & 1000.0Å away from the original interface respectively.

To get the clear vision of diffusion inside the hydrate, the concentrations have been taken on five points A, B, C, D & E corresponding to values 10Å, 30Å, 60Å, 80Å and 1000Å respectively, showing distance from the

original interface. Initially at t=0, the mole fraction equals the initial values which show that CH_4 has not yet diffused. If the concentration of methane drops below the hydrate stability limit for the given temperature and pressure, a chemical potential driving force towards dissociation will arise as shown in Figure-1 lines A, B, C and D. The sudden drop in concentrations in all four cases is due the dissociation pressure reached and hydrate completely dissociated. The maximum mole fraction decrease observed was 0.004469, 0.004565, 0.003219 and 0.004814 in all four cases respectively, this difference in fractions due to the effect of concentration gradient as moving away from the original interface.

To observe the movement of methane from solid phase to liquid, the velocity on the interface is determined by tracking the ϕ values. From this velocity the dissolution rate was calculated until 16.13 ns using the following equation [12]:

$$DR = SR \times \frac{\rho_{Hyd}}{M_G} \times \left(\frac{M_G}{M_G + (HN \times 0.018)} \right) \quad (1)$$

Where DR is Dissolution rate (mmol/m^{2}s), SR is Radius shrinkage rate (mm/s), ρ_{Hyd} is Density of hydrate (kg/m^3), M_G is Molar weight of the guest (kg/mol) and HN is Hydrate number.

The initial value of flux was high due to the initial relaxation of a system into a physical realistical interface. To show the actual dependency of dissociation on driving forces the close look on the curve has shown in the Figure-2a. The rate is decreasing gradually after this relaxed point on the curve. One reason for this is the decrease in thermodynamic driving force which is proportional to the increasing chemical potential in the surrounding aqueous solution.

The interface in this simulation is perfectly follows the power law which is proportional to square root of time showing a diffusion control process. To compare the values of dissolution rates, the flux is extrapolated to experimental time scales (Fig.2b). The flux rate after 10^4 years is 0.4544 mmol/m^{2}yr, which comparable to reference result 15 mmol/m^{2}yr.

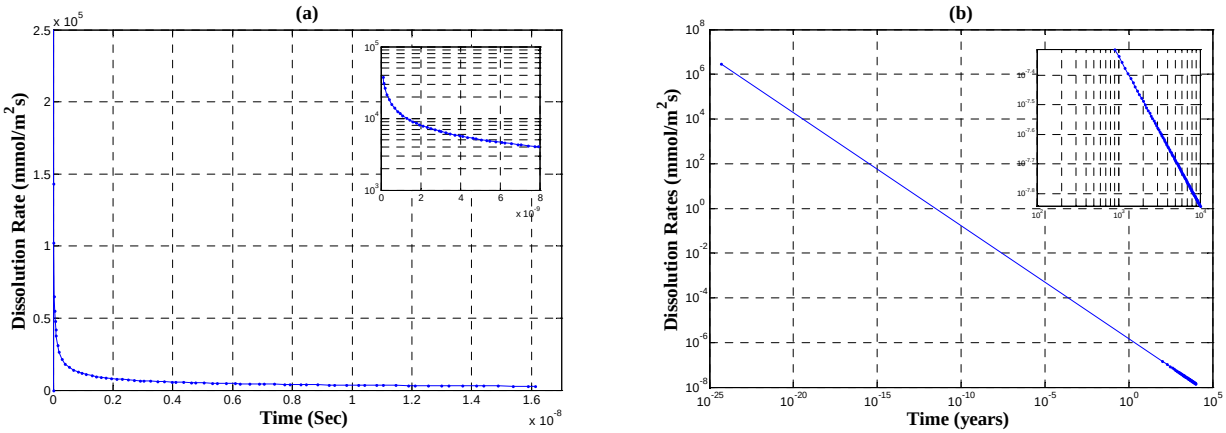

FIGURE 24: Dissolution rates and extrapolation. (a) dissolution rate until 16.13 ns. (b) extrapolation until 10000 years.

CONCLUSIONS AND FURTHER WORK

In this work phase field theory used to estimate the rates for dissociation of hydrate exposed to sea water containing methane concentration less in sea water as compare to inside of hydrate. This is necessary to maintain the fluxes of methane. The estimated methane flux is higher than what can be expected from hydrate dissociating and molecularly diffusing into the surrounding water. This is might be the effect of salinity, which is not included in the model.

There is further work done by simulating values for more temperature, pressure points. To encounter the effect of fluid flow, density change and gravity, an extended phase field model is formed. This is achieved by

coupling the phase field model with the Navier-Stokes Equations. The phase and concentration fields enter the Navier-Stokes equations as described by Conti[13-15].

$$\frac{\partial \rho}{\partial t} = -\rho \nabla . \vec{v}$$

$$\frac{\partial \vec{v}}{\partial t} + (\vec{v}.\nabla)\vec{v} = \rho \vec{g} + \nabla . \mathrm{P} .$$

Here $\rho(x, y, t)$ is the mass density, $\vec{v}(x, y, t)$ the velocity and $\vec{g}$ is the gravitational acceleration, While

$$\mathrm{P} = I\left[-p + \boldsymbol{\varepsilon}_c^2 \left(\frac{1}{2}(\nabla c)^2 + c\nabla^2 c - \nabla c \otimes \nabla c \right) + \boldsymbol{\varepsilon}_\phi^2 \left(\frac{1}{2}(\nabla \phi)^2 - \nabla \phi \otimes \nabla \phi \right) \right] + \Pi$$

is the generalization of stress tensor [1-3]. $\mathrm{P} - \Pi$ represents non-dissipative part and Π represents the dissipative part of the stress tensor. I is unit tensor, $\otimes$ represents the diadic product and p represents the pressure.

The Navier-Stokes equations couples back into time evolution partial differential equation via the convection term,

$$\frac{\partial \phi}{\partial t} + (\vec{v}.\nabla)\phi = M_\phi \left(\varepsilon_\phi^2 T \nabla^2 \phi - WTg'(\phi) - p'(\phi)(g_L - g_S) \right)$$

$$\frac{\partial c}{\partial t} + (\vec{v}.\nabla)c = \nabla . \left(\frac{v_m}{RT} Dc(1-c) \nabla \left((W_A - W_B) Tg(\phi) + (1 - p(\phi)) \frac{\partial g_S}{\partial c} + p(\phi) \frac{\partial g_L}{\partial c} \right) \right).$$

These four partial differential equations can be solved numerically. It is believed that the achieved results will be more realistic by comparing the observed fluxes with expected fluxes.

REFERENCES

1. Kvamme, B., Kuznetsova, T., Mathematical and Computer Modelling, 2009, in press
2. Svandal, A., Kvamme, B., Volume 46, Issue 3, Page 763
3. Davidson, D. W., El-Defrawy, M. K., Fuglem, M. O., & Judge, A. S. (1978). In 3rd international conference on Permafrost. p. 938-43.
4. Sloan, E. D. (1998). Clathrate hydrates of natural gases
5. Rehder, G., Kirby, S. H., Durham, W. B., Stern, L. A., Peltzer, E. T., Pinkston, J., et al. (2004). Geochimica et Cosmochimica Acta, 68(2), 285-292.
6. Gránásy, L., Börzsönyi, T., & Pusztai, T. (2002). Phys. Rev. Lett., 88(206105).
7. Kvamme, B., Graue, A., Aspenes, E., Kuznetsova, T., Gránásy, L., Tóth, G., et al. (2003). Physical chemistry chemical physics, 6(9).
8. Greiner, , W., Neise, L., & Stocker, H. (1995). Springer-Verlag New York Inc.
9. Kvamme, B., & Tanaka, H. (1995). J. Chem. Phys., 99, 7114-7119.
10. Long, D., Lovell, M. A., Rees, J. G., & Rochelle, C. A. (2009) (Vol. 319). London The Geological Society, Special Publication.
11. Nakashiki, N. (1998). Waste Management, 17(5-6), 361-367.
12. Svandal, A. (2006). University of Bergen, Bergen.
13. M. Conti, Phys. Rev. E 64 (2001) 051601.
14. M. Conti, M. Fermani, Phys. Rev. E 67 (2003) 026117.
15. M. Conti, Phys. Rev. E 69 (2004) 022601.
16. Y. Chen, H. Haflidason and J. knies, in International Geological Conference (2008).